

**Evolution of Perturbation in a
Hydrodynamically Expanding System
Formed in Relativistic Heavy Ion
Collision**

By

GOLAM SARWAR

PHYS04201204005

Variable Energy Cyclotron Centre

A thesis submitted to the

Board of Studies in Physical Sciences

In partial fulfillment of requirements

For the Degree of

DOCTOR OF PHILOSOPHY

of

HOMI BHABHA NATIONAL INSTITUTE

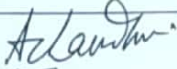
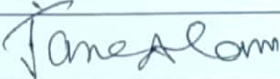
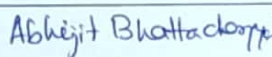
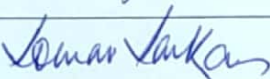
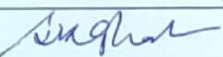


August, 2018

Homi Bhabha National Institute¹

Recommendations of the Viva Voce Committee

As members of the Viva Voce Committee, we certify that we have read the dissertation prepared by Golam Sarwar entitled "Evolution of Perturbation in a Hydrodynamically Expanding System Formed in Relativistic Heavy Ion Collision" and recommend that it may be accepted as fulfilling the thesis requirement for the award of Degree of Doctor of Philosophy.

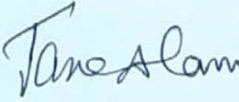
Chairman -	Prof. Asis K. Chaudhury		Date: 1/2/2019
Guide / Convener -	Prof. Jan-e Alam		Date: 1/2/2019
Co-guide - (if any)	-----		Date:
Examiner -	Prof. Abhijit Battacharyya		Date: 1/2/2019
Member 1-	Prof. Saurav Sarkar		Date: 1/2/2019
Member 2-	Prof. Sanjay Ghosh		Date: 1/2/19

Final approval and acceptance of this thesis is contingent upon the candidate's submission of the final copies of the thesis to HBNI.

I/We hereby certify that I/we have read this thesis prepared under my/our direction and recommend that it may be accepted as fulfilling the thesis requirement.

Date: 01/02/2019

Place: VECC, Kolkata


Guide

¹ This page is to be included only for final submission after successful completion of viva voce.

STATEMENT BY AUTHOR

This dissertation has been submitted in partial fulfillment of requirements for an advanced degree at Homi Bhabha National Institute (HBNI) and is deposited in the Library to be made available to borrowers under rules of the HBNI.

Brief quotations from this dissertation are allowable without special permission, provided that accurate acknowledgment of source is made. Requests for permission for extended quotation from or reproduction of this manuscript in whole or in part may be granted by the Competent Authority of HBNI when in his or her judgment the proposed use of the material is in the interests of scholarship. In all other instances, however, permission must be obtained from the author.

Golam Sarwar

DECLARATION

I, hereby declare that the investigation presented in the thesis has been carried out by me. The work is original and has not been submitted earlier as a whole or in part for a degree / diploma at this or any other Institution / University.

Golam Sarwar

List of Publications arising from the thesis

Journal

1. “ Calculation of Power Spectrum in the Little Bangs”,
G. Sarwar, S. K. Singh and J. Alam.
Int. J.M.Phys. A **33**, (2018)1850121. [[arXiv:1711.03743 \[nucl-th\]](#)].
2. “ Kinetic evolution and correlation of fluctuations in an expanding quark gluon plasma”
G. Sarwar and Jane Alam
Int. J.M.Phys. A **33**, (2018) 1850040., [[arXiv:1503.06019 \[nucl-th\]](#)].
3. “An estimate of the bulk viscosity of the hadronic medium”
G. Sarwar, S. Chatterjee and J. Alam,
J. Phys. G **44**, (2017) no.5, 055101.
[\[arXiv:1512.06496 \[nucl-th\]\]](#).

Conference proceedings

- “Temperature fluctuation in quark gluon plasma”,
G. Sarwar and J. Alam,
DAE Symp. Nucl. Phys. **60**, 718 (2015).
- “Bulk viscosity of hot and dense hadrons”, G. Sarwar, S. Chatterjee
and J. Alam.
DAE Symp. Nucl. Phys. **60**, 830 (2015).

Other publication

- “Initial Condition Dependence of Hydrodynamic Flow of Quark Gluon Plasma”,

Md. Hasanujjaman, S. K. Singh, S. Ghosh, S. Chatterjee, G. Sarwar, J. Alam
and S. Sarkar,

DAE Symp. Nucl. Phys. **60**, 808 (2015).

Chapters in books and lectures notes N. A.

Golam Sarwar

DEDICATIONS

To whom it may be appropriate
who cares most

ACKNOWLEDGEMENT

First of all I would like to express my deepest gratitude to my supervisor Prof. Jan-e Alam, whose encouragement, guidance and invaluable academic and mental support from the initial to final level enabled me to develop an understanding of the subject. I am very fortunate to have him as my supervisor. I have learned lots of physics from him, most importantly the way of research minded thinking, without his constant push and direction this thesis would not have been a reality. I am utterly thankful to him.

It is my great pleasure to thank Prof. Sanjay Gosh, Prof Sourav Sarkar, Prof. Asis K. Chaudhuri, Prof. Dinesh K. Srivastava for their encouragements and support. I am grateful to all my teachers who motivated me to seek knowledge and also to all my friends who devoted their precious moments in hours of discussions.

Academically, I also take the opportunity here to express my gratitude to all of my collaborators. I would like to thank all the past and present members in Sir's group for their all types of help, which in many occasions go beyond academic activities. It is indeed the brotherly behavior of the seniors and junior, which eased up my PhD life.

I feel, in research, over all research minded positive human environment matters greatly. Here at VECC in my PhD tenure, Ashik, Noor, Rana(Md Hasanujjaman), Mahfuzur, Shabnam, Rajendra, Asgar, Debasis, Snighda, Sushant, Sandeep da, Arghya, Pingal, Debojit da, Balaram da, Aminul da, Moin da have been gift for me in this regard. Frequent physics discussions with Santosh da, Sabya da, Trambak da, Sashi da, Partha da, Surasree di has been enriching for me. I must mention here again Prof. Jane Alam, as Academic dean for creating and habouring opportunity for such environment from official perspective. I thank all the scholars – including seniors, juniors and batch-mates, academic and non-academic members of VECC,

particularly those of Physics Division for their direct and indirect contributions in my efforts. The talented atmosphere of Theory Division is indeed admired.

I would like to acknowledge all of my family members and relatives who have been also on my side with their constant caring, supportive and helping attitude towards me. After the highest One, I am grateful to my mother and father who dreams through my and my brother's eye, see themselves in us.

I also thank people of India knowingly or unknowingly through their tax-money have been the source of financial support for this work.

In deed, for all above mentioned gifts-from research guide to parents, the praise goes to the One who actually deserves, the source of every thing, the main architect.

Golam Sarwar

Contents

Synopsis	xiii
List of Figures	xxxi
List of Tables	xxxvi
1 Introduction	1
1.1 Collision of heavy ions at relativistic energies:	4
1.2 Fluctuations and perturbations in QGP	6
1.3 Organization of thesis	7
2 Hydrodynamics and Kinetic theory	9
2.1 Hydrodynamics: Basics	9
2.1.1 Evolution of fluid:	10
2.1.2 Hydrodynamic evolution of perturbations	12
2.1.3 Closer condition for hydrodynamic solution and propagation of sound:	13
2.2 Kinetic theory: Basics	13

3	Kinetic Evolution	19
3.1	Introduction	19
3.2	Evolution of fluctuations in a non-expanding background	22
3.2.1	Fluctuations of various hydrodynamic quantities in Fourier space	22
3.2.2	Fluctuations in Fourier space and transport coefficients in relaxation time approximation	29
3.3	Evolution of fluctuation in a hydrodynamically expanding QGP background	33
3.4	Summary and discussion	35
4	Evolution of Anisotropic Perturbations	37
4.1	Introduction	37
4.2	Initial Perturbation	38
4.3	Evolution of fluctuation in energy density for a non-expanding system	44
4.4	Evolution of fluctuation in an expanding QGP background	44
4.5	Summary and discussion	51
5	The Power Spectrum of Little Bangs	53
5.1	Introduction	53
5.2	Hydrodynamic evolution of the quark gluon plasma	57
5.2.1	Initial conditions	58
5.2.2	Equation of State (EoS)	59
5.3	Evolution of anisotropies and fluctuations	60

5.4	The power spectrum	62
5.5	Results	65
5.5.1	Initial conditions from Optical Glauber Model	66
5.5.2	Initial conditions from Monte Carlo Glauber model	68
5.5.3	Pseudo-rapidity and angular distributions	70
5.5.4	Power spectrum without perturbation	70
5.5.5	Power spectrum with perturbation	78
5.5.6	Variation of C_l with T	81
5.5.7	Relation between flow harmonics and power spectrum	82
5.6	Summary and discussions	87
6	Bulk Viscosity and Pressure Fluctuation	89
6.1	Introduction	89
6.2	Correlation in pressure fluctuation and bulk viscosity in QGP phase:	91
6.3	Estimation of bulk viscosity in HRG phase	94
6.3.1	Formalism	94
6.4	Results	97
6.5	Summary and discussions	105
7	Summary and Outlook	109
A	k-space correlations	113
B	Calculations for Power Spectrum	117

B.1	Parameters for EoS:	117
B.2	C_i and v_n :	118
C	Thermodynamic Derivatives	121
	Bibliography	127

Synopsis



Homi Bhabha National Institute

SYNOPSIS OF Ph.D. THESIS

1. Name of the Student: **GOLAM SARWAR**
2. Name of the Constituent Institution: **VARIABLE ENERGY CYCLOTRON CENTRE, KOLKATA**
3. Enrolment No. : **PHYS042012040005**
4. Title of the Thesis: **EVOLUTION OF PERTURBATION IN A HYDRODYNAMICALLY EXPANDING SYSTEM FORMED IN RELATIVISTIC HEAVY ION COLLISION**
5. Board of Studies: **PHYSICAL SCIENCES**

SYNOPSIS

1 Introduction

The main aim of the heavy ion collision experiments at Relativistic Heavy Ion Collider (RHIC) and Large Hadron Collider (LHC) is to create a new state of matter called quark gluon plasma (QGP). Such a state of matter, *i.e.* QGP [1] may have existed in the early universe after a few microsecond of the Big Bang. One of the motivations to create and study QGP in the laboratory is to understand the state of the universe in the microsecond old era. The fluctuations of physical quantities from their average values can be used to understand several properties of the system *i.e.* the transport coefficients of the medium, the approach toward equilibrium, etc. The study of temperature (T) fluctuation in the cosmic microwave background radiation (CMBR) has provided crucial information about the universe when it was about 300,000 years old. This information has led to tremendous

support to the Big Bang model of cosmology. The fluctuation of T in the CMBR is introduced as a perturbation in the phase space distribution of photons. The evolution of this perturbation is studied by using Boltzmann transport equation (BTE) [2] in gravitational field with Thomson scattering in the collision term. The linear polarization resulted from the scattering is connected with the quadrupole moment of the photon's phase space distribution.

The fluctuations in the position of nucleons (with finite size) in the colliding nuclei lead to lumpiness in the spatial distribution of initial energy density(ϵ) of the system formed in Relativistic Heavy Ion Collisions Experiments (RHIC-E). The fluctuation in energy density($\Delta\epsilon$) may also originate due to the energy deposition by the propagation of energetic partons produced in the early stage of the collisions. These fluctuations may lead to observable effects similar to temperature fluctuation in CMBR. We have adopted an approach similar to the one used to study the fluctuation in CMBR. We study the evolution of perturbations by introducing a deviation, $\delta f(x, p, t)$ to the equilibrium distribution function, $f_0(p)$. The bulk in equilibrium evolves via relativistic hydrodynamics and the evolution of the fluctuations, δf over the expanding background is obtained by solving BTE.

The study of the fluctuations in the space time structure of the fireball driven by the fluctuations in the position of the nucleons in the colliding nuclei is an important contemporary issue in RHIC-E. Fluctuations in the space-time structure of the system will cause fluctuations in the thermodynamic quantities. How these fluctuations evolve in a hydrodynamically expanding system, what is their power spectrum and how they are connected with the transport coefficients has been addressed in this dissertation.

Evolution of fluctuation in a hydrodynamic medium contains information about the dissipative properties of the medium. These dissipative properties are quantified as transport coefficients. The effects of transport coefficients on the hydrodynamic evolution of the strongly interacting fireball and on various observables in RHIC-E, *e.g.* the elliptic flow, spectra of hadronic and electromagnetically interacting particles, etc have been studied extensively and and it has been found that that the matter created in heavy ion collisions behaves almost like a perfect liquid [3, 4, 5, 6, 7] with η/s close to the KSS (Kovtun, Son and Starinets) bound [8]. However, the issue of bulk viscosity is less discussed. In the present work we estimate the bulk viscosity from solution of BTE, δf .

The bulk viscosity of hadron resonance gas (HRG) has also been calculated and compared with other works. The phenomenological relevance of ζ has fuelled efforts to estimate it by using various models. In this work we also provide an estimate of ζ within the ambit of HRG model which has been quite successful in describing the low temperature QCD thermodynamics.

2 Evolution of fluctuation

To describe fluctuations caused by perturbations we have considered as small deviation, $\delta f(x, p)$ in the equilibrium single particle distribution function. The evolution of $f(x, p) = f_0(x, p) + \delta f(x, p)$ with $\delta f = f_0 \psi$ is governed by the equation,

$$p^\mu \partial_\mu f = (p \cdot u) C[f] \quad (1)$$

where f_0 is the equilibrium distribution parametrized by temperature ($T = 1/\beta$) and velocity (\vec{v}) of the fluid (QGP in the present case), $f_0(x, p) = 1/[e^{\beta(x)(u^\mu p_\mu)} \pm 1]$ with $u^\mu = \gamma(1, \vec{v})$. The energy momentum tensor can be obtained from f [9] as

$$T^{\mu\nu}(x) = \int d^3p \frac{p^\mu p^\nu}{p^0} f(\vec{x}, \vec{p}, t), \quad (2)$$

fluctuation of hydrodynamic quantities can be obtained from δf .

Evolution equation: The evolution of δf in an expanding background can be calculated by using Eq. 1. In relaxation time approximation(RTA) Eq. 1 reads:

$$\left(\frac{\partial}{\partial t} + \frac{\vec{p}}{p^0} \cdot \frac{\partial}{\partial \vec{x}} + \frac{(p^0 u_0 - \vec{p} \cdot \vec{u})}{p^0 \tau_R(x)} \right) \delta f(x, p) = - \left(\frac{\partial}{\partial t} + \frac{\vec{p}}{p^0} \cdot \frac{\partial}{\partial \vec{x}} \right) f_0(x, p) \quad (3)$$

where τ_R is the relaxation time.

In RTA, i.e. when $C[f] = -(f - f_0)/\tau_R(x)$ we get the solution [10] of Eq. 3 as:

$$\delta f(\vec{x}, \vec{p}, t) = D(t, t_0) \left[\delta f_{in}(\vec{p}, \vec{x} - \frac{\vec{p}}{p^0}(t - t_0)) + \int_{t_0}^t B(\vec{x} - \frac{\vec{p}}{p^0}(t - t'), t') D(t_0, t') dt' \right] \quad (4)$$

where

$$D(t_2, t_1) = \exp \left[- \int_{t_1}^{t_2} dt' A(p, \vec{x} - \frac{\vec{p}}{p^0}(t' - t_0), t') \right]$$

with

$$A(p, \vec{x}, t) = \frac{p^0 u_0(x) - \vec{p} \cdot \vec{u}(x)}{p^0 \tau_R(x)}$$

and

$$B(\vec{x}, t) = - \left(\frac{\partial}{\partial t} + \frac{\vec{p}}{p^0} \cdot \frac{\partial}{\partial \vec{x}} \right) f_0(x, p).$$

This δf can be used to estimate fluctuation in various thermodynamic quantities due to perturbation.

For static QGP medium, spatial component flow velocity is zero in local rest frame and temperature is independent of space-time, with $\delta f = f_0 \psi$, for massless particles the solution of BTE (Eq. 4) reduces to

$$\Psi(\vec{x}, \vec{p}, t - t_0) = \Psi_{in} \left(\left(\vec{x} - \frac{\vec{p}}{p_0}(t - t_0) \right), \vec{p} \right) \exp \left[-\frac{(t - t_0)}{\tau_R} \right]. \quad (5)$$

2.1 Hydrodynamically expanding background

QGP produced in RHIC-E in local equilibrium expands hydrodynamically due to high internal pressure into the vacuum surrounding it. The expansion of the QGP in space and time can be studied by using relativistic hydrodynamics. The conservation of energy and momentum of the fluid is governed by the equation:

$$\partial_\mu T^{\mu\nu} = 0 \quad (6)$$

where $T^{\mu\nu} = (\epsilon + P)u^\mu u^\nu - g^{\mu\nu}P$, where ϵ is the energy density, P is the pressure. The conservation of the net baryon number throughout the evolution history is controlled by the equation:

$$\partial_\mu (n_B u^\mu) = 0 \quad (7)$$

where n_B is the net baryon (baryon - antibaryon) density. In the present work we are interested in the system produced in nuclear collisions at the highest RHIC energies where n_B is negligibly small (n_B will be even smaller at LHC collision conditions) and hence $\mu_B \sim 0$. Therefore, we do not need to consider Eq. 7. In the present work Eq. 6 has been solved numerically using standard technique [11] in full (3+1) space-time dimension without making assumption on boost invariance along longitudinal direction [12] and cylindrical symmetry of the system.

2.1.1 Initial conditions

The initial conditions required to solve Eq. 6 in (3+1) dimension are as follows: the Cartesian components of initial flow velocities are: $v_x(\tau_0, x, y, z) = v_y(\tau_0, x, y, z) = 0$ and the initial energy density profile is taken as [11]:

$$\varepsilon(\tau_0, x, y, \eta_s) = \varepsilon_{GM}(x, y) \theta(Y_b - |\eta_s|) \exp \left[-\theta(|\eta_s| - \Delta\eta) \frac{(|\eta_s| - \Delta\eta)^2}{\sigma_\eta^2} \right] \quad (8)$$

where $\varepsilon_{GM}(x, y)$ is obtained from optical Glauber (OG) or Monte-Carlo Glauber (MCG) model, having the following expression-

$$\varepsilon_{GM}(x, y) = \varepsilon_0 \left[\frac{1-f}{2} n_{part}(x, y) + f n_{coll}(x, y) \right] \quad (9)$$

where n_{part} is number of participants and n_{coll} number of binary collisions between nucleons in nucleus-nucleus collisions. We have taken the value of the inelastic nucleon-nucleon cross section, $\sigma_{NN} = 42$ mb at RHIC in evaluating the n_{part} and n_{coll} . Gaussian smearing, to get the continuous distribution of energy density, which is required for hydrodynamic evolution, from energy deposition at discrete points in the MCG approach, is used as:

$$\varepsilon_{GM}(x, y) = \frac{1}{2\pi\sigma^2} \sum_i \varepsilon_{GM}(x_i, y_i) e^{-\frac{(x-x_i)^2+(y-y_i)^2}{2\sigma^2}} \quad (10)$$

where $\varepsilon_{GM}(x_i, y_i)$ is obtained from Eq(9). In the following Woods-Saxon distribution have been used to sample the nucleons from nuclei (Au in this case)

$$\rho(r) = \frac{\rho_0}{1 + e^{\frac{r-R}{\delta}}}.$$

Table 1. The values of different parameters appeared in the above expressions are given below:

Parameter	τ_0	Y_b	$\Delta\eta$	σ_η	ε_0	f	σ^2	R	δ	σ_{NN}
Value	0.6 fm/c	5.3	1.3	2.1	7.7 GeV/fm ³	0.14	0.16	6.37	0.535	42 mb

2.1.2 Equation of State (EoS)

The EoS for the QGP and the hadrons have been constructed following the procedure outlined in Ref [13], where, excluded volume model [14] for hot hadrons and pQCD results [15, 16, 13] for the QGP phase is used. For a smooth crossover, a switching function is used as in [13] and the parameters are adjusted so as to match the Lattice QCD results.

EoS for HRG phase: We choose volume of hadrons to be proportional to mass, so that volume of the hadron, $v_i = m_i/m_0$ as in [13], where m_0 is a constant. We take $m_0 = 0.9$ for this work. The

pressure of the hadronic medium is taken to be,

$$p_{HG}(T, \mu_B) = \sum_{i=1} p_i^{id}(T, \tilde{\mu}_i) \quad (11)$$

$$\tilde{\mu}_i = \mu_i - v_i p_{HG} \quad (12)$$

where $\mu_i = B\mu_B$, and B is baryon number. p_i^{id} denotes the ideal pressure of a relativistic gas comprised of i^{th} resonance and p_{HG} is the pressure after excluded volume correction is taken into account which is found by solving the above set of equations in a self-consistent way.

EoS QGP phase: The pressure of the QGP phase is taken as

$$P = \frac{8\pi^2}{45} T^4 \left[f_0 + \left(\frac{\alpha_s}{\pi}\right) f_2 + \left(\frac{\alpha_s}{\pi}\right)^{3/2} f_3 + \left(\frac{\alpha_s}{\pi}\right)^2 f_4 + \left(\frac{\alpha_s}{\pi}\right)^{5/2} f_5 + \left(\frac{\alpha_s}{\pi}\right)^3 f_6 \right] \quad (13)$$

where the coefficients f_n 's are given in [17]. The coupling, α_s has been taken from [18] calculated in three loop approximations.

$T, \mu(\equiv \mu_B)$ **dependent switching and combined EoS:** The pressure in the crossover region is taken to be

$$P(T, \mu) = S(T, \mu) P_{qgp}(T, \mu) + (1 - S(T, \mu)) P_h(T, \mu) \quad (14)$$

where the switching function $S(T, \mu)$ is taken as

$$S(T, \mu) = \exp\{-\theta(T, \mu)\} \quad (15)$$

$$\theta(T, \mu) = \left[\left(\frac{T}{T_0}\right)^r + \left(\frac{\mu}{\mu_0}\right)^r \right]^{-1} \quad (16)$$

We take $T_0 = 165$ MeV, $\mu_0 = 3\pi T_0$ and $r = 4$. These parameter values are taken to have a good agreement of our results with the lattice data [19].

2.1.3 Initial anisotropic perturbation

To simulate initial spatial anisotropy of fluctuation with different geometrical shape, we choose,

$$\delta f(p, \vec{x}, t_0) = A_0 \exp[-r(1 + a_n \cos n\theta)] \quad (17)$$

We have taken $n = 2, 3, 4, 5, \dots$ to simulate different initial anisotropy and $r = |\vec{x}|$. From this solution in coordinate space one can get various modes of fluctuations using Fourier Transformation which

will give evolution of different Fourier modes of fluctuations. We take $a_n = 0.3$ for $n = 2, 3, 4, 5$. For numerical results discussed below to see how much of initial perturbation survives over time, for comparison of initial to final value, A_0 is set to unity.

To investigate effect of such perturbation on momentum anisotropy of particles emitted from constant temperature surfaces of the evolving QGP fluid, we take δf_{in} with, A_0 not set to unity, rather

$$A_0 = K \frac{C}{(1 + p_T/B)^\beta}$$

where, $C = 9.113 \times 10^{-4}(1/MeV^2)$; $B = 1459MeV$ and $\beta = 7.7$, and K is chosen to be $K = 3.6$ so that energy density carried by the perturbation($\delta\epsilon$) is such that, $\delta\epsilon/\epsilon \sim 0.01$ (results with other values of $\delta\epsilon/\epsilon$ will also be shown). This condition ensures negligible back reaction on background from the perturbations. This power law form of momentum dependence of perturbation, which is inspired by jet parton distribution, also ensures non-equilibrium nature of this perturbation. It also ensures the condition $\delta f/f_0 \ll 1$.

2.2 Results on the evolution of perturbation

The BTE has been solved in RTA and the solution has been used to estimate the time variation of perturbation in energy density ($\Delta = \delta\epsilon/\epsilon$). The evolution of Δ in wave vector (\vec{k}) space evolves as [20]:

$$\begin{aligned} \Delta(\vec{k}, t) = & e^{-(t-t_0)/\tau} \left[\Delta(\vec{k}, t_0) \frac{\sin k(t-t_0)}{k(t-t_0)} + \frac{4\chi T(\vec{k}, t_0)}{k s \bar{T}} \{k^2 - ik_l \dot{U}_l(\vec{k}, t_0)\} \left\{ \frac{\cos k(t-t_0)}{k(t-t_0)} - \frac{\sin k(t-t_0)}{k^2(t-t_0)^2} \right\} \right. \\ & \left. + \frac{40\eta \Theta(\vec{k}, t_0)}{3 s \bar{T}} \left\{ \frac{\sin k(t-t_0)}{k(t-t_0)} + \frac{3 \cos k(t-t_0)}{k^2(t-t_0)^2} - \frac{3 \sin k(t-t_0)}{k^3(t-t_0)^3} \right\} \right]. \end{aligned} \quad (18)$$

Eq. 18 provides the connection of the fluctuation in energy density in k- space with various transport coefficients *e.g.* thermal conductivity (χ) and viscosity (η).

The spatial distribution of $\delta\epsilon/\epsilon$ for various t is depicted in Fig. 1. We observe that the maxima of the perturbation shifts from the origin ($|x| = 0$) to higher x with the progress of time. However, for expanding background, we have seen that the dissipation of fluctuation gets slower. Spatially anisotropic fluctuation breaks as it travels in an expanding QGP background. In the final state the broken parts will be connected through angular correlation. We have investigated angular correlation of pressure fluctuation for such non-equilibrium deviations. The interaction of the perturbation (δf)

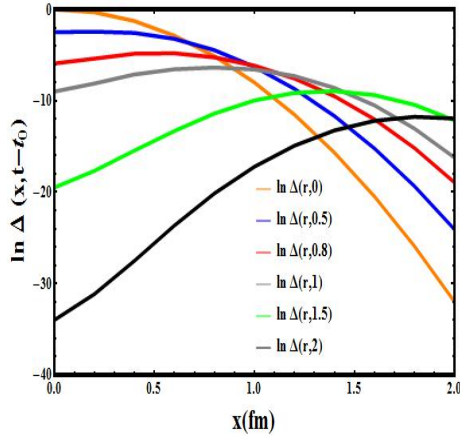


Figure 1: Evolution of the fluctuation in energy density with r coordinate at different t for a non-expanding QGP background.

with the background is incorporated through the relaxation time which is a function of temperature and hence depends on space-time coordinates for an expanding background. Therefore, it is expected that various modes of the perturbations in the Fourier space will get mixed during its propagation over the expanding background as clearly visible in Fig. 2. The peak of the fluctuation in number density ($\delta n/n$) has reduced significantly due the exponential factor determined by the relaxation time.

The dissipation of the perturbation gets slower with the expansion of the system. The effects of perturbation has better chance of survivability along the smaller dimension of the system because the expansion is faster along that direction due to larger pressure gradient. It implies that for systems with same energy density the perturbations has larger chance to survive in smaller system. Then it is expected that the presence of perturbations will be dominant in relatively smaller size systems. Fig 3 shows evolution of elliptic ($n = 2$ in Eq. 17) perturbation on the expanding QGP background, when the perturbation is given at a distance 3 fm from the origin along the x -axis. It is interesting to note that the perturbation which is moving away from the centre dissipates less compared to the one moving toward the centre. Therefore, the possibility of detection of perturbation is more if it is created near the boundary of the system.

3 Power spectrum of fluctuation

Analyzing fluctuations in Fourier modes reveal evolution of different scale, these modes are characterized by their contributions in terms of corresponding coefficients of expansion. Effect of these fluctuations are expected to be reflected in the momentum anisotropy of produced particles from

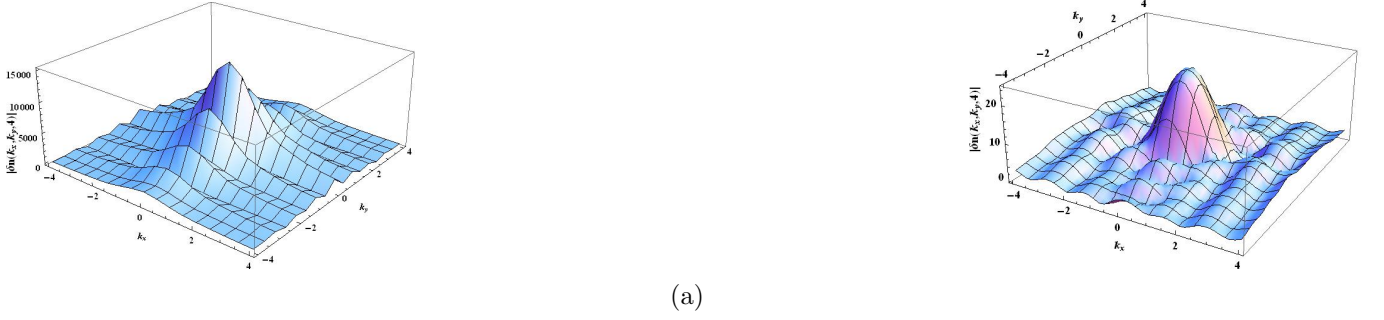


Figure 2: (Left). The fluctuations in k -space at time $\tau = 0.6$ fm/c. Right panel shows the results after a time 4 fm/c has elapsed. The mixing of k -modes is clearly visible.

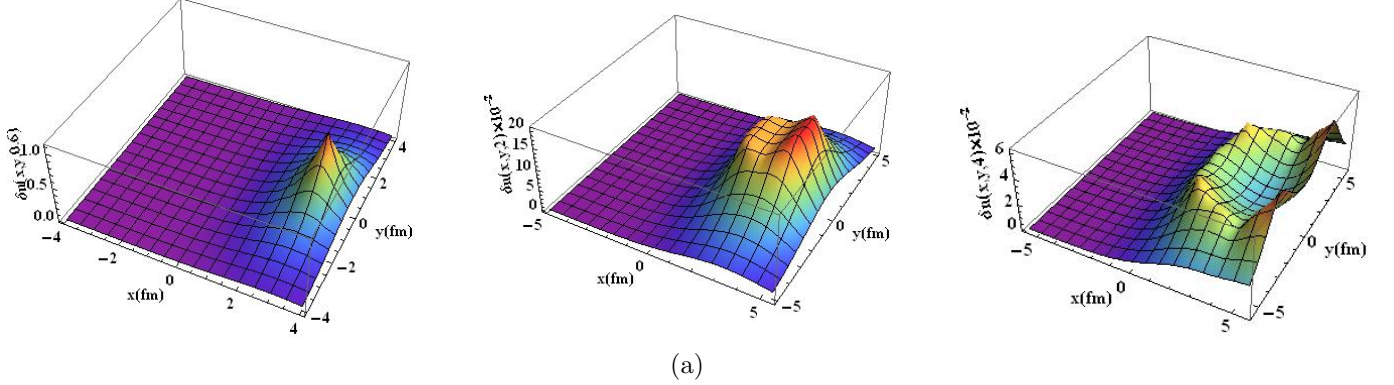


Figure 3: Evolution of the spatial anisotropy of the perturbation with initial elliptic geometry at time $\tau_0 = 0.6$ fm/c (upper panel), given at a distance of 3 fm away from the origin along x -axis. The middle (right) panel shows the results after a time 2 fm/c (4 fm/c) has elapsed.

constant temperature surfaces.

In RHIC-E in parallel to CMBR, we have estimate the power spectrum of the invariant momentum distribution of particles at constant T surfaces. The invariant momentum distribution is given by:

i) without perturbation as:

$$E \frac{dN_0}{d^3p} = \frac{g_i}{(2\pi)^3} \int_{\Sigma} d\sigma_{\mu} p^{\mu} f_0(x, p)$$

and ii) with perturbation

$$E \frac{dN}{d^3p} = \frac{g_i}{(2\pi)^3} \int_{\Sigma} d\sigma_{\mu} p^{\mu} [f_0 + \delta f(x, p)] \quad (19)$$

where, $d\sigma_{\mu}$ is the constant temperature hypersurface. Then, power spectrum can be calculated by expanding it in terms of spherical harmonics, as follows. The power spectrum of $E dN/d^3p$ can be estimated as follows:

$$E \frac{dN}{d^3p} = \bar{N} + \sum_{l=1}^{\infty} \sum_{m=-l}^l a_{lm}(p_T, T) Y_{lm}(\theta, \phi) \quad (20)$$

where

$$\bar{N} = \frac{1}{4\pi} \int d\Omega \frac{dN}{d^2p_T dy} \quad (21)$$

the coefficients, a_{lm} 's are determined as follows:

$$a_{lm}(p_T, T) = \int d\Omega Y_{lm}^* E \frac{dN}{d^3p} \quad (22)$$

For determining power spectrum without perturbation we replace EdN/d^3p by EdN_0/d^3p in Eq. 22.

Using standard techniques and properties of spherical harmonics, the angular power spectrum (C_l) of EdN/d^3p can be expressed as:

$$C_l(p_T, T) = \frac{1}{2l+1} \sum_m |a_{lm}|^2 \quad (23)$$

indicating the distribution of power of fluctuations among different angular scales determined by l .

Results on the power spectrum of the invariant momentum distribution of the particles:

In Fig. 4(a):Left) we have shown the spatial variation of perturbation, δf at initial time. The subsequent evolution of δf is governed by Boltzmann equation in relaxation time ($\tau_R(x)$) approximation. τ_R is a function of $T(x)$. The space-time variation of temperature is governed by relativistic hydrodynamics. Therefore, the evolution of perturbation is coupled to the expanding background through the temperature dependence of relaxation time.

The power spectrum (C_l) of the perturbation is depicted at temperatures 350 MeV and 170 MeV for $p_T = 0.6$ GeV. By performing power spectrum analysis of the momentum anisotropy we observe that the C_l for odd l is negligibly small initially ($T = 350$ MeV) as expected for a perturbation with symmetry under the change $\theta \leftrightarrow -\theta$ 4 implemented through Eq. 17 for $n = 2$. However, as the system cools with the progression of time the C_l for odd l appears but remains smaller than its value at even l .

Next we study the variation of C_l with temperature for different l . We observe that variation of C_l with T is similar with and without perturbation at $p_T = 0.6$ GeV, because the background dominates the evolution at this soft value of momentum. However, the behaviour is very different at $p_T = 3.0$ GeV, because the perturbation dominates the evolutions at such high value of p_T .

The C_l 's (for even l) is plotted in Fig. 4 as a function of T . We observe that for low p_T the variation of C_l with T , with and without perturbation, is qualitatively and quantitatively similar for $p_T = 0.6$ GeV because the perturbation is small. However, the variation is very different with and without perturbation for higher $p_T = 3.0$ GeV. This feature may help in tracing the non-equilibrium

effects in the expanding QGP medium which is produced in the relativistic heavy ion collisions.

4 Estimating bulk viscosity of quark gluon plasma from pressure fluctuations

It is well known that the response of the system to the external perturbation that takes the system away from equilibrium can be quantified through transport co-efficients appropriately. Green Kubo relation expresses this fact, in the domain of linear response. Using correlation of time dependent pressure fluctuation estimated from $\delta f(x, p, t)$. Using Kubo relation we have estimated bulk viscosity(ζ) of QGP, with pressure fluctuation, δP obtained from δf , as [21]

$$\zeta = \frac{V}{T} \int_0^\infty dt \langle \delta P(t) \delta P(0) \rangle.$$

Using quasi particle mass [22] for quarks and gluons we obtained bulk viscosity, where evolution of such pressure fluctuation is obtained from solution $\delta f(x, p, t)$. The temperature variation of ζ/s , where s is the entropy density, is shown the Fig 5. We find that the bulk viscosity of the system is large at low T and it reduces as T increases. It is well known that conformal symmetry breaking which is broken at low T and restored at high T . The variation of ζ/s indicates the restoration of conformal symmetry at high T .

Bulk viscosity of hot and dense hadrons The bulk viscosity of hadronic system has also been estimated by using the fluctuation of thermodynamic pressure. The hadronic resonance gas model along with the Hagedorn density of states have been used to estimate ζ . The expression has for ζ/s has been derived as [23]:

$$\frac{\zeta}{s} = - \left(\frac{\partial P}{\partial n} \right)_\epsilon \left(\frac{\partial n}{\partial s} \right) \tau_{chem}.$$

where, τ_{chem} is the chemical equilibrium time which embodies the microscopic dynamics and for all other variables standard notation has been used. The variation of bulk viscosity to entropy ratio with temperature is shown in Fig 6 [23]. Again we observe that ζ/s is small at high T .

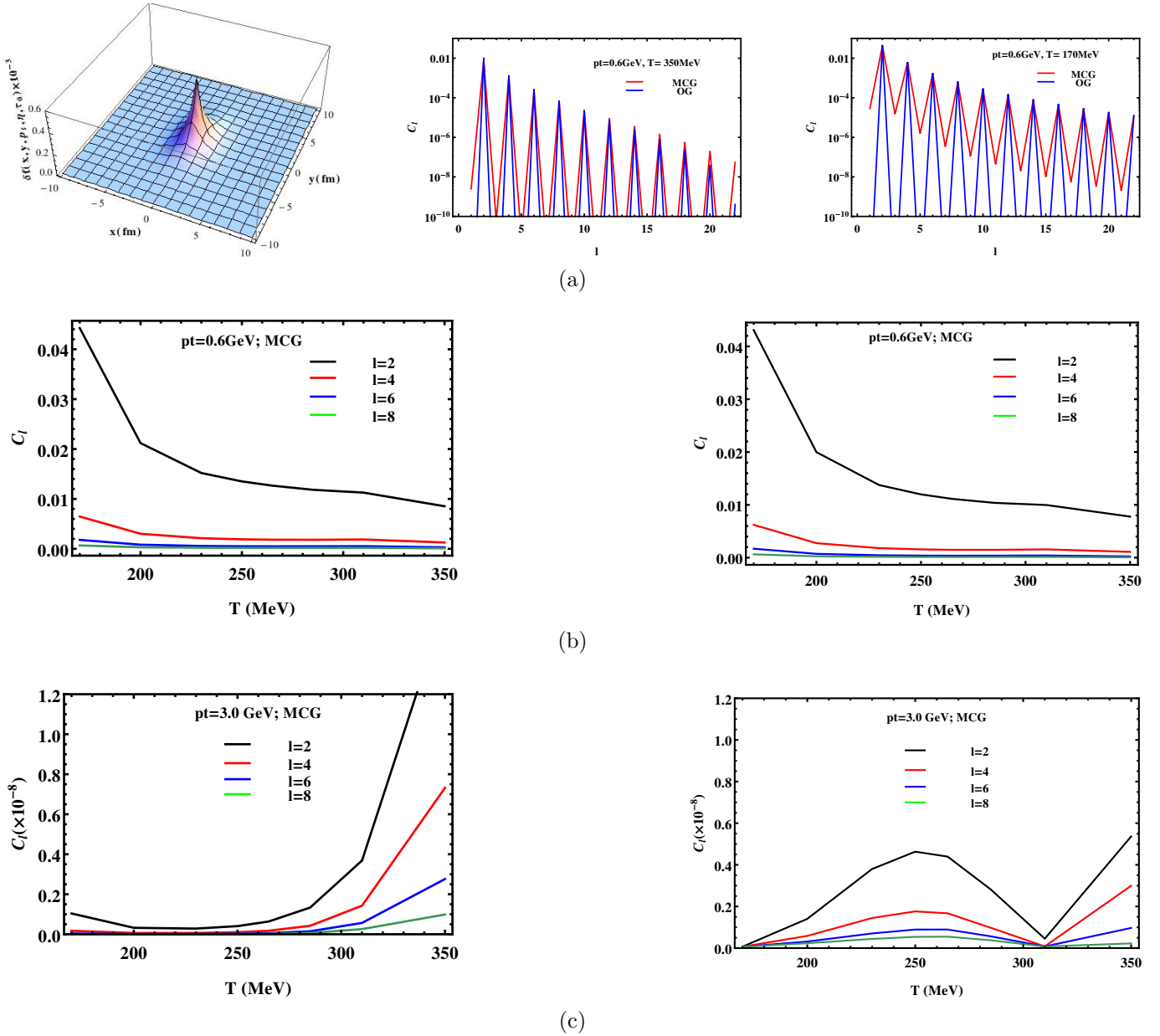


Figure 4: a) Left: The initial perturbation imparted to the expanding QGP. Middle: The power spectrum of the perturbation at $T = 350$ MeV with this perturbation. Right: The power spectrum of the perturbation at $T = 170$ MeV. The red (blue) line shows results for MCG (OG) initial conditions for $p_T = 0.6$ GeV/c . b) The temperature variation of power spectrum with MCG initial condition for different l values. Left panel: without perturbation at $p_T = 0.6$ GeV, Right panel: with perturbation at the same p_T . c) The temperature variation of power spectrum with MCG initial condition for different l values. Left panel: without perturbation at $p_T = 3.0$ GeV, Right panel: with perturbation at the same p_T .

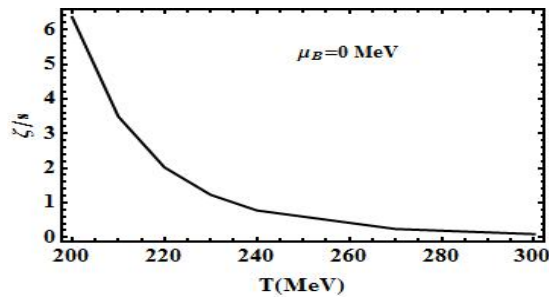


Figure 5: The variation of bulk viscosity to entropy ratio (ζ/s) as a function of temperature.

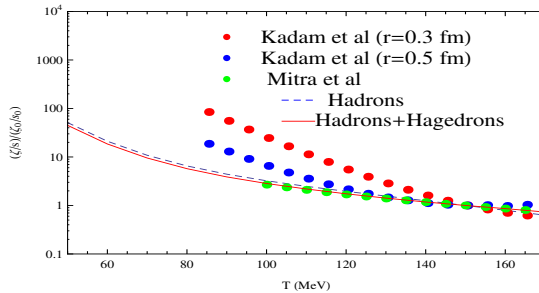


Figure 6: The variation of bulk viscosity to entropy ratio (ζ/s) as a function of temperature. The ratio is normalized at by its value at $T = 150$ MeV.

5 Summary

The evolution of perturbation in relativistic fluid introduced through the phase space distribution function has been studied using Boltzmann transport equation in relaxation time approximation. The perturbation evolves in an expanding background governed by (3+1) dimensional relativistic hydrodynamics. The temperature in turn depends on space-time coordinates of the background. The relaxation time appearing in the solution of the Boltzmann equation is a temperature dependent quantity and this couples the background with the perturbation.

We have derived a relation between the fluctuations in energy density with the transport coefficients, like shear viscosity and thermal conductivity. We have also analyzed and demonstrated how the various Fourier modes of the perturbations get mixed in an expanding background. It is shown that if a perturbation is created near the boundary of the system then it has a better chance of getting detected.

The evolution of the power spectrum of the invariant momentum distribution of particles has been estimated for Optical Glauber as well as Monte-Carlo Glauber initial conditions. The power spectrum of the momentum distribution of the particles due perturbations imparted through the phase space distribution have been evaluated at different surfaces of fixed temperatures. We have studied the variation of C_l with T and found that at high p_T the variation of C_l clearly traces the presence of perturbation.

The solution of the Boltzmann equation obtained here can be used to estimate various other physical quantities. For example, we have used this solution to estimate the fluctuation in pressure and subsequently the bulk viscosity of the QGP with the help of Kubo relation. We find that the bulk viscosity is quite high near the transition temperature (~ 200 MeV).

The bulk viscosity of hadronic system has been calculated by using HRG model and the Hagedorn density of states. The fluctuation in thermodynamic pressure has been used to determine the ζ of

QGP. The ζ/s has been estimated by using HRG model and Hagedorn density of states. The bulk viscosity of hadronic system is found to decrease with temperature. The result obtained here has been compared with other similar results available in the literature.

References

- [1] P. Braun-Munzinger and J. Stachel, *Nature*, **448**, 302 (2007); E. Shuryak *Rev. Mod. Phys.* **89**, 035001 (2017); R. Pasechnik, M. Sumbera *Universe*, **3** (2017), p. 7.
- [2] R. Durrer, *The Cosmic Microwave Background*, Cambridge University Press, 2008.
- [3] M. Gyulassy and L. McLerran, *Nucl. Phys. A* **750**, 30 (2005).
- [4] I. Arsene *et al.* (for BRAHMS collaboration), *Nucl. Phys. A* **757**, 1 (2005).
- [5] K. Adcox *et al.* (for PHENIX collaboration), *Nucl. Phys. A* **757**, 184 (2005).
- [6] B. B. Back *et al.* (for PHOBOS collaboration), *Nucl. Phys. A* **757**, 28 (2005).
- [7] J. Adams *et al.* (for STAR collaboration) *Nucl. Phys. A* **757**, 102 (2005).
- [8] P. Kovtun, D. T. Son and A. O. Starinets, *Phys. Rev. Lett.* **94**, 111601 (2005).
Phys. Rev. C **90**, 034907 (2014).
- [9] S. Weinberg, *Gravitation and Cosmology* (John Wiley & Sons, New York, 1972).
- [10] H. Levine, *Partial Differential Equations*, American Mathematical Society (1997).
- [11] Iu. Karpenko, P. Huovinen, M. Bleicher, *Comp. Phys. Comm.* **185**, 3016 (2014).
- [12] J. D. Bjorken, *Phys. Rev. D* **27**, 140 (1983).
- [13] M. Albright, J. Kapusta and C. Young, *Phys. Rev. C* **56**, 024915 (2014).
- [14] G. D. Yen, M. I. Gorenstein, W. Greiner and S.N. Yang, *Phys. Rev. C* **56** (1997) 2210.
- [15] A. Vuorinen, *Phys. Rev. D* **67**, 074032 (2003); **68**, 054017 (2003).
- [16] N. Haque, M. G. Mustafa and M. Strickland, *Phys. Rev. D* **87**, 105007 (2013).
- [17] G. Sarwar, S. K. Singh and J. Alam, *Int. J. Mod. Phys. A* **33**, 1850121(2018).

- [18] Particle data Group, J. Beringer *et al.*, Phys. Rev. D. **86**, 010001 (2012).
- [19] S. Borsányi *et al.*, Phys. Lett. B 370 (2014) 99-104.
- [20] G. Sarwar, J. Alam, Int. J. Mod. Phys. A **33**, 1850040 (2018).
- [21] H. Okumuraa, F. Yonezawab, Physica A **321** (2003) 207 – 219; J- H. Hansen, I.R. McDonald, Theory of Simple Liquids, Academic Press, London, 1986, p. 253 (Chapter 8).
- [22] M. le Bellac, Thermal Field Theory, Cambridge University Press (1996).
- [23] G.Sarwar, S. Chatterjee and J. Alam, J. Phys. G: Nucl. Part. Phys. **44** 055101 (2017).

Publications in Refereed Journals:

1. “**Calculation of Power Spectrum in the Little Bangs**”,
G. Sarwar, S. K. Singh and J. Alam.
Int. J.M.Phys. A **33**, (2018) 1850121.
2. “**Kinetic evolution and correlation of fluctuations in an expanding quark gluon plasma**”,
G. Sarwar and Jane Alam,
Int. J.M.Phys. A **33**, (2018) 1850040.
3. “**An estimate of the bulk viscosity of the hadronic medium**”,
G. Sarwar, S. Chatterjee and J. Alam,
J. Phys. G **44**, (2017) no.5, 055101

Other Publications:

a. Conference/Symposium

1. “**Temperature fluctuation in quark gluon plasma**”,
G. Sarwar and J. Alam,
DAE Symp. Nucl. Phys. **60**, 718 (2015).

2. "Bulk viscosity of hot and dense hadrons", G. Sarwar, S. Chatterjee and J. Alam.
DAE Symp. Nucl. Phys. **60**, 830 (2015).
3. "Initial Condition Dependence of Hydrodynamic Flow of Quark Gluon Plasma",
Md. Hasanujjaman, S. K. Singh, S. Ghosh, S. Chatterjee, G. Sarwar, J. Alam and S. Sarkar,
DAE Symp. Nucl. Phys. **60**, 808 (2015).

Signature of Student: *Goleam Sarwar*

Date: 28/02/2018

Doctoral Committee:

S. No.	Name	Designation	Signature	Date
1.	Prof. Asis K. Chaudhury	Chairman	<i>A. Chaudhury</i>	28/2/18
2.	Prof. Jan-e Alam	Guide/Convener	<i>Jan-e Alam</i>	28/2/18
3.	Prof. Saurav Sarkar	Member 1	<i>Saurav Sarkar</i>	28/2/18
4.	Prof. Sanjay Ghosh	Member 2	<i>Sanjay Ghosh</i>	28/2/18

List of Figures

1.1	Energy density as a function of temperature scaled by the critical temperature T_c taken from Ref. [12].	3
1.2	Illustration a typical non-central heavy-ion collision in which the eccentric shape of initial collision geometry is translated into the elliptic flow anisotropy in the final state momentum space, taken from Ref. [19]	4
1.3	Illustration of different dynamical evolution stages in a typical heavy-ion collision. taken from Ref. [19]	5
1.4	The space-time evolution of heavy-ion collision. The figure is taken from Ref. [59]	5
4.1	Evolution of the fluctuation in energy density with r at different t for a non-expanding QGP background.	39

4.2	Evolution of the spatial anisotropy of the perturbation with initial elliptic geometry at time $\tau_0 = 0.6$ fm/c (upper panel). The lower panel shows the geometry after a time 4 fm/c has elapsed. Hydrodynamic expansion of the QGP background has been taken into account. The boundary of the background has an elliptic shape with the dimension of major and minor axes are approximately 6 fm and 4 fm respectively. The colors from red to violet represent highest to lowest values of the perturbations.	39
4.3	Same as Fig. 4.2 but the spatial anisotropy has a triangular geometry at the initial time $\tau_0 = 0.6$ fm/c (upper panel). The lower panel shows the perturbation after a time 4 fm/c has elapsed.	40
4.4	Same as Fig. 4.2 but the spatial anisotropy has a quadrangular geometry at the initial time $\tau_0 = 0.6$ fm/c (upper panel). The lower panel shows the geometry after a time 4 fm/c has elapsed.	41
4.5	Same as Fig. 4.2 but the spatial anisotropy has a pentagonal geometry at the initial time $\tau_0 = 0.6$ fm/c (upper panel). The lower panel shows the results after a time 4 fm/c has elapsed.	42
4.6	Same as Fig. 4.2 but the spatial anisotropy has a hendecagonal geometry ($n = 11$) at the initial time $\tau_0 = 0.6$ fm/c (upper panel). The lower panel shows the results after a time 4 fm/c has elapsed.	43
4.7	Same as Fig. 4.6 but the perturbation is given at a distance of 2.5 fm away from the origin along x -axis. The lower panel shows the results after a time 4 fm/c has elapsed.	47
4.8	Same as Fig. 4.2 but the perturbation is given at a distance of 3 fm away from the origin along x -axis. The middle (lower) panel shows the results after a time 2 fm/c (4 fm/c) has elapsed.	48

4.9	(upper panel). The fluctuations in k -space at time $\tau = 0.6$ fm/c (upper panel). The lower panel shows the results after a time 4 fm/c has elapsed. The mixing of k -modes is visible in the lower panel. . . .	50
5.1	Initial energy density profile in the transverse plane at space time rapidity = 0 in the OG model for Au+Au central collision.	65
5.2	The constant temperature, $T = 350$ MeV surface in the time-transverse plane.	67
5.3	The constant temperature surface in the time-transverse plane for 170 MeV.	67
5.4	Same as Fig. 4.2 with MCG initial condition for a single event. . . .	68
5.5	Same as Fig. 5.1 with MCG initial condition averaged over 100 events. . . .	69
5.6	The constant temperature surface at $T = 350$ MeV for MCG initial condition.	71
5.7	Same as Fig. 5.6 for MCG initial condition at $T = 250$ MeV.	72
5.8	Same as Fig. 5.6 at $T = 170$ MeV.	72
5.9	The pseudo-rapidity (η) and angular (θ) distribution of particles at $p_T = 0.6$ GeV with OG and MCG initial conditions at $T = 350$ MeV.	73
5.10	Same as Fig. 5.9 at $T = 170$ MeV.	74
5.11	The power spectrum, C_l deduced from $dN/d^2p_T dy$ at $p_T = 0.6$ GeV for both the OG and MCG initial conditions analyzed at the surface of $T = 350$ MeV.	75
5.12	Same as Fig. 5.11 at $T = 250$ MeV.	75
5.13	Same as Fig. 5.11 at $T = 170$ MeV.	76

5.14	The initial perturbation δf given in Eq. 5.12 with $n = 2$ for $p_T = 1$ GeV at $\eta = 0$	76
5.15	The power spectrum of the perturbation at $T = 350$ MeV for perturbation shown in Fig 5.13. The red (black) line shows results for OG (MCG) initial conditions for $p_T = 0.6$ GeV/ c	77
5.16	Same as Fig 5.15 at $T = 250$ MeV	78
5.17	Same as Fig. 5.15 at $T = 170$ MeV.	79
5.18	Same as Fig 5.15 for $p_T = 1.5$ GeV/ c	80
5.19	Same as Fig 5.16 at $T = 170$ MeV	80
5.20	Same as Fig 5.17 for $p_T = 1.5$ GeV/ c	81
5.21	The temperature variation of power spectrum with OG initial condition for different l values.	83
5.22	The variation of power spectrum for even l with temperature for MCG initial condition.	84
5.23	The variation of power spectrum for odd l with temperature for MCG initial condition.	84
5.24	The variation of power spectrum with temperature for OG initial condition with perturbation at $p_T = 0.6$ GeV/ c (see text for details).	85
5.25	The variation of power spectrum of even l with temperature for MCG initial condition with perturbation at $p_T = 0.6$ GeV/ c (see text for details).	85
5.26	Same as Fig 5.22 for $p_T = 3$ GeV/ c (without perturbation).	86
5.27	Same as Fig 5.25 for $p_T = 3$ GeV/ c (with perturbation $\delta\epsilon/\epsilon \sim 0.01$).	86

5.28	Same as Fig 5.27 for $p_T = 3$ GeV/ c , but the perturbation δf , corresponds to $\delta\epsilon/\epsilon \sim 0.3$	87
6.1	The angular auto-correlation of pressure is shown at $r = 3$ fm as a function of $\Delta\phi$. The $\Delta\phi$ variation of $C_{\delta P}$ is displayed at different times such as 0.6 fm/ c (blue) 1 fm/ c (orange), 2.5 fm/ c (green), 3.5 fm/ c (red) and 4 fm/ c (black line).	92
6.2	The variation of bulk viscosity to entropy ratio (ζ/s) as a function of temperature.	93
6.3	Variation of $(\epsilon - 3P)/T^4$ with T/m_l for different values of the ratio of the masses of the heavy to light particle, m_h/m_l for vanishing chemical potential.	97
6.4	Variation of the square of the speed of sound with T for zero and non-zero net baryon density.	98
6.5	Variation of ζ/s with T/m_l for different values of the ratio of the masses of the heavy to light particle, m_h/m_l for vanishing chemical potential.	98
6.6	The temperature variation of $\zeta(T)/\zeta_0$ is shown here with $\zeta_0 = \zeta(T = 150)$ MeV.	103
6.7	Depicts the temperature variation of the bulk viscosity to entropy density ratio normalized to the value of the ratio at $T = 150$ MeV (see text) with constant relaxation time.	104

6.8	Variation of R_ζ (see text) as a function of T for hadronic resonances upto mass 2.5 GeV with (red line) and without (blue dashed line) HDS including T dependent relaxation time estimated by using Eq. 6.15. We have also displayed the same quantity as obtained in other works [170, 172].	104
6.9	The variation $(\epsilon - 3P)/T^4$ with T/m_π with (solid line) and without (dashed line) HDS. A comparison has been made with continuum extrapolated (2+1) lattice QCD data with physical quark masses [194].	105
6.10	The variation of bulk viscosity to entropy density ratio (normalized at $T = 150$ MeV) with temperature along constant S/N_B contours for $S/N_B = 30, 45$ and 300	107
6.11	The variation of R_ζ as a function of $\sqrt{s_{NN}}$ with (red line) and without (blue line) HDS.	107

List of Tables

5.1	Table 5.1: Values of different parameters used in solving the hydrodynamical equations (see text for details).	59
-----	--	----

CHAPTER 1

Introduction

The heart of matter, the nucleus of atoms are made up of neutron and protons. However, neutrons and protons are not fundamental particles, they are composed of quarks [1–3]. The dynamics of quarks are governed by Quantum Chromodynamics (QCD), which is a non-abelian $SU(3)$ gauge theory [4–6]. The interaction between quarks are mediated by gluons. Quarks carry fractional electric charge as well as a new quantum number called color charge. There are six quarks named as up, down, charm, strange, beauty and top- called quark flavors. Each quark flavor carries three color charges called red, blue and green. The $SU(3)$ gauge theory admits eight colors for gluons.

The three quark bound state (like proton and neutron) are called baryons and quark-anti-quark bound states are called mesons. Mesons and baryons are combinedly called hadrons. The QCD is firmly established as theory of strong interaction. Two of the very important properties of QCD are:

(i) Asymptotic freedom which means that at very high energy the color coupling becomes weak i.e., at very high energy or at short distance the strength of interaction between quarks are small. The coupling strength, $\alpha_s = g^2/(4\pi)$ varies with square of the momentum transfer(Q^2) as:

$$\alpha_s(Q^2) = \frac{12\pi}{(33 - 2N_f)} \ln \frac{Q^2}{\Lambda_{QCD}^2},$$

where N_f is the number of flavor.

(ii) Quark confinement or infrared slavery -the quarks are permanently confined within hadrons. At the low momentum, corresponding to the characteristic scale of bound quarks in hadrons, the coupling strength becomes very large i.e. at the characteristic length scale of dimension of hadrons the interaction strength is very high and hence the quarks remain bound within the hadronic size.

The question one may ask is: whether one can create a situation where quarks are not bound within the hadronic size. According to the big bang model of cosmology such a situation prevailed when the universe was a few microsecond old.

Just after the discovery of the asymptotic freedom in non-abelian gauge theory [7–10] Collins and Perry [11] showed that at very high density the properties of nuclear matter is governed by its fundamental degrees of freedom i.e., by quarks and gluons and not by hadrons. Subsequently calculations based on lattice QCD (Fig. 1.1) showed that at high temperature ($\sim 170\text{MeV}$) hadronic matter goes a phase transition from hadrons to quarks and gluons [12, 13]. At high temperature and density the nuclear matter will melt down to quarks and gluons, that is to say that at high temperature and/or density the quarks will not be confined within the hadronic size but move in a larger volume [14]. Therefore, the question is whether in the laboratory we can create a thermalized state of quarks and gluons called Quark Gluon Plasma(QGP) that prevailed in the microsecond old universe.

It is expected that QGP may be produced by colliding nuclei at relativistic energies i.e., at energies of Relativistic Heavy Ion Collider (RHIC) and Large Hadron Collider (LHC).

The main aim of heavy ion programs at RHIC and LHC is to create quark gluon

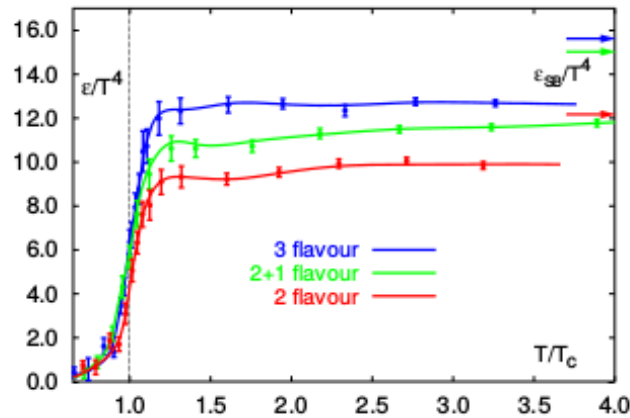


Figure 1.1: Energy density as a function of temperature scaled by the critical temperature T_c taken from Ref. [12].

plasma, a state of matter that might have existed in the micro-second old universe.

One of the compulsion to study the QCD phase transition is to understand the non-abelian gauge theory in medium and to understand the dynamics of similar transition in the early universe. This is especially important because the universe has undergone several other transitions *e.g.* Electroweak, GUT, etc, but among these the QCD transition is the only one which is accessible through the presently available accelerator energy. The QGP may have existed in the micro-second old universe [15] and may exist in the core of neutron star [16], implying that the study of QGP is crucial in understanding the early universe and compact astrophysical objects like neutron stars also.

In colliding experiments two relativistically contracted heavy ions are made to collide (Fig. 1.2) to produce a hot and dense system of quark gluon plasma which subsequently revert to hadrons. The hot and dense system produced in these collisions will have very small life time $\sim 10 fm/c$ and volume $\sim O(100 fm^3)$ (which can be estimated from HBT interferometry [17]). As a consequence it is not possible to use direct probe to characterize the system produced in such collisions. Therefore, particles (hadrons, leptons, photons) produced in the collision through various interactions are detected at various kinematic regions [18] to predict the properties of

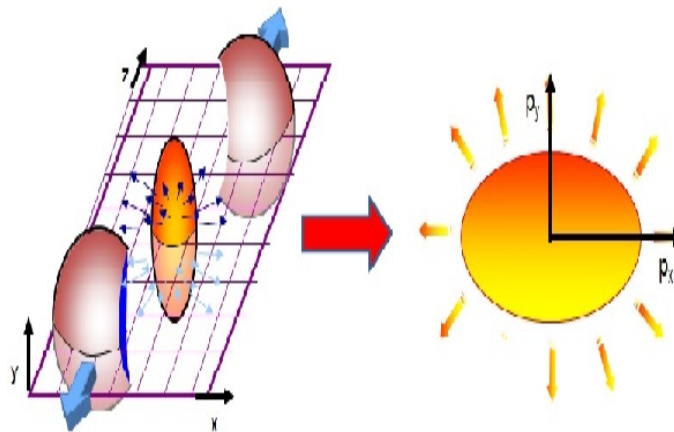


Figure 1.2: Illustration a typical non-central heavy-ion collision in which the eccentric shape of initial collision geometry is translated into the elliptic flow anisotropy in the final state momentum space, taken from Ref. [19]

the system.

Some of the well-known signals proposed as the signature of QGP formation in the nuclear collisions at high energies are: J/ψ suppression [20–23], thermal photon and leptons [24–27], thermal distribution of hadrons [28], jet quenching [29–32], azimuthal anisotropy [33–49] strangeness enhancement [50–54], fluctuation in charged particle ratio [55, 56], heavy quark anisotropic co-efficient [57], etc.

1.1 Collision of heavy ions at relativistic energies:

The over all picture (Fig. 1.3) of the collision emerge as follows [57, 58]:

Two Lorentz contracted nuclei moving with high energy collide to create a system of quarks and gluons- generated from the nucleons of the colliding nuclei. A part of the kinetic energy of the partons (quarks and gluons) of the colliding nucleons get converted to thermal energy through random collisions- creating a thermal system of quarks and gluons [60]. This hot system of quarks and gluons or QGP expands against vacuum due to high internal pressure. The expansion of this system is described by relativistic hydrodynamics. This is demonstrated in Fig 1.4. The two

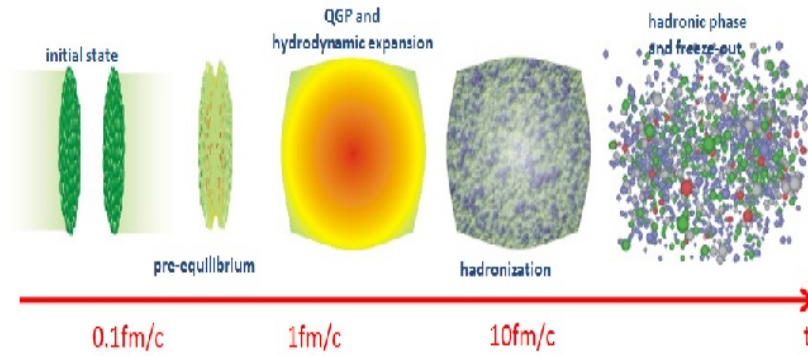


Figure 1.3: Illustration of different dynamical evolution stages in a typical heavy-ion collision. taken from Ref. [19]

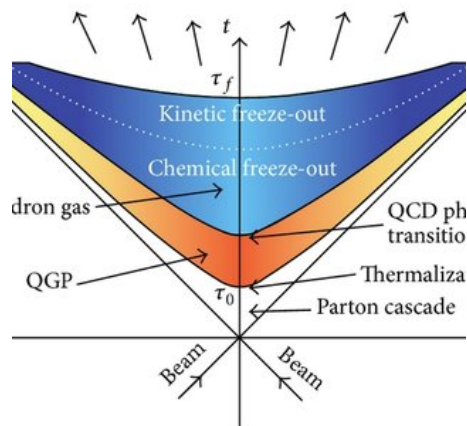


Figure 1.4: The space-time evolution of heavy-ion collision. The figure is taken from Ref. [59]

nuclei collide at the origin and subsequently the thermalized system is formed at a proper time $\tau = \tau_0$ (where $\tau = \sqrt{t^2 - z^2}$)¹. The system expands and consequently cooled down to a temperature $T = T_c$, where T_c is the transition temperature for QGP to hadronic phase. That is at $T = T_c$ the system reverts to hadronic system. The resulting hadronic matter keeps on expanding and cools as long as they can maintain equilibrium through interaction. The hadrons maintain chemical and kinetic equilibrium through inelastic and elastic interaction among them. The evolution point at which the in-elastic interaction ceases the number of hadronic species get fixed is called chemical freeze-out [61]. Once the mean free path of the hadrons becomes comparable to the dimensions of the system or their inelastic as well as elastic scattering rate becomes less than their expansion rate, the hadrons decouple and hit the detector with the momentum that it had after the last scattering. The temperature of the system at which the freeze-out occurs is called the freeze-out temperature (T_f).

1.2 Fluctuations and perturbations in QGP

The initial energy density used as input to the hydrodynamical equations governs the nature of the solution of hydrodynamic equations. For example a fluctuating initial energy density will subsequently give rise to fluctuation in hydrodynamic quantities like, number density, pressure, energy density, etc. However, with the propagation of time the fluctuations may dissipate. Measurement of some observable like elliptic flow, triangular flow, etc of hadrons or of some penetrating probes (like photons and dileptons) may help in understanding such fluctuations. In the present work the power spectrum with initial state fluctuation has been estimated and compared with the power spectrum originating from a smooth initial condition. The fluctuating

¹One makes a coordinate transformation from (t, z) to (τ, η) , where $\tau = \sqrt{t^2 - z^2}$ and $\eta = \frac{1}{2} \ln \frac{t+z}{t-z}$. τ is called proper time and η is called space-time rapidity.

initial energy density has been calculated using Monte-Carlo Glauber model and the smooth one has been calculated using Optical Glauber model.

In RHIC-E perturbation in the hydrodynamic medium may be caused by external agencies like propagation of energetic jets through medium. How will this perturbation evolve in an expanding background controlled by hydrodynamics with fluctuating and smooth initial conditions [62,63]. Such theoretical studies have also been performed in the present dissertation.

The deviation of the system from equilibrium may be treated as response of the system to external perturbation, or the external perturbation shifts the system away from equilibrium. Such shift may be accounted for through the shift (δf) in the equilibrium phase space distribution (f_0). The evolution of δf can be studied by solving Boltzmann transport equation in an expanding background, which has been done here. The power spectrum due to external perturbation has been calculated with fluctuating as well as smooth hydrodynamic background.

It has been shown theoretically that the variation of the power spectrum with temperature in an appropriate momentum window can be used to trace the presence of non-equilibrium process in the system. Fluctuation in pressure has been used to estimate the bulk viscosity of QGP. For comparison, the bulk viscosity of hadronic system has also been estimated using hadronic resonance gas model including Hagedorn density of state.

1.3 Organization of thesis

In the next chapter, basics of hydrodynamics and kinetic theory are briefly discussed. In chapter 3 kinetic evolution of perturbations both for static and relativistic hydrodynamically expanding background is presented. Results for kinetic evolution of anisotropic perturbation with different geometric shape are presented

in chapter 4. In chapter 5 we discuss the evolution of power spectrum of momentum anisotropy of particles in the QGP phase due to non-equilibrium perturbations and initial state inhomogeneity. We present, in chapter 6, an estimation of contribution of phase space to the bulk viscosity of hadron resonance gas using fluctuation in number density and also estimation of bulk viscosity of QGP phase using correlation of pressure fluctuation, which is calculated using kinetic evolution, discussed in chapter 3. We dedicate chapter 7 for summary and outlook. In the appendix we keep some calculations related to previous chapters. We present details derivation of correlation of fluctuation (appendix A), parameterization of equation of state, connection between power spectrum and various flow harmonics (appendix B) and various thermodynamic relations (appendix C) used in estimating the bulk viscosity of hadronic matter in the appendices.

CHAPTER 2

Theoretical Tool for Studying Fluids

2.1 Hydrodynamics: Basics

The collective behavior of the QGP produced in RHIC-E can be studied by using relativistic hydrodynamics. In hydrodynamic description [64,65], fluid is modeled as collection of fluid cells in spatial dimensions [66]. The fluid is characterized by fields of quantities related to fluid cells (fluid particles). These fields are defined over such space time points that a fluid cell is considered to be a point in this hydrodynamic description. The field variables are local thermodynamic quantities and velocities of the fluid cells.

These cells are defined in a manner that they contain many constituent particles. The size of the cell is much larger than the mean free path of the particles, which are the degree of freedom of the fluid. But the size of the cell is smaller than the size of the system. The fields that characterizes the cells, are four velocity($u^\mu(x)$) energy density ($\epsilon(x)$) and conserved charge densities, where $x = (t, \vec{x})$.

2.1.1 Evolution of fluid:

In this description, fluid is characterized by hydrodynamic fields. Therefore, the space time evolution of the fluid, is expressed in terms of evolution of these hydrodynamic fields.

The evolution equations for fields are obtained from conservation equations of quantities that remain conserved during such evolution. To do that conserved quantities are expressed in terms of such fields. If there are extra conditions (e.g., second law of thermodynamics) to be fulfilled during evolution, the corresponding expressions are devised suitably to comply with that.

Here, one gets evolution equations for velocity, temperature, chemical potential (or any thermodynamic quantity) fields, namely, from conservation of energy momentum (symmetric) tensor($T^{\mu\nu}(x)$) and current of conserved charges($J_Q^\mu(x)$). For that these conserved currents($T^{\mu\nu}(x)$ and $J_Q^\mu(x)$) are expressed in terms of quantities (fields) of these fluid cells. While forming the expressions, it is done in such a way that the conservation equations become consistent with laws of thermodynamics and thermodynamic conditions on the system. In this regard, covariant form of thermodynamic laws are used, where fluid cell velocity are explicitly included, and four currents corresponding to thermodynamic quantities are introduced.

The hydrodynamic evolution equation is described by the conservation of energy momentum and conserved charges:

$$\partial_\mu T^{\mu\nu} = 0 \tag{2.1}$$

and

$$\partial_\mu J_Q^\mu = 0, \tag{2.2}$$

where,

$$T^{\mu\nu}(x) = \epsilon(x)u^\mu(x)u^\nu(x) + P(x)\Delta^{\mu\nu}(x) \quad (2.3)$$

is the energy momentum tensor for ideal (non-dissipative) fluids; where $\Delta^{\mu\nu} = g^{\mu\nu} + u^\nu u^\mu$ is the projection transverse to fluid four velocity u^μ , with $u_\mu u^\mu = -1$ and $g^{\mu\nu} = \text{diag}(-1, 1, 1, 1)$, $\epsilon(x)$ and $P(x)$ are respectively energy density and pressure measured in rest frame of the fluid.

The current corresponding to the conserved quantity Q (e.g. net baryon number, net electric charge, strange number etc.) for a relativistic system is defined as

$$J_Q^\mu(x) = n_Q(x)u^\mu(x). \quad (2.4)$$

With these forms along and with thermodynamic [67] relations the isentropic condition is reproduced as conservation of entropy current, $\partial_\mu(s(x)u^\mu) = 0$, where $s(x)$ is the entropy density of the fluid cell.

For a dissipative system energy momentum tensor is given by [68]

$$T^{\mu\nu}(x) = \mathcal{E}(x)u^\mu(x)u^\nu(x) + \mathcal{P}(x)\Delta^{\mu\nu}(x) + (q^\mu u^\nu + q^\nu u^\mu) + \Sigma^{\mu\nu} = T_{ideal}^{\mu\nu}(x) + \Delta T^{\mu\nu}(x), \quad (2.5)$$

where $\Delta T^{\mu\nu}$ represents the dissipative part, and the conserved current is given by

$$J^\mu = \mathcal{N}_Q u^\mu + j^\mu, \quad (2.6)$$

where q^μ , $\Sigma^{\mu\nu}$ and j^μ are transverse to u^μ , and $\mathcal{E}(x) = \epsilon(x) + \delta\epsilon(x)$, $\mathcal{P}(x) = P(x) + \delta P(x)$, $\mathcal{N}_Q = n_Q(x) + \delta n_Q(x)$; $\epsilon(x), P(x)$ and $n_Q(x)$ follows equilibrium equation of state. Detail form of components of this form of energy momentum tensor are chosen by the condition that conservation equations with them, along with second law of

thermodynamics produces the the entropy generation condition $\partial_\mu(s(x)u^\mu(x)) \geq 0$ [65]. Problem of causality and instability in the solutions of conservation equations are two things that are also kept into consideration while getting form of q^μ and $\Sigma^{\mu\nu}$. If they are expressed in terms of first order gradients of these fields times dissipative coefficient, then within the ambit of linear response theory, correlations of them gives dissipative quantities.

In the present work we consider the expanding background as an ideal fluid of QGP. The equation of state(EoS) required to solve hydrodynamic equations for QGP and late hadrons are mentioned latter. The initial condition used in the current work too to be mentioned later.

2.1.2 Hydrodynamic evolution of perturbations

Evolution of hydrodynamic perturbation can be studied in this framework. For that perturbations should be chosen as deviation from the average local equilibrium value. Then propagation of such hydrodynamic perturbations can be studied within the ambit of hydrodynamics, whether it is noise or single perturbation at a point. Due to inherent defining property of hydrodynamics, this will address only slower or longer modes of fluctuations and perturbations present in the medium.

To study scales of shorter modes within hydrodynamic framework one use higher order hydrodynamics [69]. But there is break down problem of second order viscous hydrodynamics [70], corresponding limits have been investigated in [71].

Evolution of these perturbation of hydrodynamic scales can be studied using the conservation equations Eq. 2.1 and Eq. 2.2 where field quantities are to be written including their perturbations.

.

If there is external source that drives the evolution then that comes in the equations

as $\partial_\mu T^{\mu\nu} = S^\nu$ and $\partial_\mu J_Q^\mu = s_Q$, where S^ν is source for supplying energy momentum to the medium cells, and s_Q is source representing extra conserved charge put in the medium during its evolution.

Thermal noise type source can also create fluctuations in the system. In case of studying evolution of hydrodynamic fluctuations one can choose S^μ to represent hydrodynamic noise having form $S^\mu = \partial_\nu \Delta T_{noise}^{\mu\nu}$ [62]. The source of such perturbation, for QGP medium created in RHIC-E, can also be due to energy momentum deposited in the medium by propagating heavy quarks and jets. Corresponding equations involves evolution of background and evolution of perturbations.

2.1.3 Closer condition for hydrodynamic solution and propagation of sound:

In general, for solutions of the conservation equations Eqs. 2.1 and 2.2 extra conditions relating components of conserved currents are required to close the equations. For fluids one of such condition is equation of state which represents relation between different thermodynamic quantities.

Usually for the evolution of QGP one supplies equation state from lattice QCD calculations. Propagation of fluctuations is coupled to the hydrodynamic background through relaxation time. Propagation of perturbation encodes the dissipative properties of the medium as well as speed of sound. Correlations of these fluctuations give information of the transport coefficient [62].

2.2 Kinetic theory: Basics

Kinetic theory describes the system in terms of single particle distribution function, $f(x, p)$. Number of particles in the volume $d^3x d^3p$ centered at (x, p) is written as

$f(x, p)d^3x d^3p$. In the domain of kinetic theory, evolution of the system is then described in terms of evolution $f(x, p)$. Under the assumption of molecular chaos Ludwig Boltzmann derived the famous transport equation that governs the evolution of $f(t, \vec{x}, \vec{p})$, which reads

$$p^\mu \partial_\mu f = C[f],$$

where $C[f]$ is the collision term containing the collision of particles.

Under assumption of two particle local interaction $C[f]$ can be written as,

$$C[f] = \frac{1}{2} \int \frac{d^3\vec{k}}{k_0} \int \frac{d^3\vec{k}'}{k'_0} \int \frac{d^3\vec{p}'}{p'_0} W_{pk \rightarrow p'k'} \{f_{p'} f_{k'} (1 \pm f_p)(1 \pm f_k) - f_p f_k (1 \pm f_{p'})(1 \pm f_{k'})\}.$$

where, with four momentum notation $p \equiv (p_0, \vec{p})$, $W_{pk \rightarrow p'k'}$ is the collisional transition rate, that involves information of interaction among the particles. The first term within the curly bracket gives the rate for $p'k' \rightarrow pk$ increases the number of particles of momentum p in d^3x , where as the second term gives the same for reduction rate of number of particles of momentum p in d^3x . Factors like $(1 \pm f_p)(1 \pm f_k)$ accounts for effect of quantum statistics for availability of phase space for the outgoing particles. The plus sign in these factor indicates Bose enhancement and minus stands for Pauli blocking.

Collision term of this form, makes the evolution equation an integro-differential equation. It is impossible to find the general analytic solution of this equation. However numerical methods can help in this regard [72, 73]. For specific situation, like if the system is slightly away from equilibrium, approximate methods can be used to solve this equation. In such situation linearization of $C[f]$ in terms of the deviation becomes valid. Then, relaxation time approximation can be use to

linearize the collision term. In this approximation $C[f]$ reads:

$$C[f] = -p_\mu u^\mu \frac{\delta f}{\tau_R}$$

where $\delta f = f - f_0$, f_0 is equilibrium distribution function and τ_R is relaxation time.

To solve the equation one needs initial condition and relaxation time as input. The relaxation time represents the interaction dynamics.

Once, $f(x, p)$ is known all local thermodynamic quantities can be evaluated. Number density, $n(x)$ of the particle can be expressed as:

$$n(x) = \int d^3p f(x, p).$$

In a similar manner particle current density in the volume element can be written as

$$\vec{j}(x) = \int d^3p \frac{\vec{p}}{p_0} f(x, p),$$

where $\vec{p}/p_0 = \vec{v}_p$ is velocity of on shell particles of momentum \vec{p} . Then the particle four current at the space time point, $N^\mu(x) \equiv (n(x), \vec{j})$, can be written as:

$$N^\mu(x) = \int \frac{d^3p}{p_0} p^\mu f(x, p).$$

Entropy density $s(x)$ of the system can be written as

$$s(x) = - \int d^3p f(x, p) \{ \ln f(x, p) - 1 \}$$

and entropy three current density

$$\vec{S} = - \int d^3p \vec{v}_p f(x, p) \{ \ln f(x, p) - 1 \}.$$

For, particles flowing Fermi-Dirac(FD) and Bose-Einstein(BE) statistics, the entropy four current takes the form,

$$S^\mu = - \int \frac{d^3p}{p^0} p^\mu f(x, p) \{ \ln f(x, p) + a \tilde{f}(x, p) \ln \tilde{f}(x, p) \},$$

where, $\tilde{f}(x, p) = 1 - a f(x, p)$, $a = 1$ for Fermions and $a = -1$ for Bosons.

The equilibrium distribution is achieved when entropy is maximum. Equilibrium form of distribution can also be obtained by requiring integrand of $C[f]$ to be zero, which represents the fact that there is no net gain in respective phase space cell due to collision [72].

The energy momentum tensor per unit volume can be defined in compact form as:

$$T^{\mu\nu} = \int \frac{d^3p}{p^0} p^\mu p^\nu f(x, p),$$

where

$$f_{eq}(x, p) = \frac{1}{e^{\beta x p_\mu u^\mu - \alpha(x)} + a},$$

where, $a = 0$, gives MB distribution, $a = 1$ for FD and $a = -1$ for BE distributions. Where $\beta(x)$ and $\alpha(x)$ are inverse of temperature field and chemical potential field respectively.

To get the energy momentum tensor where dissipation is present due to gradients of the fields, the distribution function is expressed as a sum of equilibrium and a additional term($\delta f(x, p)$) which takes into account gradients of hydrodynamic fields. To get $\delta T^{\mu\nu}$ for hydrodynamic fields, δf is expressed in gradients of hydrodynamic fields, and equation of motion for quantities forming $\delta T^{\mu\nu}$ can be obtained from Boltzmann equation. However, this δf can be assigned to take account of any type

of source of deviation from equilibrium. The additional part of distribution function (δf), when expressed in the basis of these independent gradients, represents the non-equilibrium process in a fluid cell which originates from gradients of the fields (like velocity of the cell w.r.t the lab frame and temperature) of equilibrium distribution of the cell. The form of the δf in terms the gradients of hydrodynamic fields can be constructed using the Boltzmann equation. For that the fields should correspond to the parameter fields of equilibrium part of the distribution function, where the equilibrium part alone is assigned to give the thermodynamic quantities.

Kinetic theory is used to study the system created in RHIC-E, to understand the approach towards equilibrium i.e. how the system of partons released from individual nucleons due to collision of heavy ions at relativistic energies lead to the formation of QGP [74–80]. Kinetic theory is also used to simulate the evolution of jet partons through the QGP medium.

CHAPTER 3

Kinetic Evolution of Perturbations

This chapter contains part of paper [81]. The microscopic evolution of perturbations, which is examined within the ambit of Boltzmann Transport Equation (BTE) in a static as well as a hydrodynamically expanding background, has been presented in this chapter.

3.1 Introduction

The fluctuations of physical quantities from their average values can be used to understand several properties of the system *i.e.* the transport coefficients of the medium, the approach toward equilibrium, etc. The study of temperature (T) fluctuation in the cosmic microwave background radiation (CMBR) has provided crucial information about the universe when it was about 300,000 years old. This information has led to tremendous support to the Big Bang model of cosmology. The polarization of the photons resulting from the Thomson scattering at the decoupling surface infected by density fluctuation gets reflected in the quadrupole moment of the phase space distribution of the incident photon. The fluctuation of T in the CMBR is introduced as a perturbation in the phase space distribution of photons. The evolution of this perturbation is studied by using Boltzmann transport equation

(BTE) [82] in gravitational field. The linear polarization resulted from the Thomson scattering is connected with the quadrupole moment of the photon's phase space distribution.

The fluctuations in the position of nucleons (with finite size) in the colliding nuclei lead to lumpiness in the spatial distribution of initial energy density of the system formed in Relativistic Heavy Ion Collisions Experiments (RHIC-E). The fluctuation in energy density may also originate due to the energy deposition by the propagation of energetic partons produced in the early stage of the evolution. These fluctuations may lead to observable effects similar to temperature fluctuation in CMBR. We have adopted an approach similar to the one followed to study the fluctuation in CMBR. We study the evolution of perturbations by introducing a deviation, $\delta f(x, p, t)$ in the equilibrium distribution function, $f_0(p)$. The bulk in equilibrium evolves via relativistic hydrodynamics and the evolution of the fluctuations, δf over the equilibrated expanding background is treated within the ambit of BTE [72]. In contrast to this the propagation of perturbation has been studied using hydrodynamics in Refs. [62, 83–86]. δf may be used to estimate the fluctuations in various thermodynamic quantities as we will see below. In the present work the equilibrated background is assumed to be quark gluon plasma (QGP) expected to be produced in RHIC-E.

The fluctuations in the thermodynamic quantities (e.g., hot spots created in the initial state of the collisions [87]) can be related to perturbations in the phase space distributions in the hydrodynamic limit. Fluctuations in thermodynamic quantities have been proposed as signals of the critical end point in the QCD phase transition [88, 89]. Dissimilar fluctuations in partonic and hadronic phases in the net electric charge and baryon number may shed light on the QCD phase transition in RHIC-E [90]. Event by event fluctuations in the ratio of positively to negatively charged pions may be used as an indicator of QCD transition [91] as well as for understanding the chemical equilibrium in the system formed in RHIC-E [92]. Evo-

lution of these fluctuations near the critical end point has been studied by using BTE [93]. Kinetic theory approach has also been adopted to study fluctuations in particle and energy densities [94]. In Ref. [95] it has been argued that the perturbations in hot QGP travel longer distance to reach the border of the medium giving rise to the possibility of detectable signatures of these perturbations.

The study of the fluctuations in the space time structure of the fireball driven by the fluctuations in the position of the nucleons in the colliding nuclei is an important contemporary issue in RHIC-E. Fluctuations in the space-time structure of the system will infect fluctuations in the thermodynamic quantities. How will these fluctuations evolve with time in a hydrodynamically expanding system and how are they connected with the transport coefficients for matter formed in RHIC-E are addressed in this work.

In Ref. [96] role of non-equilibrium processes on the evolution of QGP was studied within the framework of Parton-Hadron String Dynamics (PHSD) transport approach. It was found that the event-by-event fluctuations on collective variables estimated by the microscopic PHSD model is large due to non-equilibrium processes. However, the ensemble averaged results from these events is close to the results obtained in (2+1)-dimensional viscous hydrodynamics. In this context the study of the evolution of perturbations in the microscopic approach is crucial. Therefore, the present study of the perturbations in a hydrodynamically expanding background within the ambit of kinetic theory is appropriate. This is not only expected to achieve better microscopic understanding of the physics but also avoid question of breaking down of hydrodynamic description of fluctuation [70].

The mode by-mode analysis of the perturbation in the expanding background is discussed bellow. In the next section we discuss the evolution of fluctuations in a non-expanding background and present a relation between energy fluctuation in Fourier space and viscous coefficient. Section 3.3 is devoted to discuss the progres-

sion of fluctuations in a hydrodynamically expanding QGP background. Results based on this formalism are presented in Ch. 4 and section 6.2 of Ch. 6 is dedicated to summary and discussions.

3.2 Evolution of fluctuations in a non-expanding background

In the following we discuss the connection of δf , a small deviation of phase space distribution from its equilibrium value with the fluctuations in various thermodynamic variables and its time evolution in a non-expanding background within the framework of BTE (results with expansion will be discussed in section 3.3). The phase space distribution function, $f(\vec{x}, \vec{p}, t)$ of a system slightly away from equilibrium, at time t , position \vec{x} , momentum \vec{p} can be written as [98],

$$f(\vec{x}, \vec{p}, t) = f_0(p)\{1 + \Psi(\vec{x}, \vec{p}, t)\} = f_0(p) + f_0\Psi(\vec{x}, \vec{p}, t) \quad (3.1)$$

where $f_0(p)$ is the phase space distribution function in equilibrium and $\Psi(\vec{x}, \vec{p}, t)$ is the fractional deviation from $f_0(p)$. $\Psi(\vec{x}, \vec{p}, t)$ can be used to estimate the fluctuations in various thermodynamic quantities in the system. The evolution of Ψ is governed by BTE, which in turn provides the relation between the dissipative effects and fluctuations in the hydrodynamic limit.

3.2.1 Fluctuations of various hydrodynamic quantities in Fourier space

A given fluctuations in spatial coordinate can be expressed in terms of various k -modes in Fourier space. These k -modes or wave number modes can be connected to the wave length ($\lambda = 2\pi/k$) modes, which in turn is related to the angular size (ϑ) of

the fluctuations through the relation: $\vartheta = \lambda/d$ [99], where d is the angular diameter as is usually done in analyzing temperature fluctuations in the universe. Fourier analysis is also important to understand what are the k -modes of the fluctuations that dissipate during the evolution of the system. For example it is important to determine the viscous horizon in heavy ion collisions [83]. The energy momentum tensor, $T^{\mu\nu}$ of the system under study can be written as: $T^{\mu\nu} = \bar{T}^{\mu\nu} + \Delta T^{\mu\nu}$, where the equilibrium (ideal) part, $\bar{T}^{\mu\nu}$ is determined by $f^0(p)$ and the dissipative part, $\Delta T^{\mu\nu}$ is determined by Ψ , *i.e.*

$$T^{\mu\nu} = \int d^3p \frac{p^\mu p^\nu}{p^0} f(\vec{x}, \vec{p}, t) \quad (3.2)$$

where $f(\vec{x}, \vec{p}, t)$ is given by Eq. 3.1. The $\bar{T}^{\mu\nu}$ of the system in equilibrium can be obtained from Eq. 3.2 by setting $\Psi = 0$. The metric, $g^{\mu\nu}$, in Minkowski space-time is taken as $g^{\mu\nu} = (-1, 1, 1, 1)$. We assume that the momentum, \vec{p} can be written as $p_i = p n_i$, *i.e.* $\vec{p} = |\vec{p}| \hat{n}$ where \hat{n} is a unit vector and $d^3p = p^2 dp d\Omega$, $d\Omega$ being solid angle associated with n_i which satisfies $\int d\Omega n_i n_j = 4\pi \delta_{ij}/3$ and $\int d\Omega n_i n_j n_k = 0$. It is straightforward to obtain various components of T^μ_ν from Eq. 3.2. The deviation of the components of the stress energy tensor, $\Delta T^{\mu\nu}$ from their ideal values can be expressed in terms of the perturbation, Ψ as follows:

$$\begin{aligned} \Delta T^0_0 &= - \int p^2 dp d\Omega \epsilon f_0(p) \Psi(\vec{x}, \vec{p}, t), \\ \Delta T^0_i &= \int p^2 dp d\Omega p n_i f_0(p) \Psi(\vec{x}, \vec{p}, t), \\ \Delta T^i_j &= \int p^2 dp d\Omega \frac{p^2}{\epsilon} n^i n_j f_0(p) \Psi(\vec{x}, \vec{p}, t) \end{aligned} \quad (3.3)$$

where $\epsilon = p^0 = -p_0 = \sqrt{p^2 + m^2}$ and m is the mass of the particle. It is to be noted that the integral, $\int d^3p p n_i f_0(p) = 0$, since in equilibrium the system is isotropic *i.e.* all directions are equally probable in its rest frame, the phase space average of momentum vector then is zero.

The ideal part of the stress energy tensor in the hydrodynamic limit is given by,

$$\bar{T}_\nu^\mu = (\bar{\rho} + \bar{P})U^\mu U_\nu - \bar{P}g_\nu^\mu, \quad (3.4)$$

where $U^\mu = dx^\mu/d\tau = \gamma(1, \vec{v})$ is the four velocity of the fluid and τ is the proper time. The relations among various components of $\bar{T}^{\mu\nu}$ and the thermodynamic variables are: $\bar{T}_0^0 = -\bar{\rho}$, $\bar{T}_i^0 = -\bar{T}_0^i = 0$, and $\bar{T}_j^i = \bar{P}\delta_j^i$. Therefore, $\bar{\rho} = \int p^2 dp d\Omega \epsilon f_0(p)$, is the average energy density. Other thermodynamic quantities like pressure, number density etc can be estimated in a similar way. Equilibrium distribution is isotropic, therefore, integration over $d\Omega$ will simply give 4π . If the fluid is slightly away from equilibrium with space time dependent fluctuations in energy density, pressure, velocity, etc., then the system will evolve toward equilibrium through dissipative processes. In such situation the components of the energy momentum tensors can be explicitly expressed in terms of the thermodynamic variables as:

$$\begin{aligned} T_0^0(x_i, t) &= -\{\bar{\rho} + \delta\rho(x_i, t)\}, \\ T_i^0(x_i, t) &= -T_0^i = (\bar{\rho} + \bar{P})v_i, \\ T_j^i(x_i, t) &= \{\bar{P} + \delta P(x_i, t)\}\delta_j^i + \Sigma_j^i(x_i, t), \\ \Delta T_i^i &= 0, \end{aligned} \quad (3.5)$$

where v_i is the i^{th} component of the velocity perturbation. One can choose a frame which is moving with velocity close to the velocity of the fluid, so that the fluid velocity measured from this frame is small. From Eq. 3.5, we get $\Sigma_j^i = T_j^i - \delta_j^i T_k^k/3$. By using Eqs. 3.3, 3.4 and 3.5 we get,

$$\begin{aligned} \delta\rho(x_i, t) &= -\delta T_0^0(x_i, t), \\ v_i(x_i, t) &= \frac{\delta T_i^0(x_i, t)}{(\bar{\rho} + \bar{P})}, \\ \delta T_j^i(x_i, t) &= \delta P(x_i, t)\delta_j^i + \Sigma_j^i(x_i, t), \end{aligned} \quad (3.6)$$

with $\delta P(x_i, t) = \delta T_i^i(x_i, t)/3$. The shear stress, $\Sigma_j^i(x_i, t)$ can be expressed in terms of shear viscous coefficient, η as $\Sigma_j^i(x_i, t) = -\eta(\frac{\partial U_i}{\partial x_j} + \frac{\partial U_j}{\partial x_i} - \frac{2}{3}\delta_j^i \frac{\partial U_l}{\partial x_l})$ and the thermal conductivity (χ) is defined through the relation, $\delta T_j^0 = -\chi(\frac{\partial T}{\partial x_i} + T \frac{\partial U}{\partial t})$ [67]. The term $\frac{\partial U}{\partial t}$ is absent in non-relativistic domain.

It is useful to express these quantities, *i.e.* various components of $\delta T^{\mu\nu}$ in Fourier or k -space because expansion of these quantities in terms the spherical harmonics (Y_{lm}) will enable to connect the angular scales set by l in terms of k analogous to the determination of angular scale in CMBR [82]. In k -space these quantities are marked by tilde ($\tilde{}$) as:

$$\tilde{\Sigma}_j^l(k_i, t) = -i\eta(\tilde{U}^l k_j + \tilde{U}_j k^l - \frac{2}{3}\delta_j^l k^r \tilde{U}_r) \quad (3.7)$$

and

$$\delta \tilde{T}_i^0(k_i, t) = -\chi \left[ik_i \tilde{T}(k_l, t) + \tilde{T}(k_l, t) \frac{\partial \tilde{U}_i}{\partial t} \right]. \quad (3.8)$$

By using Eqs. 3.3 and 3.6 the fluctuations in k -space can be expressed in terms of Fourier mode, Ψ as:

$$\begin{aligned} \delta \tilde{\rho}(k_i, t) &= \int p^2 dp d\Omega \epsilon f_0(p) \tilde{\Psi}(k_i, p, n_i, t), \\ \tilde{v}_i(k_l, t) &= -\frac{1}{(\bar{\rho} + \bar{P})} \int p^2 dp d\Omega p n_i f_0(p) \tilde{\Psi}, \\ \tilde{\Sigma}_j^i(k_l, t) &= \int p^2 dp d\Omega \frac{p^2}{\epsilon} (n_i n_j - \frac{1}{3}\delta_{ij}) f_0(p) \tilde{\Psi}, \\ \delta \tilde{P}(k_i, t) &= \frac{1}{3} \int p^2 dp d\Omega \frac{p^2}{\epsilon} f_0(p) \tilde{\Psi} \end{aligned} \quad (3.9)$$

where $\tilde{\Psi}$ is the Fourier transform of Ψ . Now we take the zenith direction along \vec{k} and then the angular dependence of $\tilde{\Psi}(k_i, p, n_i, t)$ can be expressed in terms of angles between \hat{k} and \vec{n} . Depending on the symmetries of the problem under consideration $\tilde{\Psi}$ can be expanded in a series of suitably chosen basis functions e.g, for axial symmetry in terms of Legendre polynomials and in absence of such symmetry it can be

expressed in terms of spherical harmonics [100].

The vector component n_i and tensor components $(n_i n_j - \frac{1}{3} \delta_{ij})$, appearing in the expressions for $v_i(k_l, t)$ and $\Sigma_j^i(k_l, t)$ respectively, can be converted into functions of θ (angle between \vec{k} and \vec{n}), by taking contraction with suitable tensors made out of the components of \hat{k} . If we contract n_i with k_i then we get $k \hat{k} \cdot \hat{n} = k \cos \theta = k P_1(\hat{k} \cdot \vec{n})$ and by contracting $(n_i n_j - \frac{1}{3} \delta_{ij})$ with $(\hat{k}_i \hat{k}_j - \frac{1}{3} \delta_{ij})$ we get $\frac{2}{3} \frac{1}{2} (3(\hat{k} \cdot \hat{n})^2 - 1) = \frac{2}{3} \frac{1}{2} (3 \cos^2 \theta - 1) = \frac{2}{3} P_2(\hat{k} \cdot \hat{n})$, where P_l s are Legendre polynomials. For axial symmetric distribution of \vec{p} it helps to connect different co-efficient of expansion of $\tilde{\Psi}$ in terms of Legendre polynomials with corresponding scalar quantities obtained from $v_i(k_l, t)$ and $\Sigma_j^i(k_l, t)$ due to orthogonality relation satisfied by P_l 's. We define the scalar quantities like Δ , θ and σ as in [101], which, as will be seen later allow us to get evolution equation for the Fourier modes. The fluctuation in energy density in Fourier space is given by,

$$\Delta(k_i, t) = \frac{\delta \tilde{\rho}(k_i, t)}{\bar{\rho}} = -\frac{\delta \tilde{T}_0^0(k_i, t)}{\bar{\rho}}, \quad (3.10)$$

Similarly we define energy flux,

$$\theta(k_i, t) = ik^j \tilde{v}_j = \frac{ik^j \delta \tilde{T}_j^0(k_i, t)}{(\bar{\rho} + \bar{P})}, \quad (3.11)$$

and the shear stress as,

$$(\bar{\rho} + \bar{P}) \sigma(k_l, t) = -(\hat{k}_i \hat{k}_j - \frac{1}{3} \delta_{ij}) \tilde{\Sigma}_j^i(k_l, t), \quad (3.12)$$

The quantity, $\theta(k_i, t) = ik^j \tilde{v}_j$ originates from the velocity gradient. θ and σ can be expressed in terms of the shear viscous coefficient (η) and thermal conductivity (χ) as follows:

$$\sigma(\vec{k}, t) = -\frac{4}{3} \frac{\eta}{\bar{\rho} + \bar{P}} ik^j \tilde{v}_j(\vec{k}, t) \quad (3.13)$$

and

$$\theta(\vec{k}, t) = \frac{\chi}{\bar{\rho} + \bar{P}} (k^2 \tilde{T}(k_l, t) - ik_l \tilde{T}(k_l, t) \dot{v}_l(k_l, t)). \quad (3.14)$$

The left hand side of both the equation above can be estimated from the solution BTE. Fourier transformation of these equations in frequency space will lead to dispersion relation. This relation can be used to determine those k (wave number) values which will dissipate due to viscous effects, and this will determine the viscous horizon.

Now Eqs. 3.9, 3.10, 3.11 and 3.12 can be used to obtain the fluctuations in the energy density, pressure and velocity in k -space as:

$$\begin{aligned} \Delta(k_i, t) &= \frac{1}{4\pi} \int d\Omega \frac{\int p^2 dp \epsilon f_0(p) \tilde{\Psi}(k_i, p, n_i, t)}{\int p^2 dp \epsilon f_0(p)}, \\ \frac{\delta \tilde{P}(k_i, t)}{\bar{P}} &= \frac{1}{4\pi} \int d\Omega \frac{\int p^2 dp (p^2/\epsilon) f_0(p) \tilde{\Psi}(k_i, p, n_i, t)}{\int p^2 dp (p^2/\epsilon) f_0(p)}, \\ \theta(k_i, t) &= \frac{ik}{4\pi} \int d\Omega (\hat{k} \cdot \hat{n}) \frac{\int p^2 dp f_0(p) \tilde{\Psi}(k_i, p, n_i, t)}{\int p^2 dp (\epsilon + p^2/3\epsilon) f_0(p)}, \\ \sigma(k_i, t) &= -\frac{1}{4\pi} \int d\Omega ((\hat{k} \cdot \hat{n})^2 - \frac{1}{3}) \frac{\int p^2 dp f_0(p) \tilde{\Psi}(k_i, p, n_i, t)}{\int p^2 dp (\epsilon + p^2/3\epsilon) f_0(p)}. \end{aligned} \quad (3.15)$$

To understand the angular scale determined by the multipole number l (as used in the appendix A to find the angular correlations) we expand $\tilde{\Psi}$ in terms of Legendre polynomials for an axially symmetric distribution as:

$$\tilde{\Psi}(\vec{k}, \hat{n}, p, t) = \sum_{l=0}^{\infty} (-i)^l (2l+1) \Psi_l(\vec{k}, p, t) P_l(\hat{k} \cdot \hat{n}), \quad (3.16)$$

The l is related to angular resolution of the anisotropies, *i.e.* smaller angular scale will require larger l and vice versa. The temperature fluctuations (ΔT) may be

obtained from Eq. 3.16 by using the relation [101]:

$$\Delta T/\bar{T} = -(\partial \ln f_0 / \partial \ln p)^{-1} \Psi \quad (3.17)$$

For simplicity we will consider the massless limit, $m = 0$ which gives the relation $\epsilon = p$. The energy density is a scalar quantity whereas the velocity and the shear tensor are vector and tensor respectively and these aspects are also bound to reflect in the corresponding fluctuations. Therefore, the orthogonality of P_l 's ensure that the fluctuations in scalar, vector and tensor quantities are dictated by the coefficients Ψ_0 , Ψ_1 and Ψ_2 which are obtained by substituting Ψ from Eq. 3.16 in Eq. 3.15 and performing the angular integration as,

$$\begin{aligned} \Delta(k_i, t) &= \delta \rho(k_i, t) / \bar{\rho} = \int p^2 dp p f_0(p) \Psi_0(k_i, p, t) / \bar{\rho}, \\ \delta P(k_i, t) / \bar{P} &= \int p^2 dp p f_0(p) \Psi_0(k_i, p, t) / \bar{\rho} \\ \theta(k_i, t) &= 3i k^j \delta T_j^0 / (4\bar{\rho}) = \frac{3}{4} k \int p^2 dp p f_0(p) \Psi_1(k_i, p, t) / \bar{\rho} \\ \sigma(k_i, t) &= \frac{1}{2} \int p^2 dp p f_0(p) \Psi_2(k_i, p, t) / \bar{\rho} \end{aligned} \quad (3.18)$$

where $\bar{\rho} = \int p^2 dp p f_0(p)$. The above set of equations can be written in a more compact form through the expansion of the function $F(\vec{k}, \hat{n}, t)$ which is obtained by integrating δf over the magnitude of momentum, \vec{p} .

$$F(\vec{k}, \hat{n}, t) = \int p^2 dp p f_0(p) \Psi(\vec{k}, p, n_i, t) / \bar{\rho} \quad (3.19)$$

therefore, F has the angular dependence of Ψ and consequently F can be expressed as:

$$F(\vec{k}, \hat{n}, t) = \sum_{l=0}^{\infty} (-i)^l (2l+1) F_l(\vec{k}, t) P_l(\hat{k} \cdot \hat{n}). \quad (3.20)$$

with

$$F_l(\vec{k}, t) = \int p^2 dp p f_0(p) \Psi_l(\vec{k}, p, t) / \epsilon_0 \quad (3.21)$$

The fluctuations in terms of F_l 's are now given by

$$\Delta(\vec{k}, t) = F_0(\vec{k}, t), \quad \delta P(\vec{k}, t)/\bar{P} = F_0(\vec{k}, t), \quad \theta(\vec{k}, t) = 3/4kF_1(\vec{k}, t), \quad \sigma(\vec{k}, t) = 1/2F_2(\vec{k}, t). \quad (3.22)$$

Using the relation $\sigma(\vec{k}, t) = -4\eta ik^j v_j(\vec{k}, t)/3(\bar{\rho} + \bar{P})$, and writing $ik^j v_j(\vec{k}, t) = \Theta(\vec{k}, t)$ we get an important relation which connects the fluctuation (F_2) with the transport coefficient (η),

$$F_2(\vec{k}, t) = -\frac{8\eta}{3(\bar{\rho} + \bar{P})}\Theta(\vec{k}, t) \equiv -\frac{8}{3\bar{T}}\frac{\eta}{\bar{s}}\Theta(\vec{k}, t) \quad (3.23)$$

where the thermodynamic relation, $\bar{h} = \bar{\rho} + \bar{P} = \bar{s}\bar{T}$, among enthalpy density (\bar{h}), entropy density (\bar{s}) and temperature (\bar{T}) has been used. The η appears as a coefficient of 2^{nd} rank tensor involving gradient in the i th direction of the j th component of velocity, as a result the $l = 2$ term appears in the expression for η in Eq. 3.23. In a similar way, using Eq. 3.22 the bulk viscosity ζ can be related to the fluctuation in pressure (F_0) as: $\delta P = -ik_l v^l \zeta$.

3.2.2 Fluctuations in Fourier space and transport coefficients in relaxation time approximation

The temperature fluctuations, $\Delta T(\theta, \phi)$ in CMBR is generally expanded in Laplace series in terms of spherical harmonics, $Y_{lm}(\theta, \phi)$. The maximum value of l is determined by the angular resolution of the detector which can be connected to the wave number (k) corresponding to the Fourier transform of the spatial anisotropy. Therefore, in analogy with fluctuations in the CMBR the spatial anisotropy is studied here in Fourier space. But first we briefly discuss it in coordinate space.

The BTE, $p^\mu \partial_\mu f = C[f]$ in absence of external force and in the relaxation time

approximation (similar approximation were used *e.g.* in Refs [102–104]) reduces to

$$\frac{\partial \Psi}{\partial t} + \frac{p^i}{\epsilon} \frac{\partial \Psi}{\partial x^i} = -\frac{\Psi(\vec{x}, \vec{p}, t)}{\tau_R}. \quad (3.24)$$

for Ψ . In Eq. 3.24 τ_R is the relaxation time. For the present work the relaxation time can be estimated as the inverse of the reaction rate of the quarks and gluons using pQCD cross sections and Hard Thermal Loop Approximations [105]. The solution of Eq. 3.24 for a given initial (at time t_0) distribution, $\Psi_{in}(\vec{x}, \vec{p}, t_0)$ is [109]:

$$\Psi(\vec{x}, \vec{p}, t - t_0) = \Psi_{in} \left(\left(\vec{x} - \frac{\vec{p}}{p_0} (t - t_0) \right), \vec{p} \right) \exp \left[-\frac{(t - t_0)}{\tau_R} \right] \quad (3.25)$$

Knowing Ψ it is straightforward to estimate the fluctuation in energy density from the following expression:

$$\Delta(\vec{x}, t - t_0) = \frac{\int p^2 dp d\Omega \epsilon f_0(p) \Psi(\vec{x}, \vec{p}, t - t_0)}{\int p^2 dp d\Omega \epsilon f_0(p)}. \quad (3.26)$$

The solution of Eq. 3.24 given by Eq. 3.25 is useful to study the time evolution of spatial anisotropy of the matter.

Now we would like to derive a relation between the fluctuation in energy density and transport coefficients. To facilitate this we write Eq. 3.24 for massless particles (as the case may be for partonic plasma produced in RHIC-E) in k -space:

$$\frac{\partial \Psi}{\partial t} + ik(\hat{k} \cdot \hat{n}) \Psi = -\frac{\Psi(\vec{k}, \vec{p}, t)}{\tau_R}. \quad (3.27)$$

With the help of Eq. 3.19, Eq. 3.27 can be reduced to an equation describing the time evolution of F as

$$\frac{\partial F}{\partial t} + ik(\hat{k} \cdot \hat{n}) F = -\frac{F(\vec{k}, t)}{\tau_R}. \quad (3.28)$$

This equation has the following solution,

$$F(\vec{k}, \hat{n}, t) = F(\vec{k}, \hat{n}, t_0) \exp \left[-\left(\frac{1}{\tau_R} + ik\mu \right) (t - t_0) \right] \quad (3.29)$$

where $\hat{k} \cdot \hat{n} = \mu$. The value of $F(\vec{k}, \hat{n}, t)$ can be obtained from its value at initial time, t_0 . Eq. 3.29 is a general expression for the fluctuations in the sense that all the quantities, *e.g.* Δ , θ , σ , discussed above at time t can be obtained from this expression if their corresponding initial values are supplied. Expanding $F(\vec{k}, \hat{n}, t)$ as in Eq. 3.20 and using the orthogonality relations of $P_l(\mu)$ s we get,

$$F_l(\vec{k}, t) = \frac{1}{2} e^{-\frac{(t-t_0)}{\tau_R}} \sum_{s=0}^{\infty} (-i)^{(s-l)} (2s+1) F_s(\vec{k}, t_0) \int_{-1}^{+1} d\mu P_l(\mu) P_s(\mu) e^{-ik\mu(t-t_0)}. \quad (3.30)$$

For $l = 0, 1, 2$ we have,

$$\begin{pmatrix} F_0(k, t) \\ F_1(k, t) \\ F_2(k, t) \end{pmatrix} = \begin{pmatrix} I_0 & (-i)3I_1 & (-5)\frac{1}{2}(3I_2 - I_0) \\ I_1 & (-i)3I_2 & (-5)\frac{1}{2}(3I_3 - I_1) \\ \frac{1}{2}(3I_2 - I_0) & (-i)\frac{1}{2}(I_3 - I_1) & (-5)\frac{1}{4}(9I_4 - 6I_2 + I_0) \end{pmatrix} \begin{pmatrix} F_0(k, t_0) \\ F_1(k, t_0) \\ F_2(k, t_0) \end{pmatrix}$$

where $I_n \equiv I_n(k, t)$ and $\alpha = k(t - t_0)$

$$I_n(\alpha) = \int_{-1}^{+1} d\mu \mu^n e^{-i\mu\alpha},$$

for $n = 0$ I_0 is given by

$$I_0(\alpha) = (-i) 2 \frac{\sin \alpha}{\alpha}$$

The following relations may be used to obtain $I_j(\alpha)$ for $j = 1, 2, \dots$

$$I_{n+k}(\alpha) = \frac{1}{(-i)^k} \frac{d^k I_n}{d^2 \alpha}.$$

Therefore, the energy density fluctuation at time t is given by:

$$\Delta(\vec{k}, t) = \frac{1}{2} e^{-\frac{(t-t_0)}{\tau_R}} \sum_{s=0}^{\infty} (-i)^s (2s+1) F_s(\vec{k}, t_0) \int_{-1}^{+1} d\mu P_s(\mu) e^{-ik\mu(t-t_0)}. \quad (3.31)$$

Taking terms up to $s = 2$ in the expression for $\Delta(\vec{k}, t)$ we get,

$$\Delta(\vec{k}, t) = \frac{1}{2} e^{-\frac{(t-t_0)}{\tau_R}} \sum_{s=0}^2 (-i)^s (2s+1) F_s(\vec{k}, t_0) \int_{-1}^{+1} d\mu P_s(\mu) e^{-ik\mu(t-t_0)}. \quad (3.32)$$

Performing the integration over μ we get,

$$\begin{aligned} \Delta(\vec{k}, t) = & e^{-\frac{(t-t_0)}{\tau_R}} [F_0(\vec{k}, t_0) \left\{ \frac{\sin k(t-t_0)}{k(t-t_0)} \right\} + 3F_1(\vec{k}, t_0) \left\{ \frac{\cos k(t-t_0)}{k(t-t_0)} - \frac{\sin k(t-t_0)}{\{k(t-t_0)\}^2} \right\} \\ & - 5F_2(\vec{k}, t_0) \left\{ \frac{\sin k(t-t_0)}{k(t-t_0)} + \frac{3 \cos k(t-t_0)}{(k(t-t_0))^2} - \frac{3 \sin k(t-t_0)}{(k(t-t_0))^3} \right\}]. \end{aligned} \quad (3.33)$$

This is the fluctuations in energy density, from which the fluctuations in temperature can be obtained by using the relation: $\delta\rho/\bar{\rho} = 4\delta T/T$ for $\rho \sim T^4$. We use Eqs. 3.22, 3.23 and 3.33 to obtain the energy density fluctuation in terms of transport coefficients as:

$$\begin{aligned} \Delta(\vec{k}, t) = & e^{-(t-t_0)/\tau_R} [\Delta(\vec{k}, t_0) \frac{\sin k(t-t_0)}{k(t-t_0)} \\ & + \frac{4}{k} \frac{\chi}{s} \frac{T(\vec{k}, t_0)}{\bar{T}} \{k^2 - ik_l \dot{U}_l(\vec{k}, t_0)\} \left\{ \frac{\cos k(t-t_0)}{k(t-t_0)} - \frac{\sin k(t-t_0)}{k^2(t-t_0)^2} \right\} \\ & + \frac{40}{3} \frac{\eta}{s} \frac{\Theta(\vec{k}, t_0)}{\bar{T}} \left\{ \frac{\sin k(t-t_0)}{k(t-t_0)} + \frac{3 \cos k(t-t_0)}{k^2(t-t_0)^2} - \frac{3 \sin k(t-t_0)}{k^3(t-t_0)^3} \right\}]. \end{aligned} \quad (3.34)$$

Eq. 3.34 provides the connection of the fluctuation in energy density in Fourier space with various transport coefficients *e.g.* thermal conductivity (χ) and viscosity (η). It may be easily checked that the above solution satisfies the condition, $\Delta(\vec{k}, t) \rightarrow \Delta(\vec{k}, t_0)$ in the limit $t \rightarrow t_0$. It is interesting to note that the $k \sim 0$ mode (or large wave length mode) which is insensitive to spatial gradient is damped by the exponential time dependence only. $\Delta(k=0, t_0)$ represents the mode of the initial

perturbation that takes the whole system (as in $k \rightarrow 0$, length scale of inhomogeneity $\lambda \rightarrow \infty$) slightly away from its equilibrium value. However, the non-zero k modes, in addition to the exponential decay, are damped out also due to spatial gradient which is signaled by the presence of terms involving shear viscosity and thermal conductivity in Eq. 3.34.

The fluctuation in energy density in position space can be obtained by taking Fourier transformation of Eq. 3.34 as,

$$\frac{\delta\rho}{\bar{\rho}}(\vec{x}, t) = \int \frac{d^3k}{(2\pi)^3} \Delta(\vec{k}, t) \exp(i\vec{k}\cdot\vec{x}) \quad (3.35)$$

If the initial ($t = t_0$) energy density fluctuation, gradient of velocity, viscosity to entropy ratio and temperature of the system in equilibrium are known then Eqs. 3.34 and 3.35 can be used to get fluctuations at any time, $t > t_0$. The derivation of angular correlation function for these fluctuation has been given Angular correlation function for these fluctuation has been given in the appendix A.

3.3 Evolution of fluctuation in a hydrodynamically expanding QGP background

So far we have considered the evolution of the fluctuations in a non-expanding background. However, in a realistic scenario in RHIC-E the system expands due to high internal pressure. Therefore, in this section we include the effects of the expansion on the spatial anisotropy through the solutions of relativistic hydrodynamics. The fluid velocity and all the thermodynamic quantities become function of space time coordinates to be determined by the solution of the hydrodynamical equations.

The evolution of δf is governed by the BTE, $p^\mu \partial_\mu f = (p \cdot u)C[f]$ [72, 73, 98]. For an expanding system under the relaxation time approximation BTE reduces to the

following [102–104, 106–108]):

$$\left(\frac{\partial}{\partial t} + \frac{\vec{p}}{p^0} \cdot \frac{\partial}{\partial \vec{x}} + \frac{(p^0 u_0 - \vec{p} \cdot \vec{u})}{p^0 \tau_R(x)} \right) \delta f(x, p) = - \left(\frac{\partial}{\partial t} + \frac{\vec{p}}{p^0} \cdot \frac{\partial}{\partial \vec{x}} \right) f_0(x, p) \quad (3.36)$$

The solution of Eq. 3.36 is given by [109]:

$$\delta f(x, p) = D(t, t_0) \left[\delta f_{in}(p, \vec{x} - \frac{\vec{p}}{p^0}(t - t_0)) + \int_{t_0}^t B(\vec{x} - \frac{\vec{p}}{p^0}(t - t'), t') D(t_0, t') dt' \right] \quad (3.37)$$

where

$$D(t_2, t_1) = \exp \left[- \int_{t_1}^{t_2} dt' A(p, \vec{x} - \frac{\vec{p}}{p^0}(t' - t_0), t') \right] \quad (3.38)$$

with

$$A(p, \vec{x}, t) = \frac{u_0(x) - \vec{p} \cdot \vec{u}(x)/p_0}{\tau_R(x)} \quad (3.39)$$

and

$$B(\vec{x}, t) = - \left(\frac{\partial}{\partial t} + \frac{\vec{p}}{p^0} \cdot \frac{\partial}{\partial \vec{x}} \right) f_0(x, p) \quad (3.40)$$

For

$$f_0(x, p) = f_{eq} = \frac{1}{e^{\beta(x)(u^\mu p_\mu)} - 1} \quad (3.41)$$

The expression for B reduces to:

$$B(\vec{x}, t) = -f_{eq}(1 + f_{eq}) \frac{p^\mu}{p^0} \partial_\mu [\beta(x) u^\mu p_\mu] \quad (3.42)$$

We took the relaxation time as $\tau_R^{-1}(x) = 1.1\alpha_s T(x)$ [105] (we have taken constant value of $\alpha_s = 0.2$ here), $\beta = 1/T(x)$, $u^\mu(x) = (\gamma, \gamma \vec{v})$ is the four velocity of the fluid and $\gamma(x) = u^0(x) = (1 - v(x)^2)^{-1/2}$. The interaction of the expanding background with the fluctuation is implemented through the relaxation time which depends on T and the space-time variation of the temperature and velocity fields are determined by the solution of the relativistic hydrodynamic equations. Eq. 3.37 provides the space-time evolution of fluctuation in phase space distribution for an expanding QGP

background. This equation may be used to estimate various auto-correlations and fluctuations in thermodynamic quantities which can be measured experimentally.

3.4 Summary and discussion

We have discussed a formalism for studying evolution of perturbations in QGP background. The formalism discussed is relevant for studying space-time evolution of fluctuations in any relativistically expanding background. In this chapter we have presented a theoretical study of evolution of perturbation in both expanding and non-expanding background. For non-expanding background evolution of different Fourier modes of perturbations have been discussed under relaxation time approximation. Explicit relations between fluctuations and transport coefficients have been derived. Evolution of angular power spectrum of the anisotropies in a non-expanding background has been estimated in the appendix [A](#).

CHAPTER 4

Evolution of Spatially Anisotropic Perturbations

This chapter contains part of paper [81]. Evolution of spatially anisotropic perturbation created in the system formed after Relativistic Heavy Ion Collisions is discussed in this chapter. Spatial anisotropic perturbations with different geometry have been evolved through Boltzmann equation. It is observed that the trace of such fluctuation survive the evolution. Within the relaxation time approximation analytical results have been obtained for the evolution of these anisotropies. The mixing of various Fourier (or k) modes of the perturbations during the evolution of the system is discussed. This study is very useful in understanding the presumption that the measured anisotropies in the data from heavy ion collisions at relativistic energies imitate the initial state effects.

4.1 Introduction

In the previous chapter we have discussed the formalism we have developed for studying the evolution of perturbations using Boltzmann Transport equation in both static and hydrodynamically expanding QGP background. In this chapter we discuss

our study of the evolution different anisotropic perturbation. Authors in Ref. [97] has discussed deposition of energy by the away side mini-jet in the non-equilibrium framework. Corresponding perturbation in the medium has clear anisotropic form in space, as mini-jet deposits energy along its path. Therefore, instead of Gaussian type perturbation, consideration of anisotropic perturbation in space will be more appropriate in such cases.

In this work we have used BTE to study the anisotropic fluctuations. The description of the evolution of anisotropy induced fluctuations within the ambit of kinetic theory approach helps in getting better microscopic insight on the evolution. Moreover, kinetic theory approach has validity over a wider range of phase space compared to hydrodynamical descriptions. In the two sections below we present results on the evolution of fluctuations in a static and subsequently for a realistic scenario of expanding background respectively.

4.2 Initial Perturbation

To simulate initial spatial anisotropy with different geometry, we choose,

$$\delta f(p, \vec{x}, t_0) = A_0 \exp[-r(1 + a_n \cos n\phi)] \quad (4.1)$$

We have taken $n = 2, 3, 4, 5$ and 11 to simulate different initial anisotropy. A_0 is set to unity for numerical results discussed below. From the solution in coordinate space one can get Fourier modes of fluctuations using Fourier Transformation which will give evolution of different Fourier modes of fluctuations. We take $a_n = 0.3$ for $n = 2, 3, 4, 5$ and 11.

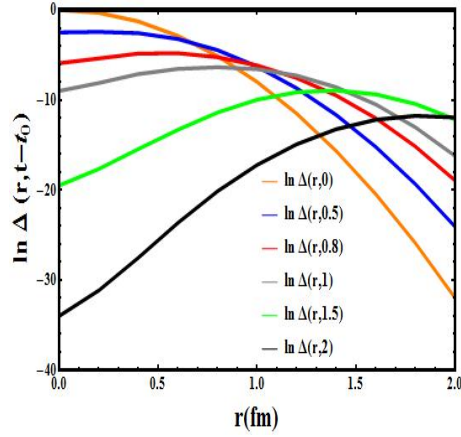


Figure 4.1: Evolution of the fluctuation in energy density with r at different t for a non-expanding QGP background.

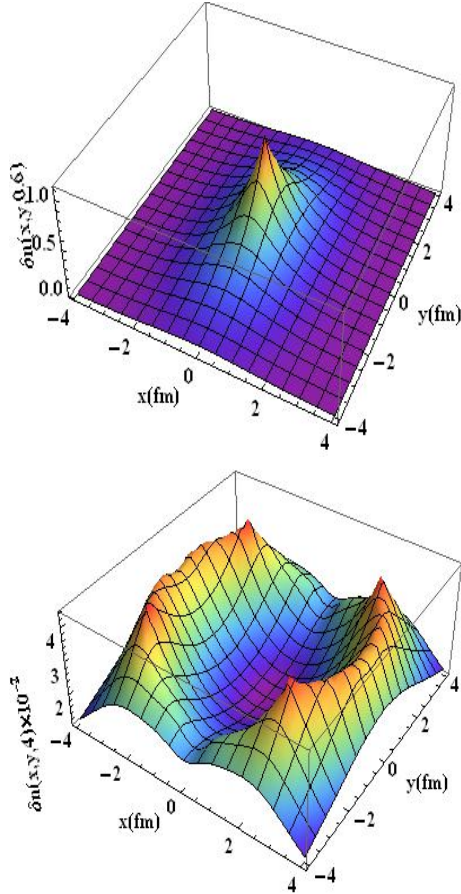


Figure 4.2: Evolution of the spatial anisotropy of the perturbation with initial elliptic geometry at time $\tau_0 = 0.6$ fm/c (upper panel). The lower panel shows the geometry after a time 4 fm/c has elapsed. Hydrodynamic expansion of the QGP background has been taken into account. The boundary of the background has an elliptic shape with the dimension of major and minor axes are approximately 6 fm and 4 fm respectively. The colors from red to violet represent highest to lowest values of the perturbations.

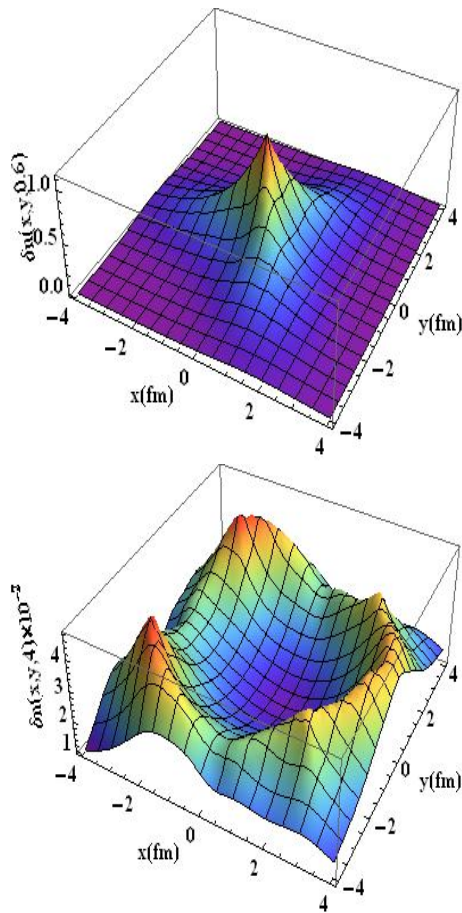


Figure 4.3: Same as Fig. 4.2 but the spatial anisotropy has a triangular geometry at the initial time $\tau_0 = 0.6$ fm/c (upper panel). The lower panel shows the perturbation after a time 4 fm/c has elapsed.

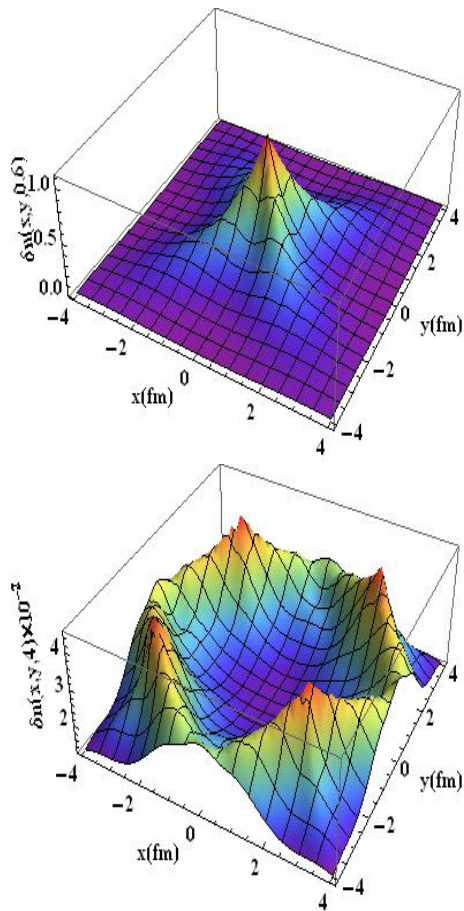


Figure 4.4: Same as Fig. 4.2 but the spatial anisotropy has a quadrangular geometry at the initial time $\tau_0 = 0.6$ fm/c (upper panel). The lower panel shows the geometry after a time 4 fm/c has elapsed.

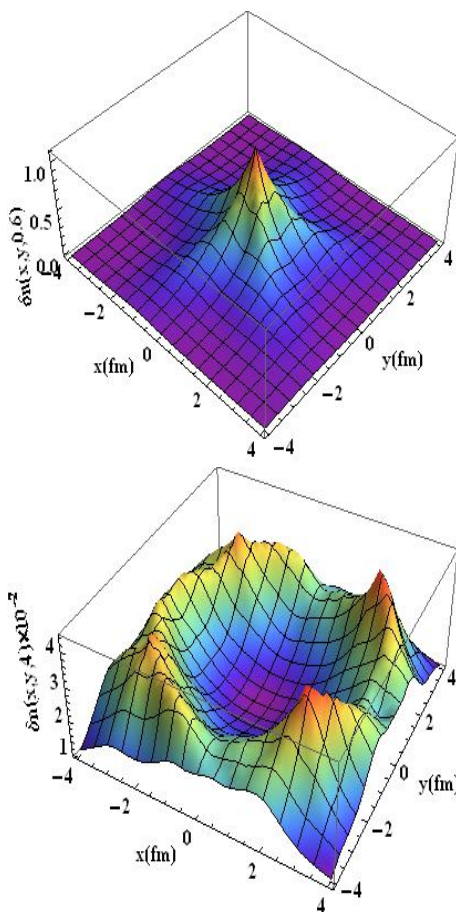


Figure 4.5: Same as Fig. 4.2 but the spatial anisotropy has a pentagonal geometry at the initial time $\tau_0 = 0.6$ fm/c (upper panel). The lower panel shows the results after a time 4 fm/c has elapsed.

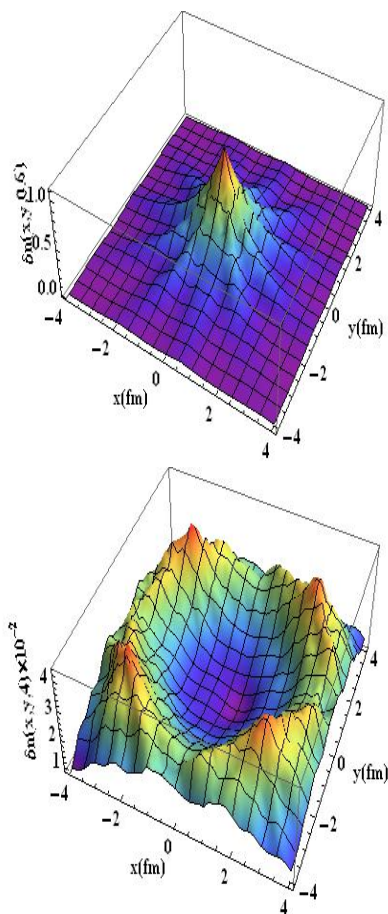


Figure 4.6: Same as Fig. 4.2 but the spatial anisotropy has a hendecagonal geometry ($n = 11$) at the initial time $\tau_0 = 0.6$ fm/c (upper panel). The lower panel shows the results after a time 4 fm/c has elapsed.

4.3 Evolution of fluctuation in energy density for a non-expanding system

We display the spatial variation of the fluctuation in Fig. 4.1 at different times for a non-expanding background. We substitute Eq. 3.25 in Eq. 3.26 with Ψ_{in} as a Gaussian in space at the initial time and evaluate the evolution of the fluctuation. For the sake of illustration we take $T = 400$ MeV and $\tau \sim 1$ fm/c. The results indicate a rapid dissipation and displacement of the peak of the fluctuations with increase in time. The displacement of the peak of the initial fluctuation given by Eq. 4.1 centered at $r = |\vec{x}| = 0$ is governed by the factor, $\vec{x} - \vec{p}(t - t_0)/p_0$ appearing in the solution for Ψ (Eq. 3.25) and the dissipation is controlled by the relaxation time, τ_R involves in the exponential factor in the same equation. The dissipation will slow down in an expanding medium because the relaxation time will increase with decreasing temperature due to expansion.

4.4 Evolution of fluctuation in an expanding QGP background

In this section we would like to do some case study of how a given spatial anisotropy characterized by some geometric shape will evolve with space and time in an expanding QGP medium governed by relativistic hydrodynamics. This will give us some idea on the evolution of elliptical or triangular anisotropic perturbations created in the collisions.

We present the results now for a realistic scenario where the background QGP is expanding hydrodynamically.

The space time variation of quantities such as energy density and flow velocity is

governed by relativistic hydrodynamics. Therefore, we solve the equation:

$$\partial_\mu \bar{T}^{\mu\nu} = 0 \quad (4.2)$$

with the assumption that net baryon number density (n_B) is zero at the central rapidity region, hence we need not consider the equation $\partial_\mu(n_B u^\mu) = 0$. We also assume boost invariance [110] along the longitudinal direction and solve the Eq. 4.2 numerically with equation of state $\bar{P} = \bar{\rho}/3$ for initial condition taken from optical Glauber at the highest RHIC energy ($\sqrt{s_{NN}} = 200$ GeV) for Au+Au collision. The hydrodynamic solutions [111] for flow velocity and temperature ($\bar{T} = [30\bar{\rho}/(g\pi^2)]^{1/4}$) have been used to study the space time evolution of the fluctuations in an expanding background.

Taking the value of the temperature dependent relaxation time relevant for QCD plasma [105] the evolution of initial spatial anisotropies introduced through Ψ_{in} (or δf) have been studied. It is to be noted that due to expansion the temperature decreases and hence the relaxation time increases which slows down the dissipation. Therefore, the dissipation of the perturbation gets slower with the expansion of the system. The effects of perturbation has better chance of survivability in the direction of lesser extent because the expansion is faster along that direction due to larger pressure gradient. It implies that systems with same energy density the perturbations has larger chances to survive in systems with smaller size. Then it is expected that the presence of perturbations will be dominant in relatively smaller size systems. In Fig. 4.2 the evolution of the initial elliptic spatial anisotropy of the perturbation (upper panel), realized by taking $n = 2$ in Eq. 4.1 is depicted. The initial thermalization time is taken as $\tau_0 = 0.6$ fm/c. The evolution is studied up to $\tau = 4$ fm/c. The red to violet colors used in the figures for distinct visibility, represent correspondingly the highest to lowest values of the perturbations. For $n = 2$ the anisotropy has an elliptic shape having stronger gradient along x -axis resulting

in faster expansion along x compared to y axis. Therefore, the propagation of the perturbation generates a pattern similar to the one generated in water waves by the impact of a stick on the still water surface. This kind of pattern is clearly observed in the lower panel of Fig. 4.2 such type of fluctuation may be created by the propagation of jets through the QGP. It may be observed that the solution of BTE given in Eq. 3.37 is subjected to two different kinds of mechanism - (a) dissipation of the fluctuations and (b) hydrodynamic expansion of the background. The expansion velocity will be larger along x -axis than along y -axis due to different pressure gradient imposed by the initial geometry of the fluctuation. This results in the splitting of the fluctuation as observed in the lower panel of Fig. 4.2. By switching off the dissipation (appearing through the exponential term in $D(t, t_0)$) we have noticed that the fluctuation still splits in two parts but the peak of the fluctuation does not reduce significantly. It is also important to note that the two oppositely propagating perturbations are correlated which may have interesting observable effects.

Moreover, if the perturbation is created near the boundary of the system then the wave propagating outward will dissipate less than the one moving inward. The results in Fig. 4.2 indicate a rapid dissipation of the peak. The peak has been reduced by more than 90% at a time $\tau = 4 \text{ fm}/c$. The expansion of the QGP background is governed by the equation of state *i.e.* by the velocity sound in the QGP (the maximum displacement is determined by the sound horizon: *i.e.* the distance traveled by the sound wave: $\int_{\tau_0}^{\tau} d\tau c_s(\tau) d\tau$. We have taken the sound velocity, $c_s = 1/\sqrt{3}$, independent of τ for the expanding QGP background). The displacement of the fluctuation (primarily δf) is regulated by the factor: $\vec{x} - \vec{p}(t - t_0)/p_0$ appearing in Ψ (Eq. 3.25). Therefore, the net displacement is determined by the combination of these two factors. The dissipation of the fluctuation is dictated by the relaxation time which is a function of space-time coordinate through the relation: $\tau_R^{-1} \sim T(t, \vec{x})$. Therefore, the amplitude of the displacement becomes a space time dependent quantity which is evident from the results displayed in Fig. 4.2.

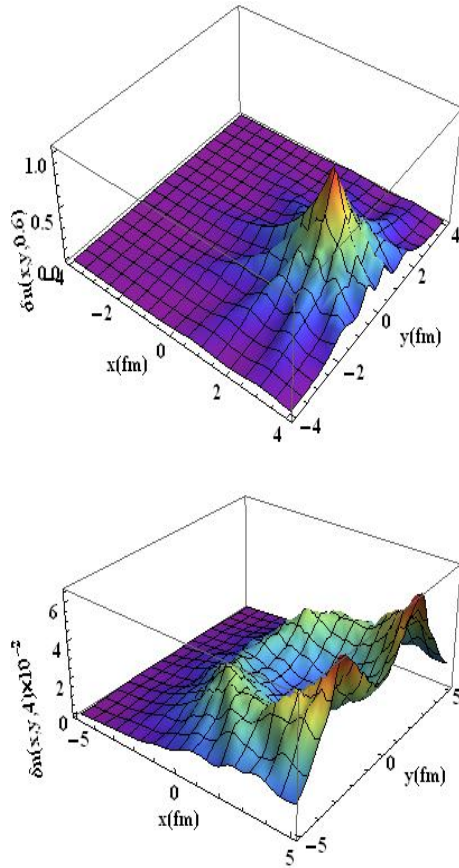


Figure 4.7: Same as Fig. 4.6 but the perturbation is given at a distance of 2.5 fm away from the origin along x -axis. The lower panel shows the results after a time 4 fm/c has elapsed.

The spatial anisotropic structure of the system formed in RHIC-E can be understood with the help of Fourier analysis in terms of its various coefficients. Work on the space-time evolution of the angular power spectrum for more realistic initial condition for the hydrodynamical solution derived from Glauber Monte-Carlo techniques is discussed in Ch. 5.

In Figs. 4.3 - 4.5 the evolution of the spatial anisotropic perturbations with different initial geometry like triangular, quadrangular and pentagonal for $n = 3, 4$ and 5 respectively have been depicted. We would like to see how these anisotropies dissipate. The perturbations introduce pressure gradient in the system. The magnitude of the perturbation gets reduced by the force arising due to pressure imbalance. It is observed that the spatial anisotropies of such perturbations dissipate fast. The

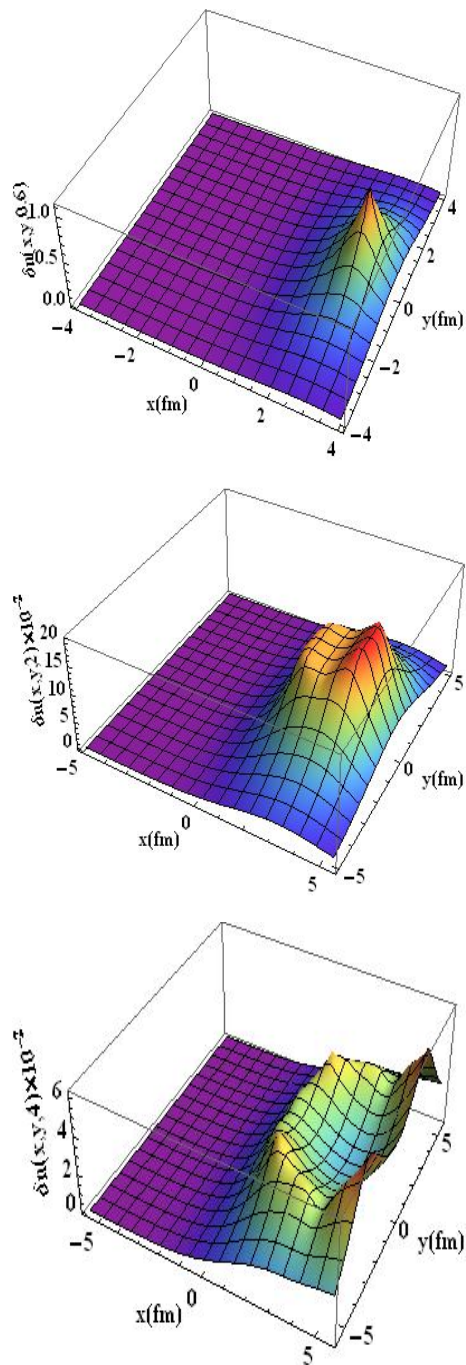


Figure 4.8: Same as Fig. 4.2 but the perturbation is given at a distance of 3 fm away from the origin along x -axis. The middle (lower) panel shows the results after a time 2 fm/c (4 fm/c) has elapsed.

propagation of these anisotropic perturbations are affected primarily by the velocity of sound in the QGP background as well as by the velocity of the fluctuation appearing in Ψ as $\vec{x} - \vec{p}(t - t_0)/p_0$, and hence, on the thermal mass of the degrees of freedom that constitute the perturbation. The splitting of the peaks are resulted from the expanding background with different magnitude of velocities due to different pressure gradient imposed by the initial geometry of the fluctuation. The propagating waves for the perturbation take shape analogous to water waves created on the calm surface if perturbed initially with similar geometric shape. Theoretical analysis of the angular power spectrum of the anisotropies arising from such perturbations in the evolving stage will shed light on possibility of selecting out the signatures of the early stage of the evolving matter.

In Fig. 4.6 we display an initial perturbation (introduced at $r = 0$) with smaller angular dimension implemented through a hendecagonal ($n = 11$) geometric shape to check whether such perturbations survive the evolution (upper panel). The fate of the perturbation after space-time evolution is depicted in the lower panel of Fig. 4.6. We observe that the perturbations of small angular size dissipate substantially. In fact, the perturbation with size corresponding to $n = 5$ and $n = 11$ look similar at a time 4 fm/c after the initial time. We introduce the initial perturbation at distance 2.5 fm away from the origin along the positive x -axis (upper panel, Fig. 4.7). It is clear from the results displayed in Fig. 4.7 (lower panel) that the perturbation moving outward (away from the centre) has suffered less dissipation compared to the one propagating inward and hence has a better chance to carry detectable signature.

An elliptic perturbation is imparted near the boundary (Fig. 4.8, upper panel), 3 fm away from the center along the (positive) x -axis. The fate of the perturbation after 2 fm/c and 4 fm/c are shown in the middle and lower panels of Fig 4.8 respectively. It is interesting to note that the perturbation propagating away from the center dissipates less and the one moving toward the center of the background QGP decay fast. Therefore, if any perturbation is created near the boundary the possibility of

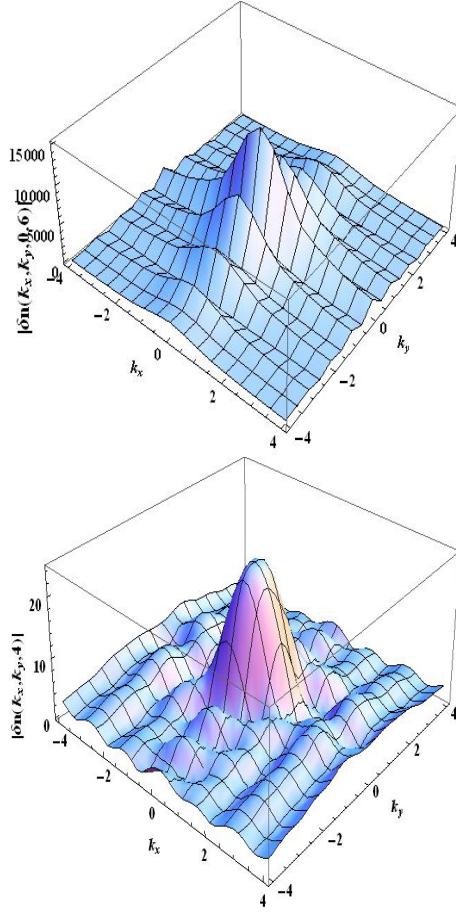


Figure 4.9: (upper panel). The fluctuations in k -space at time $\tau = 0.6$ fm/c (upper panel). The lower panel shows the results after a time 4 fm/c has elapsed. The mixing of k -modes is visible in the lower panel.

getting it detected is more.

The evolution of fluctuation, $\delta n(k_x, k_y, t)$ obtained by integrating $\delta \tilde{f}$ over p in transverse k -space is depicted in Fig. 4.9 for the initial shape at time 0.6 fm/c realized with $n = 2$ (Eq.4.1). We observe that the pattern of the perturbation changes substantially from its initial distribution (upper panel) due to the mixing of various k -modes (lower panel) at a later time (4 fm/c). The perturbation is propagating over a hydrodynamically expanding background which makes all the variables like, temperature (\bar{T}), flow velocity (v), pressure (\bar{P}), energy density (ϵ), etc explicit functions of time and space. The interaction of the perturbation (δf) with the background is incorporated through the relaxation time which is a function of temperature and hence space-time coordinates. Therefore, it is expected that various

modes of the perturbations in the Fourier space will get mixed during its propagation over the expanding background as clearly visible in Fig. 4.9 (lower panel). The peak of the fluctuation has reduced significantly due the exponential factor determined by the relaxation time. We discuss the evolution of correlation of anisotropic pressure perturbation in chapter 6.

4.5 Summary and discussion

The evolution of fluctuations have been studied in Refs [62, 68, 83–85, 95, 112] using relativistic hydrodynamical model. In contrast we use a more microscopic approach to investigate the evolution of fluctuations within the framework of BTE in a relativistically expanding QGP background. The background of the spatial fluctuations has been assumed as a thermalized expanding QGP. The expansion of the background has been dealt with the (2+1) dimensional relativistic hydrodynamical model. The evolution of initial spatial anisotropic perturbations with different geometry have been studied and analytical results have been obtained. It is found that the perturbations dissipate during its propagation, however, the creation of such anisotropic perturbations near the boundary of the plasma may lead to detectable effects. Theoretical analysis of these anisotropies will help in understanding the early stage of the matter. The mixing of various k -modes of the perturbations during the course of evolution has been demonstrated.

CHAPTER 5

Power Spectrum of Momentum Anisotropy and Trace of Non-equilibrium

This chapter contains part of paper [113]. Here effect of initial state fluctuations of produced system in RHIC, as well as effect of non-equilibrium perturbations on power spectra of final parton momentum anisotropy is discussed.

5.1 Introduction

At Relativistic Heavy Ion Collider (RHIC) and Large Hadron Collider (LHC) heavy nuclei are made to collide to create quark matter or quark gluon plasma (QGP) - a state of matter that prevailed in the micro-second old universe according to the cosmological Big Bang (BB) model. In this regard the production of QGP in nuclear collisions at relativistic energies is dubbed as Little Bangs (LB). One of the compulsion to study the QCD phase transition in Relativistic Heavy Ion Collision Experiments (RHIC-E) is to understand the non-abelian gauge theory in medium and to understand the dynamics of similar transition in the early universe. This is especially important because the universe has undergone several other transitions *e.g.* Electroweak, GUT, etc, but among these the QCD transition is the only one

which is accessible through the presently available accelerator energy. The study of the temperature fluctuation in the cosmic microwave background radiation (CMBR) originated from the recombination era (about 300,000 years after the BB) has provided crucial knowledge in supports of BB model [82, 114] and matter content of the universe. The polarization of photons due to Thomson scattering from the anisotropic decoupling surface (where the photon had suffered the last interactions) results in the non-zero quadrupole moment of the phase space distribution of the incident photon. This anisotropic fluctuations in density, for example, may be caused by the propagation of gravitational wave in the early universe. The temperature fluctuation in the CMBR is introduced as a perturbation in the phase space distribution of photons. The evolution of this perturbation is studied by using Boltzmann transport equation (BTE) [82, 101] in gravitational field. The linear polarization due to the scattering is connected with the quadrupole moment of the phase space distribution of photon.

In this work we would like to perform a theoretical analysis of LB following procedure similar to the one used in the analysis of CMBR. Study of fluctuation can be useful to characterize the state of the matter and also to put constraints on models [63, 115–118, 120–123]. Power spectrum in RHIC-E has been discussed by several authors in Refs. [86, 124–126]. In Ref. [86] the root mean square of various flow harmonics has been calculated and shown strong similarities with the power spectrum of CMBR. Mócsy and Sorensen [124] has extracted the power spectrum of the system produced in RHIC-E by using data on transverse momentum (p_T) correlations. In Ref. [126] data from ALICE collaboration has been used to estimate p_T fluctuation and subsequently expanded in Laplace series to estimate the power spectrum analogous to temperature fluctuation in CMBR. In Ref. [125] relativistic heavy ion collision events have been generated by using HIJING [127] and redistributed the produced particles to emulate flow effects to reproduce elliptic flow to some required value.

As mentioned before the state of the matter, the QGP created in RHIC-E imitates the condition that prevailed in the micro-second old universe. The space time evolution of the matter is governed by fluid dynamics for both BB and LB. However, there are glaring differences too. For example, the relevant interactions, characteristic length and time scales in LB and BB are very different, primarily because of the pertinence of gravity in the BB.

In the present work we will study the power spectrum due to fluctuations in the initial energy density that may arise naturally due to the quantum fluctuation of the finite "lump-like" nucleons within the colliding nuclei [87, 94]. These fluctuations evolve hydrodynamically [62, 83–85, 95, 112]. The bulk matter *i.e.* QGP created in RHIC-E with very high temperature and pressure will expand relativistically against vacuum. This expansion is treated in the present work by solving relativistic hydrodynamic equations in (3+1) dimensions with initial conditions derived from Optical as well as Monte-Carlo Glauber model [128]. The equation of state (EoS) is taken from lattice QCD. The system will revert to hadrons due to the cooling caused by the expansion. In the hadronic phase the system may continue to expand hydrodynamically until the mean free path of the constituents become too large to maintain equilibrium. When the hadrons cease to interact, their momenta get frozen and hit the detector with those values of frozen momenta. However, it has been shown that the chemical freeze-out of the hadrons takes place near the quark-hadron transition boundary, meaning that the system may be out of chemical equilibrium in the hadronic phase and the evolution of the hadronic phase can not be studied using hydrodynamics, it may require hybrid model approach (hydro+URQMD [129]) which is beyond the scope of the present work. Therefore, we will evaluate the power spectrum of QGP phase only in this work.

We will also study the power spectrum of anisotropic fluctuations in momentum space inflicted through the phase space distribution that may drive the system slightly away from equilibrium. The correlation that survive the evolution can be

observed in the final state and which may be connected to the initial state correlation [63, 120–122]. The variation of the power spectrum with time will indicate the dissipation of fluctuations created during the evolution. The nature of the variation may help in differentiating the fluctuations produced in the initial state from those created afterward. The evolution of such anisotropic fluctuations is dictated by the Boltzmann transport equation (BTE). The propagation of the jets through QGP may cause such fluctuations [130]. Therefore, we intend to study the evolution of the fluctuations through BTE in a hydrodynamically expanding QGP background. The BTE is solved in relaxation time (τ_R) approximation, τ_R has been taken from calculations done by using hard thermal loop approximation in QCD. In principle, τ_R is a function of temperature (T) and baryonic chemical potential (μ_B), however, as discussed below in the present case we need to consider the T dependence only. The change in T due to expansion of the bulk is controlled by relativistic hydrodynamics. This change in T affects evolution of the fluctuation (solution of the BTE) through the relaxation time, indicating a direct coupling between the anisotropic fluctuation and bulk expanding background. The BTE has been solved with initial conditions containing spatial anisotropies to be specified later.

The initial energy density distribution, $\epsilon(\tau, x, y, \eta)$ of the bulk matter created in RHIC-E can be estimated by using Glauber model. In the present work, both the Optical Glauber (OG) as well as the Monte-Carlo Glauber (MCG) models have been used to demonstrate the sensitivity of the results on initial conditions of the bulk matter. The finite size of the colliding nucleons with quantum fluctuations in the nuclear beams will create "lumpiness" in $\epsilon(\tau, x, y, \eta)$. This can be seen very clearly in $\epsilon(\tau, x, y, \eta)$ calculated using MCG. We study the evolution of these fluctuations using hydrodynamics at the surfaces of constant T . Power spectrum due to fluctuations caused by phase space perturbations has also been estimated. In the present work we make an attempt to evaluate the fluctuations in RHIC-E in keeping close resemblance with analysis of temperature fluctuation in cosmic

microwave radiation (CMBR). The power spectrum will be evaluated at various stages of the evolving system to understand how it changes with time.

This chapter is organized as follows. In the next section we will briefly discuss the evolution of the quark gluon plasma within the framework of relativistic hydrodynamics followed by discussions on the initial conditions and equation of state used in this work in the successive subsections. The evolution of the fluctuations within the scope of BTE has been discussed in section 5.3. The power spectrum has been evaluated in section 5.4. Section 5.5 is devoted to present the results and section 5.6 is dedicated to summary and discussions.

5.2 Hydrodynamic evolution of the quark gluon plasma

The expansion of the QGP in space and time can be described by applying relativistic hydrodynamics. The conservation of energy and momentum of the fluid is governed by the equation:

$$\partial_\mu T^{\mu\nu} = 0 \tag{5.1}$$

where $T^{\mu\nu} = (\epsilon + P)u^\mu u^\nu - g^{\mu\nu}P$. Here ϵ is the energy density, P is the pressure, $u^\mu = \gamma(1, \vec{v})$ is the four velocity of the fluid and $\gamma = 1/\sqrt{1 - v^2}$. The conservation of the net baryon number throughout the evolution history is controlled by the equation:

$$\partial_\mu (n_B u^\mu) = 0 \tag{5.2}$$

where n_B is the net baryon (baryon - antibaryon) density. However, in the present work we are interested in the system produced in nuclear collisions at the highest RHIC energies where n_B is negligibly small (n_B will be even smaller at LHC collision conditions) and hence $\mu_B \sim 0$. Therefore, we do not need to consider Eq. 5.2. In the

present work Eq. 5.1 has been solved numerically using standard technique [131] in full (3+1) space-time dimension without assuming boost invariance along longitudinal direction [110] and cylindrical symmetry of the system. The initial conditions and equation of state (EoS) used here are discussed briefly below.

5.2.1 Initial conditions

The initial conditions required to solve Eq. 5.1 in (3+1) dimension are as follows: The Cartesian components of initial flow velocities are: $v_x(\tau_0, x, y, z) = v_y(\tau_0, x, y, z) = 0$ and the initial energy density profile is taken as [131]:

$$\varepsilon(\tau_0, x, y, \eta_s) = \varepsilon_{GM}(x, y) \theta(Y_b - |\eta_s|) \exp \left[-\theta(|\eta_s| - \Delta\eta) \frac{(|\eta_s| - \Delta\eta)^2}{\sigma_\eta^2} \right] \quad (5.3)$$

where $\varepsilon_{GM}(x, y)$ is obtained from OG or MCG model, having the following expression

$$\varepsilon_{GM}(x, y) = \varepsilon_0 \left[\frac{1-f}{2} n_{part}(x, y) + f n_{coll}(x, y) \right] \quad (5.4)$$

We have taken the value of the inelastic nucleon-nucleon cross section at RHIC energy as, $\sigma_{NN} = 42$ mb in evaluating the number of participants, n_{part} and number of collisions, n_{coll} . In MCG model approach the energy density is deposited at discrete points, but for hydrodynamic evolution we need a continuous distribution of energy density. Therefore, we use Gaussian smearing to get the energy density as:

$$\varepsilon_{GM}(x, y) = \frac{1}{2\pi\sigma^2} \sum_i \varepsilon_{GM}(x_i, y_i) e^{-\frac{(x-x_i)^2 + (y-y_i)^2}{2\sigma^2}} \quad (5.5)$$

where $\varepsilon_{GM}(x_i, y_i)$ is obtained from Eq(5.4). To sample the nucleons from nuclei (Au in this case), we use the following Woods-Saxon distribution

$$\rho(r) = \frac{\rho_0}{1 + e^{\frac{r-R}{\delta}}}$$

The values of different parameters appeared in the above expressions are tabulated below.

Table 5.1: Table 5.1: Values of different parameters used in solving the hydrodynamical equations (see text for details).

Parameter	τ_0	Y_b	$\Delta\eta$	σ_η	ε_0	f	σ^2	R	δ	σ_{NN}
Value	0.6 fm/c	5.3	1.3	2.1	7.7 Gev/fm ³	0.14	0.16	6.37	0.535	42 mb

5.2.2 Equation of State (EoS)

The EoS for the QGP and the hadrons have been constructed following the procedure outlined in Ref [132]. We use excluded volume model [133] for hot hadrons and pQCD results [132,134,135] for the QGP phase. For a smooth crossover, a switching function is used as in [132] and the parameters are adjusted so as to match the Lattice QCD results. A brief description of the model used is as follows. We choose volume of hadrons to be proportional to mass, $v_i = m_i/m_0$ as in [132], where m_0 is a constant. We take $m_0 = 0.9$ for this work. The pressure of the hadronic medium is taken to be

$$p_{HG}(T, \mu_B) = \sum_{i=1} p_i^{id}(T, \tilde{\mu}_i) \quad (5.6)$$

$$\tilde{\mu}_i = \mu_i - v_i p_{HG} \quad (5.7)$$

where $\mu_i = B\mu_B$ and B is baryon number. p_i^{id} denotes the ideal pressure of a relativistic gas comprised of i^{th} resonance and p_{HG} is the pressure after excluded volume correction is taken into account which is found by solving the above set of equations in a self-consistent way.

The pressure of the QGP phase is taken as

$$P_{qgp} = \frac{8\pi^2}{45} T^4 \left[f_0 + \left(\frac{\alpha_s}{\pi}\right) f_2 + \left(\frac{\alpha_s}{\pi}\right)^{3/2} f_3 + \left(\frac{\alpha_s}{\pi}\right)^2 f_4 + \left(\frac{\alpha_s}{\pi}\right)^{5/2} f_5 + \left(\frac{\alpha_s}{\pi}\right)^3 f_6 \right] \quad (5.8)$$

where the coefficients f_n 's are given in the appendix B.1. The coupling, α_s has been taken from [136] calculated in three loop approximations. The pressure in the crossover region is taken to be

$$P(T, \mu_B) = S(T, \mu) P_{qgp}(T, \mu_B) + (1 - S(T, \mu)) P_h(T, \mu_B) \quad (5.9)$$

where the switching function $S(T, \mu)$ is taken as

$$S(T, \mu_B) = \exp\{-\theta(T, \mu_B)\} \quad (5.10)$$

$$\theta(T, \mu_B) = \left[\left(\frac{T}{T_0}\right)^r + \left(\frac{\mu_B}{\mu_0}\right)^r \right]^{-1} \quad (5.11)$$

We take $T_0 = 165$ MeV, $\mu_0 = 3\pi T_0$ and $r = 4$. With these parameter values we find a good agreement of our results with the lattice data [137].

5.3 Evolution of anisotropies and fluctuations

Evolution of phase space perturbation(δf) is obtained as discussed in Ch. 3.3. Once δf is known, perturbations in various thermodynamic quantities *e.g.* in energy density (ϵ), entropy density (s) etc can be obtained as follows. Deviation from the equilibrium value in the thermodynamic quantities may be incorporated through the deviation in the distribution function as discussed in Ch. 3.2.1.

The evolution of the flow velocity, energy density, pressure etc can be obtained from the solution of hydrodynamic equations. Temperature can be estimated from its dependence on energy density. The interaction of the expanding background

(hydrodynamics) with the perturbations (δf) at each space-time point is enforced through temperature (appearing through τ_R) and flow velocity which are obtained from the solution of the relativistic hydrodynamic equations. Therefore, the fluctuations involve interaction between equilibrium (hydrodynamics) and non-equilibrium (BTE) degrees of freedom. We assume that the effects of the out-of-equilibrium perturbation on the equilibrated background is negligibly small.

The formalism discussed there in chapter 3 can be used to any system where the fluctuations are evolving in an expanding background aided by: (a) initial distribution δf_{in} appearing in Eq. 3.37, (b) τ_R which is determined by the interaction at the microscopic level, (c) flow velocity and temperature determined by the solutions of hydrodynamic equations which needs, initial energy density and velocity distributions as well as the EoS.

In the present work we will apply this formalism to the system formed in RHIC-E. Therefore, we will use QCD based calculations for estimating $\tau_R(T)$ as: $\tau_R^{-1}(x) = 1.1\alpha_s T$ performed in Ref. [105] in HTL (Hard Thermal Loop approximation). We have used QCD equation of state (section 5.2.2) for solving hydrodynamical equations.

The power spectra have been evaluated for the following two scenarios for: (i) the fluctuation in the initial energy density obtained in OG and MCG models, (ii) fluctuations caused by perturbations in phase space distribution. The latter one has been evolved through BTE in an expanding thermal QGP background as discussed. To simulate different types of initial spatial anisotropy one may choose,

$$\delta f(p, \vec{x}, t_0) = A_0 \exp[-r(1 + a_n \cos n\vartheta)] \quad (5.12)$$

where n can be taken as $n = 2, 3, 4, 5, \dots$ to simulate different geometry for the initial anisotropy (see also [124]). We have set the perturbation centered around $r = |\vec{x}| = 0$ here. To investigate effect of such perturbation on momentum anisotropy

of particles emitted from constant temperature surfaces of the evolving QGP fluid, we take initial perturbation, δf with

$$A_0 = K \frac{C}{(1 + p_T/B)^\beta} \quad (5.13)$$

where, $C = 9.113 \times 10^{-4}$ (1/MeV²), $B = 1459$ MeV, $\beta = 7.7$ and $K = 3.6$ such that energy density carried by the perturbation($\delta\epsilon$) satisfy $\delta\epsilon/\epsilon \sim 0.01$. The power spectrum for other values of $\delta\epsilon/\epsilon$ will also be shown. This condition ensures negligible back reaction on background from the perturbations. This power law form of momentum dependence of perturbation, which is inspired by jet parton distribution, also ensures non-equilibrium nature of this perturbation. It also ensures the condition $\delta f/f_0 \ll 1$.

5.4 The power spectrum

We are now equipped to study the evolution of the power spectrum of the angular distribution of the particles which originates due to:

(i) fluctuations in initial energy density profile evaluated in OG and MCG models by using the momentum distributions of particles at various surfaces of constant temperatures with the help of mathematical expression given in [138]:

$$E \frac{dN_0}{d^3p} = \frac{g_i}{(2\pi)^3} \int_{\Sigma} d\sigma_{\mu} p^{\mu} f_0(x, p) \quad (5.14)$$

where $d\sigma_{\mu}$ is the surface element, p^{μ} is the 4-momenta of the particle and in Milne

coordinate these are expressed as follows [64, 131]:

$$\begin{aligned} d\sigma_\mu &= (\tau_f dx_f dy_f d\eta_f, -\tau_f d\tau_f dy_f d\eta_f, -\tau_f d\tau_f dx_f d\eta_f, -\tau_f d\tau_f dx_f dy_f) \\ &= \left(1, -\frac{\partial\tau_f}{\partial x_f}, -\frac{\partial\tau_f}{\partial y_f}, -\frac{\partial\tau_f}{\partial\eta_f}\right) \tau_f dx_f dy_f d\eta_f \\ p^\mu &= (m_T \cosh(y - \eta_f), p_x, p_y, m_T \sinh(y - \eta_f)/\tau_f) \end{aligned}$$

where η_f is the fluid rapidity, τ_f is the proper time, x_f and y_f are transverse coordinate for the fluid. p_x, p_y are the fluid momenta in Cartesian coordinate, y ($= \frac{1}{2} \ln \frac{p_0 + p_z}{p_0 - p_z}$) is the particle rapidity and $m_T = \sqrt{p_T^2 + m^2}$ is the transverse mass of the particle. In the above equation subscript f stands for fluid. Therefore,

$$p^\mu d\sigma_\mu = \left[m_T \cosh(y - \eta_f) - p_x \frac{\partial\tau_f}{\partial x} - p_y \frac{\partial\tau_f}{\partial y} - \frac{m_T \sinh(y - \eta_f)}{\tau_f} \frac{\partial\tau_f}{\partial\eta_f} \right] \tau_f dx_f dy_f d\eta_f$$

For massless particles, y is given by

$$y = -\ln \left[\tan \left(\frac{\theta}{2} \right) \right]$$

which is same as the pseudo-rapidity (η) of the particle.

(ii) We estimate the power spectrum of the perturbation in the momentum distribution of particles. The perturbation, δf has been obtained by solving Boltzmann equation in relaxation time approximation in an expanding QGP background. δf can be used to estimate perturbations in thermodynamic quantities as mentioned earlier. We use $f = f_0 + \delta f$ to estimate the p_T distribution of particles using Cooper-Fryer formula [138] as:

$$E \frac{dN}{d^3p} = \frac{g_i}{(2\pi)^3} \int_\Sigma d\sigma_\mu p^\mu [f_0 + \delta f(x, p)] \quad (5.15)$$

Now the quantities, EdN_0/d^3p or EdN/d^3p can be expanded in Laplace series in terms of spherical harmonics, $Y_{lm}(\theta, \phi)$ at a given transverse momentum (p_T) and

T . We identify pseudo-rapidity, η as the polar angle through the relation, $\eta = -\ln\{\tan(\theta/2)\}$.

The power spectrum of the fluctuations in the transverse momentum (p_T) distribution of particles can be estimated at surfaces of constant temperatures to understand its evolution as the system cooled down with the progression of time. The power spectrum of EdN/d^3p has been estimated as follows:

$$E \frac{dN}{d^3p} = \bar{N} + \sum_{l=1}^{\infty} \sum_{m=-l}^l a_{lm}(p_T, T) Y_{lm}(\theta, \phi) \quad (5.16)$$

where

$$\bar{N} = \frac{1}{4\pi} \int d\Omega \frac{dN}{d^2p_T dy} \quad (5.17)$$

the coefficients, a_{lm} 's are determined as follows:

$$a_{lm}(p_T, T) = \int d\Omega Y_{lm}^* E \frac{dN}{d^3p} \quad (5.18)$$

For determining power spectrum without perturbation we replace EdN/d^3p by EdN_0/d^3p in Eq. 5.18. The terms in Eq. 5.16 with different l corresponds to different angular scales: terms with larger l will have smaller angular resolution, $\theta_l = \pi/l$, [82] determines the value of the maximum l i.e. l_{max} . For heavy ion experiments at RHIC and LHC the resolution in pseudo-rapidity will govern the value of l_{max} .

Using standard techniques and properties of spherical harmonics, the angular power spectrum (C_l) of EdN/d^3p can be written as:

$$C_l(p_T, T) = \frac{1}{2l+1} \sum_m |a_{lm}|^2 \quad (5.19)$$

indicating the distribution of power of fluctuations among different angular scales determined by l . In CMBR fluctuation, C_l for the temperature fluctuation, $\Delta T(\theta, \phi)/T$ has been calculated theoretically and compared with experimental data which has

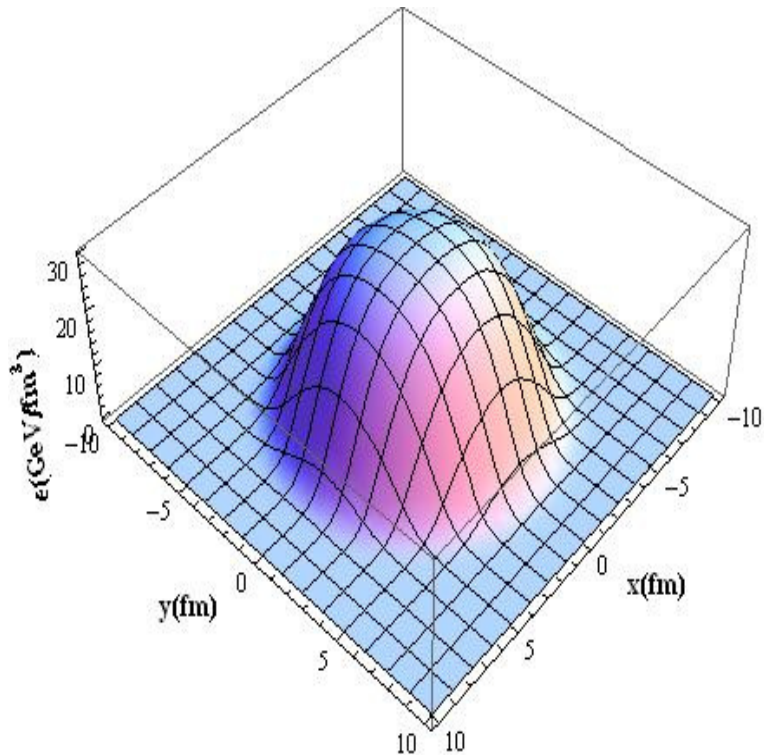


Figure 5.1: Initial energy density profile in the transverse plane at space time rapidity $= 0$ in the OG model for Au+Au central collision.

helped in understanding the matter content of the universe. The power spectrum, C_l 's are related to the various flow harmonics [139–144] as shown in appendix B.2.

5.5 Results

We have solved the (3+1) dimensional relativistic ideal hydrodynamic equations with initial conditions (due to OG and MCG models) and EoS described above to study the evolving QGP. The Boltzmann transport equation has been solved in relaxation time approximation in the evolving background to study the effects of perturbation on the phase space. The solution of BTE has been used to estimate the power spectrum. We present the results for the following two sets of conditions:

(i) The power spectrum of EdN_0/d^3p due to fluctuations in initial energy density.

We estimate the power spectrum of the p_T distributions of particles ($dN_0/d^2p_T dy$) for

OG and MCG initial conditions at surfaces of constant temperatures, say T_S , defined as $T(x, y, \tau, \eta_s) = T_S$ (where η_s is space-time rapidity) which implies, $\tau = \tau(x, y)$ on the surface at $\eta_s = 0$. We will evaluate the power spectrum at $T = T_S = 350$ MeV which is close to the initial temperature, near the transition temperature (T_c), at $T_S = T_c = 170$ MeV and at some intermediary temperature, $T = T_S = 250$ MeV to understand how the power spectrum evolve from the initial to the transition point.

(ii) The power spectrum of EdN/d^3p which contains the perturbations has also been estimated for $T_s = 170, 250$ and 350 MeV.

5.5.1 Initial conditions from Optical Glauber Model

First we consider (i): in Fig. 5.1 the initial energy density profile due to OG model is displayed for central Au + Au collision at $\sqrt{s_{NN}} = 200$ GeV. The thermalization time has been taken as $\tau_i = 0.6$ fm/c. Other parameters regarding the initial condition are displayed in table 5.1 in section 5.2.1. The profile evaluated at zero space-time rapidity has isotropic symmetry with sharp fall near the boundaries.

In Figs. 5.2 and 5.3, the surfaces of constant temperatures evolved hydrodynamically for initial energy density (shown in Fig. 5.1) have been depicted. Fig. 5.2 (Fig. 5.3) shows the result for $T = 350$ (170) MeV. We observe no qualitative change in the shape of the surfaces except at lower temperature the space-time size of the surface becomes larger. It is important to note that the energy density profile and consequently the constant temperature surfaces are smooth - not showing any distinct fluctuations because of the absence of fluctuation in the initial energy density profile in OG model.

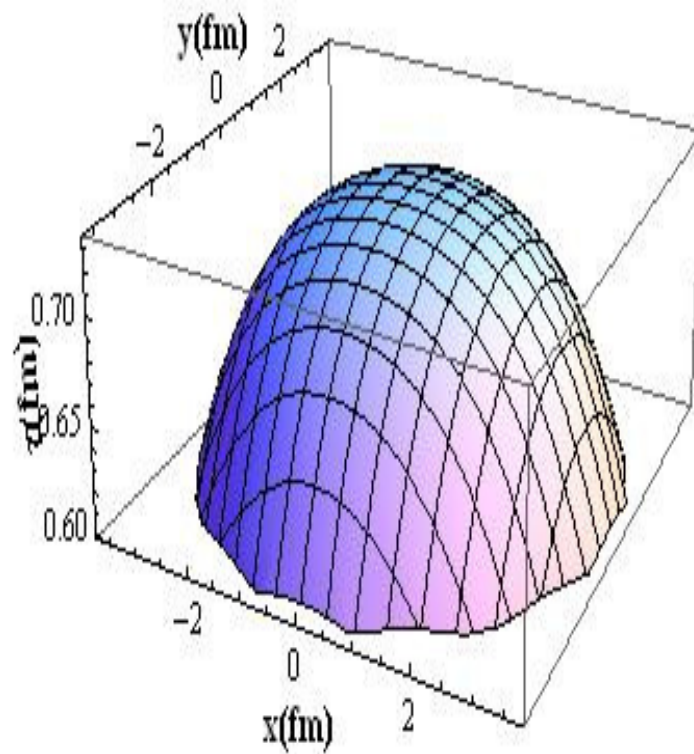


Figure 5.2: The constant temperature, $T = 350$ MeV surface in the time-transverse plane.

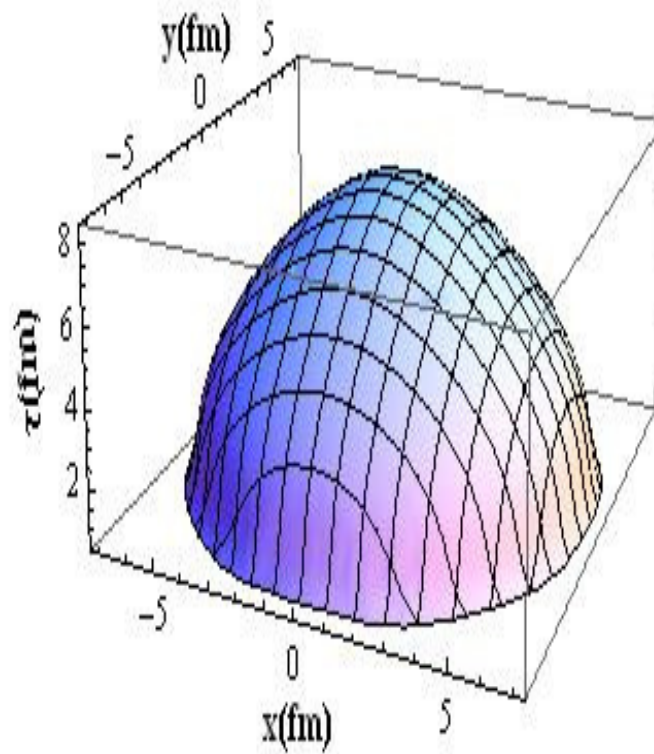


Figure 5.3: The constant temperature surface in the time-transverse plane for 170 MeV.

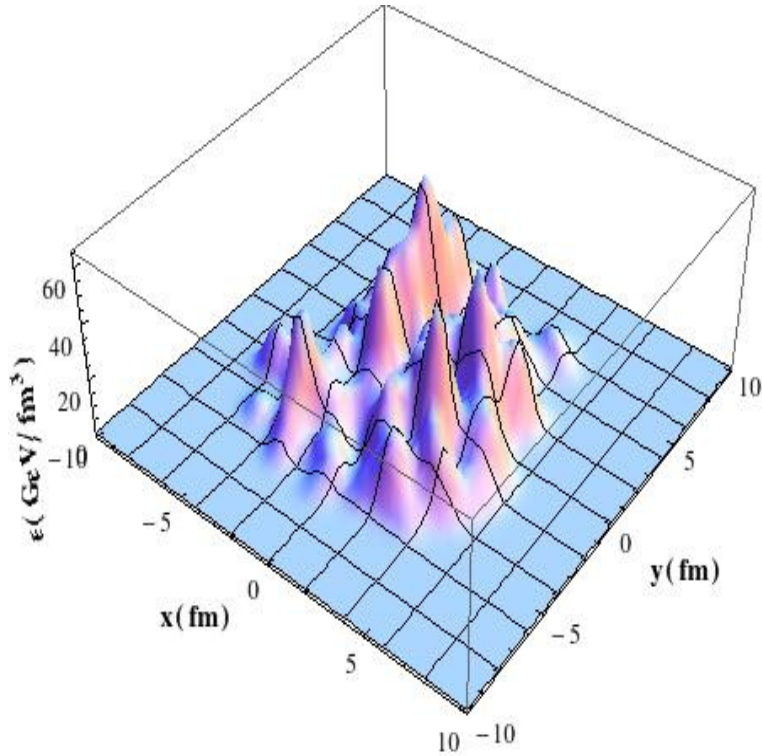


Figure 5.4: Same as Fig. 4.2 with MCG initial condition for a single event.

5.5.2 Initial conditions from Monte Carlo Glauber model

Similar to the OG initial condition we plot the initial energy density profile evaluated in MCG model for 0 – 5% centrality collision of Au + Au at $\sqrt{s_{NN}} = 200$ GeV in Fig. 5.4 at $\tau_0 = 0.6$ fm. We observe lumpiness of complicated nature in the initial energy density profile at various position in the transverse plane due to the collisions of nucleons with fluctuating positions in the beam nuclei.

However, averaging of energy density over 100 events smoothen the energy density profile to a great extent. The result displayed in Fig. 5.5 has been obtained by averaging over 100 events. We will use this profile as an input to rest of the works.

The constant temperature surface at $T = 350(250)$ MeV is displayed in (τ, x, y, η_s) coordinate in Fig. 5.6 (Fig. 5.7) for MCG initial condition. It is observed that the initial energy density in MCG model has more fluctuations than that of OG model in space time coordinate. These inhomogeneities will create pressure imbalance with

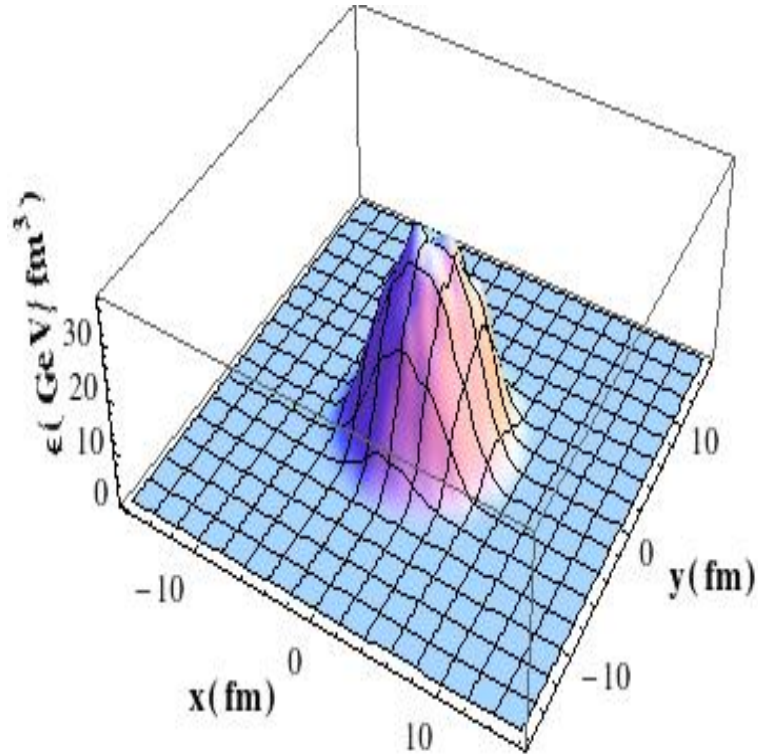


Figure 5.5: Same as Fig. 5.1 with MCG initial condition averaged over 100 events.

the neighbouring zones - higher density domains will exert larger pressure and hence will expand faster to smoothen the inhomogeneities. As a result the inhomogeneity will reduce and their distributions will change. We observe that the size of the surface in space-time coordinate has increased at lower temperature. The fluctuations at the surface at $T = 350$ MeV resulting from the inhomogeneities in the initial energy density profile have reduced in magnitude at $T = 250$ MeV surface as the system evolve hydrodynamically. The domains of higher energy densities (Fig. 5.5) will take longer time to reach a given temperature as can be seen from Fig. 5.6 where for certain domains τ is larger compared to others. We observe that the differences in the values of $\tau(x, y)$ at various points in $x - y$ plane is smaller in the $T = 170$ MeV surface than at $T = 350$ or 250 MeV surfaces. Indicating that the system is approaching toward a homogeneous one in coordinate space and through expansion this inhomogeneities get transferred to momentum space. However, the magnitude of fluctuations have reduced in real space at lower temperature, $T = 170$ MeV

(Fig. 5.8).

5.5.3 Pseudo-rapidity and angular distributions

In Fig. 5.9, the η (upper panel) and θ (lower panel) distributions of particles have been displayed at the surface of constant temperatures, $T = 350$ MeV. We find that the fluctuations in differential particle numbers is larger at MCG than OG model, which is clearly visible both in the η and θ distributions. However, with progress in time or with the reduction of temperature at $T = 170$ MeV (Fig. 5.10) the total number of particles increase and more particles appear at larger η enhancing the width of the distributions. The θ distribution shows a plateau over a larger domain of θ as compared to the distribution at $T = 350$ MeV. Moreover, the peak of the invariant momentum distribution is larger at $T = 170$ MeV than at $T = 350$ MeV, because of the increase in the normalization resulting from larger freeze-out surface. It is also observed that the changes in fluctuation is larger for a system with MCG initial condition than OG initial condition. The difference in fluctuation between OG and MCG model at $T = 170$ MeV is smaller than the difference at $T = 350$ MeV.

5.5.4 Power spectrum without perturbation

Next we would like to investigate - how the power spectrum of the fluctuations caused by initial energy density profiles evolves. We study the power spectrum of particle spectra, EdN_0/d^3p at the surfaces of constant temperatures at $T = 350, 250$ and 170 MeV. The angular distribution of particles at constant p_T has been analyzed by decomposing it in terms of spherical harmonics as discussed in section 4.

The power spectrum of the distribution, C_l has been plotted in Fig. 5.11 for the angular distribution of the spectra at $T = 350$ MeV for the OG and MCG initial

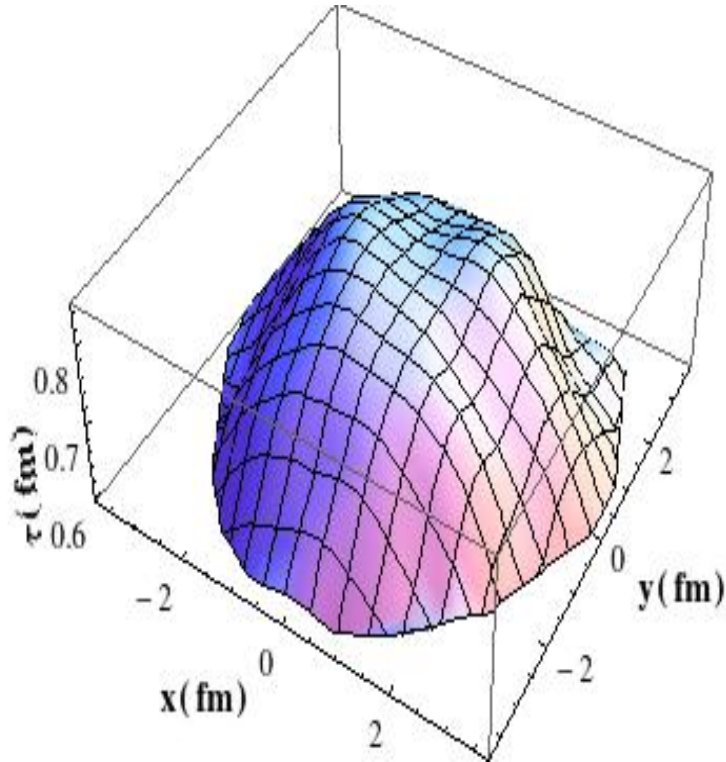


Figure 5.6: The constant temperature surface at $T = 350$ MeV for MCG initial condition.

conditions. We clearly find that the power spectrum corresponding to the odd l 's are negligibly small because the distribution is an even function of θ .

In Figs. 5.12 and 5.13 the power spectrum for the angular distribution at the surface of $T = 250$ and 170 MeV respectively have been depicted. We observe that there is no significant change in the power spectrum for the OG initial conditions at lower temperatures. With time, the spatial inhomogeneities in $x - y$ plane (which are translated into momentum space due to force caused by pressure gradient) of the system gets reduced as the system favours to erase out any pressure imbalance, however, for systems without fluctuation as in OG case, does not show much change. In case of OG initial conditions the system is symmetric, (Fig. 5.1) therefore, with the evolution from higher to lower temperatures (Fig. 5.2 and 5.3) there is no significant change in the power spectrum.

However, for MCG initial condition, the system is inhomogeneous (Fig. 5.5). The

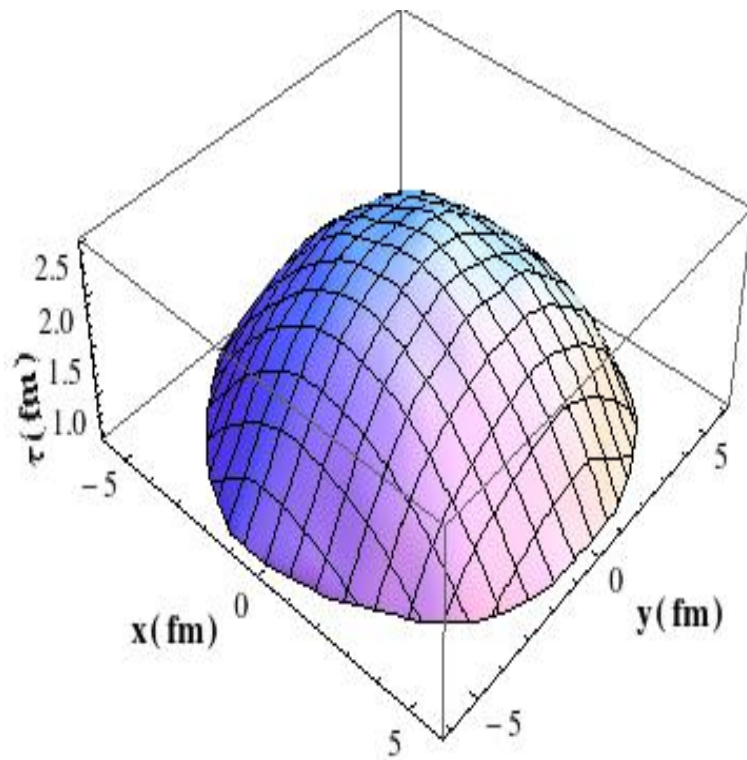


Figure 5.7: Same as Fig. 5.6 for MCG initial condition at $T = 250$ MeV.

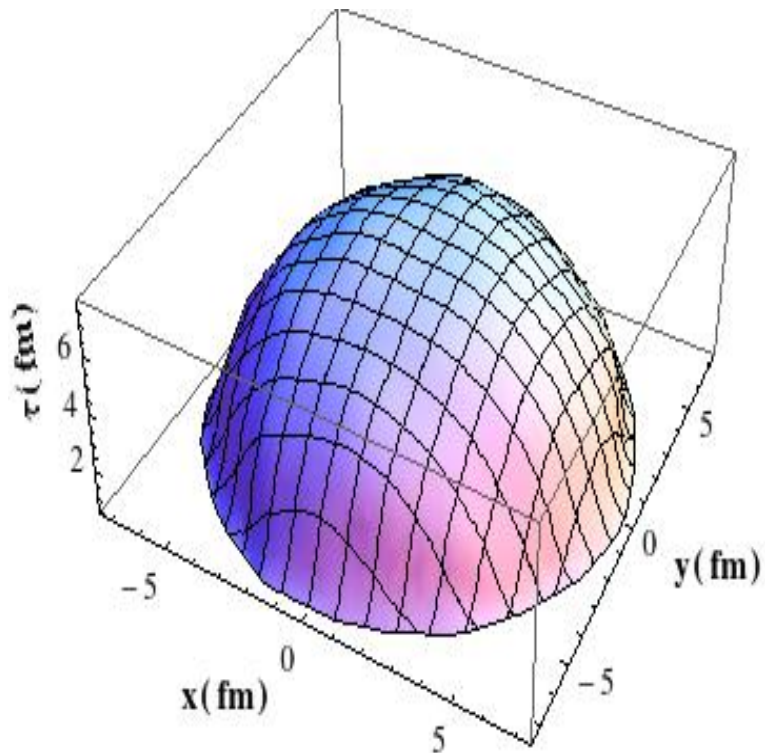


Figure 5.8: Same as Fig. 5.6 at $T = 170$ MeV.

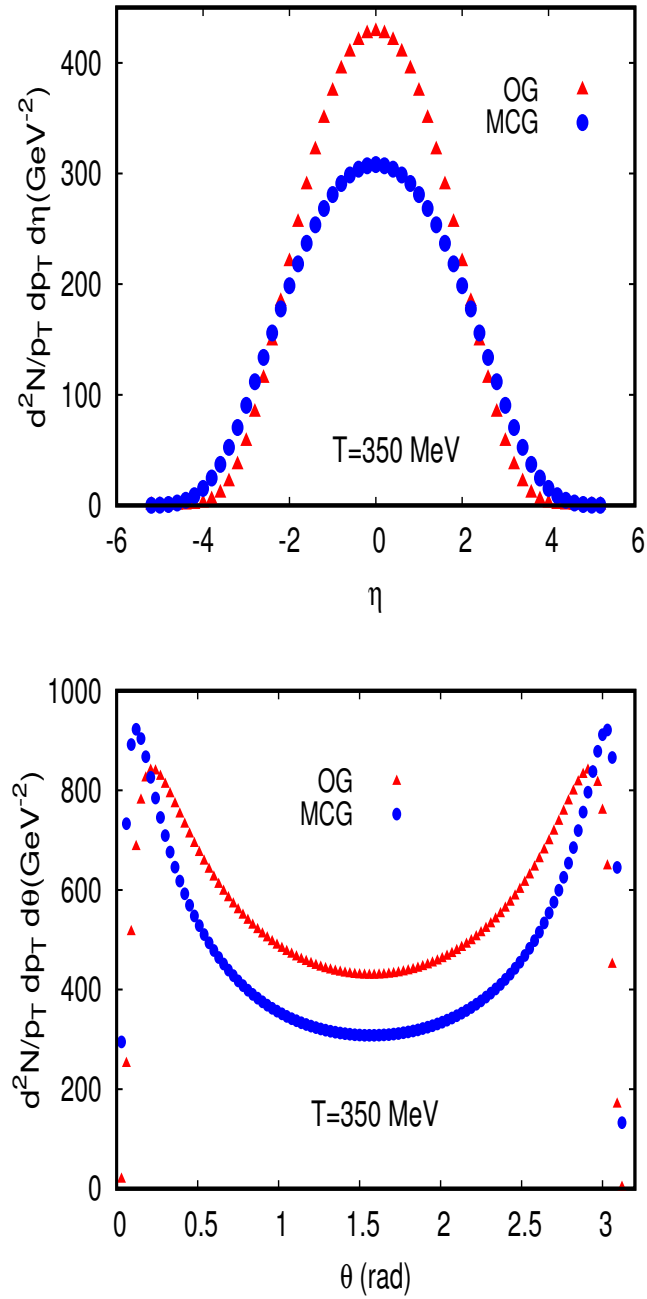


Figure 5.9: The pseudo-rapidity (η) and angular (θ) distribution of particles at $p_T = 0.6$ GeV with OG and MCG initial conditions at $T = 350$ MeV.

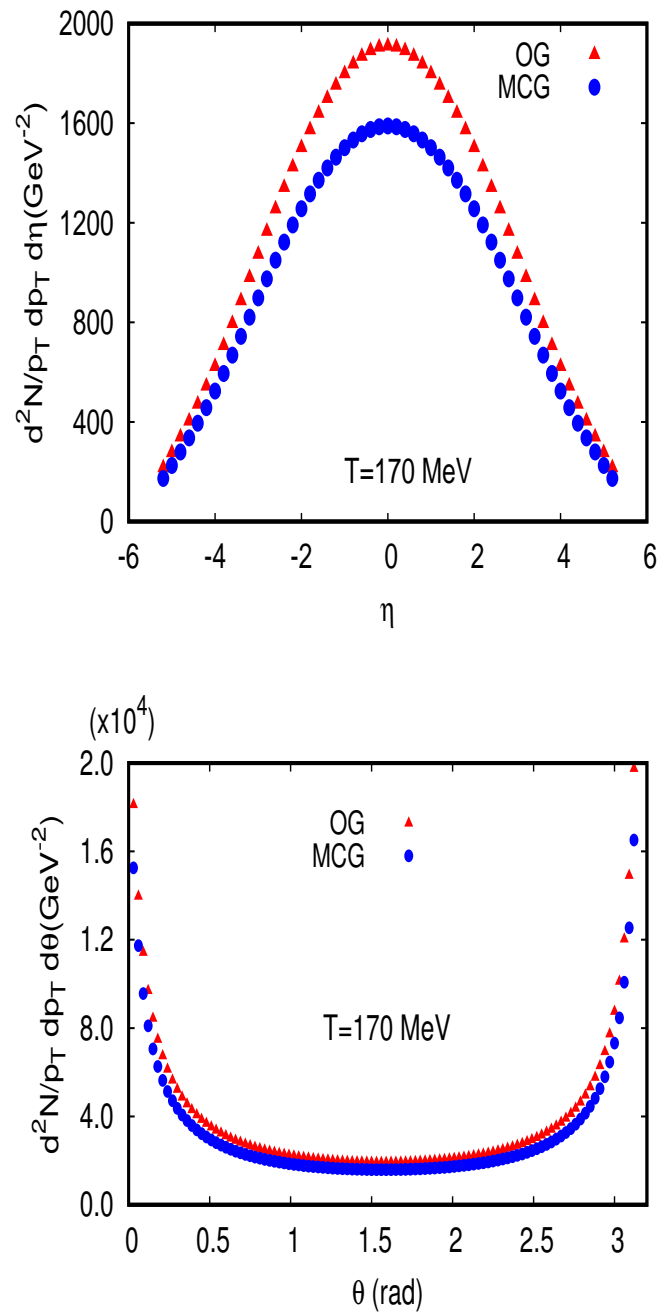


Figure 5.10: Same as Fig. 5.9 at $T = 170$ MeV.

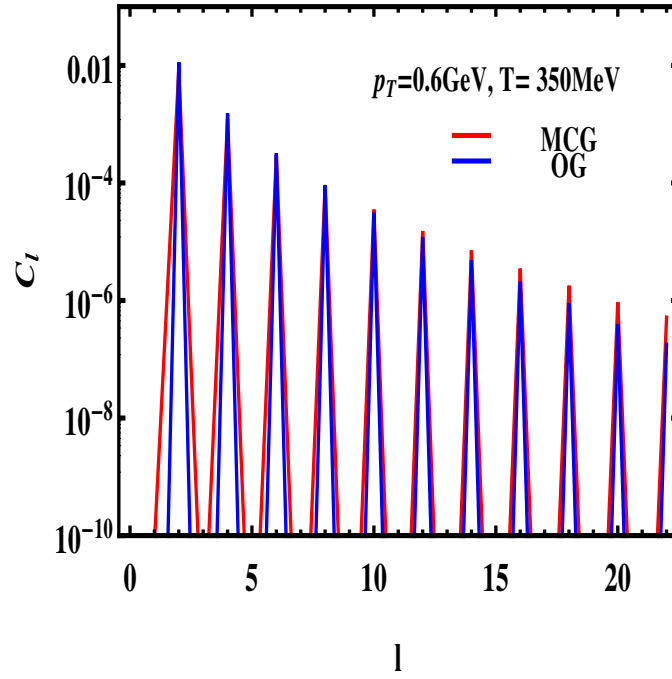


Figure 5.11: The power spectrum, C_l deduced from $dN/d^2p_T dy$ at $p_T = 0.6$ GeV for both the OG and MCG initial conditions analyzed at the surface of $T = 350$ MeV.

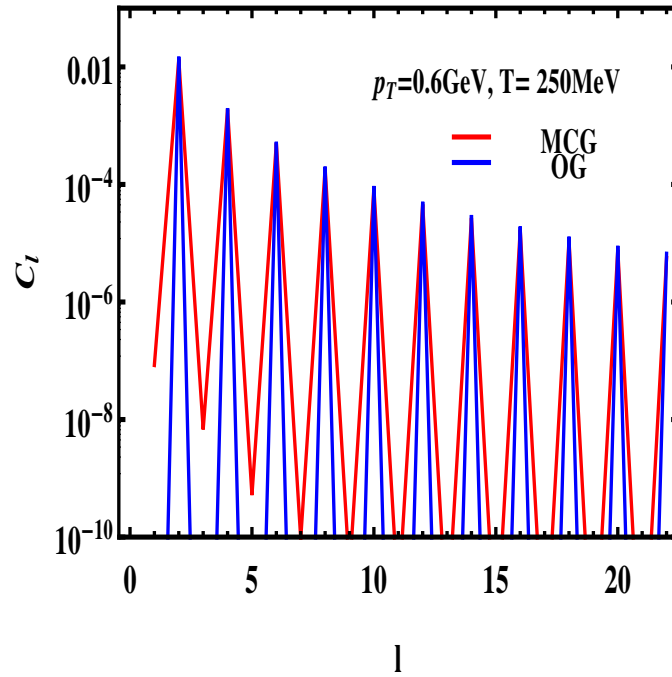


Figure 5.12: Same as Fig. 5.11 at $T = 250$ MeV.

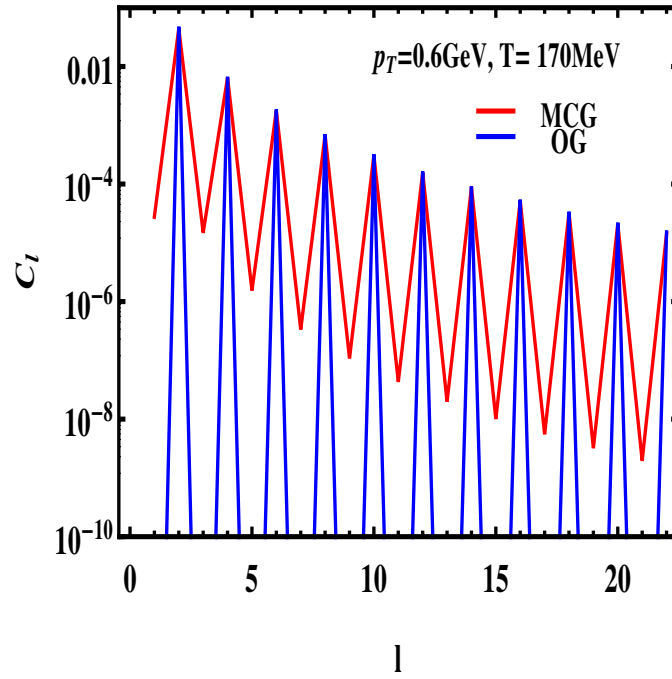


Figure 5.13: Same as Fig. 5.11 at $T = 170$ MeV.

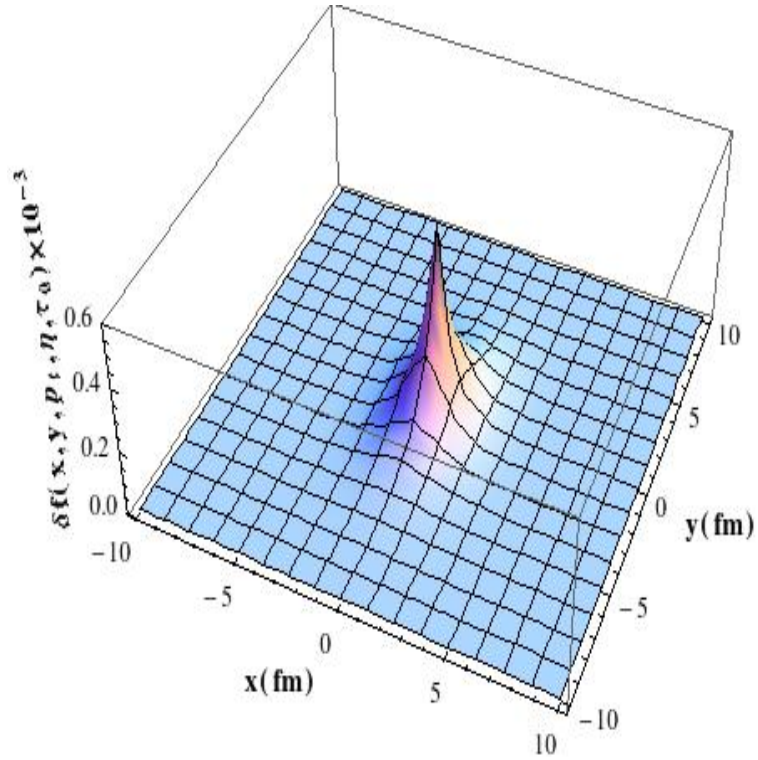


Figure 5.14: The initial perturbation δf given in Eq. 5.12 with $n = 2$ for $p_T = 1$ GeV at $\eta = 0$.

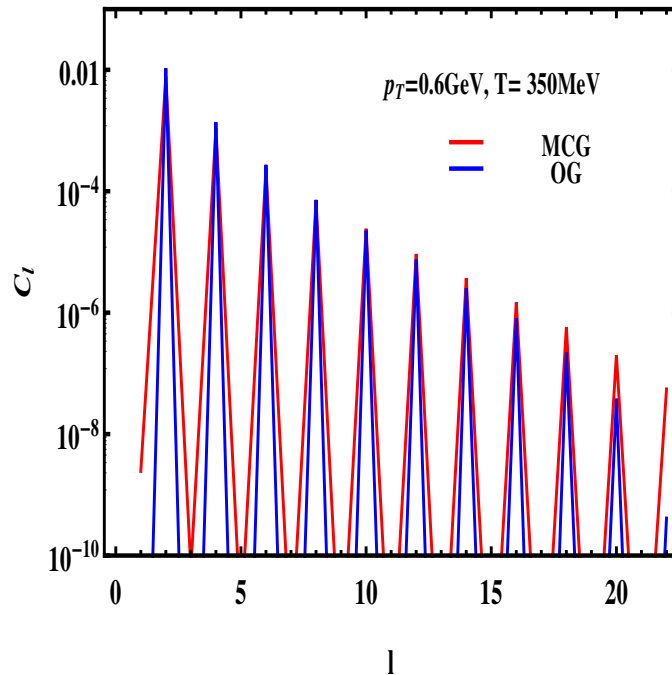


Figure 5.15: The power spectrum of the perturbation at $T = 350$ MeV for perturbation shown in Fig 5.13. The red (black) line shows results for OG (MCG) initial conditions for $p_T = 0.6$ GeV/ c

pressure gradients caused by the inhomogeneity acts in favor of reducing it during the course of expansion from higher to lower temperature. Therefore, it is clearly seen that the power spectrum of the system appears to be different at $T = 250$ MeV (Fig. 5.12) as the contribution from odd l are enhanced compared to its value at $T = 350$ MeV (Fig. 5.11). We also note that C_l 's increase with lowering of temperatures both for OG and MCG initial conditions (see later). It is well known that smaller (larger) l 's resolve larger (smaller) angular anisotropy. The value of l sets the angular scale, $\theta_l = \pi/l$. The most interesting aspect is that at lower temperatures ($T = 170$ MeV, Fig. 5.13), the power spectrum at odd l 's appear with non-zero values. The enhancement of the odd l 's is a signature of the presence of inhomogeneities in the initial condition. The increase in C_l 's for large l at lower temperature ($T = 170$ MeV) indicates appearance of smaller angular fluctuations.

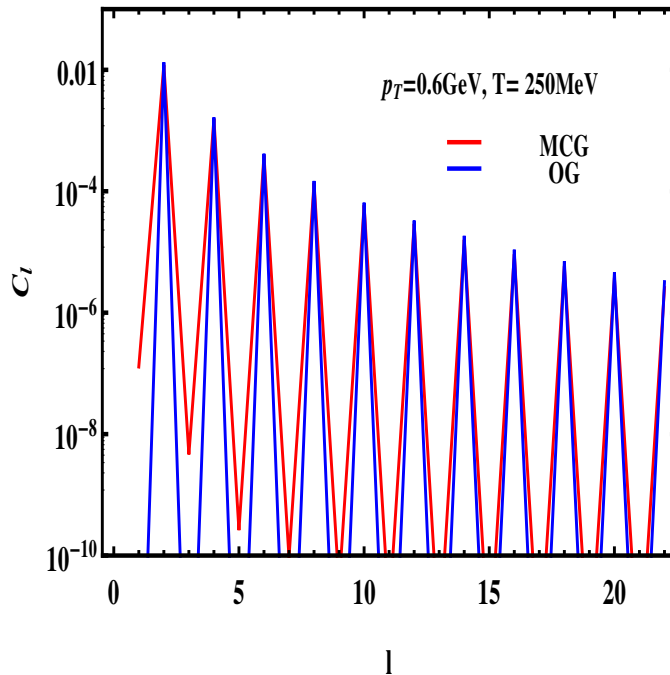


Figure 5.16: Same as Fig 5.15 at $T = 250$ MeV

5.5.5 Power spectrum with perturbation

So far we have discussed the evolution of power spectrum created in the initial collision dynamics. However, fluctuations represented by δf may be caused by other sources also, *e.g.* propagation of jets through the medium may create such fluctuations. Therefore, next we make some case studies on the propagation of fluctuations by introducing perturbations, $\delta f(\vec{p}, \vec{x}, t)$ in phase space distribution. In Fig. 5.14 the initial perturbation δf , obtained by solving BTE (Eq. 5.12 for $n = 2$) has been displayed. We study the power spectrum of EdN/d^3p for the perturbation shown in Fig. 5.14. C_l at $T = 350, 250$ and 170 MeV, for both OG and MCG are depicted in Figs. 5.15, 5.16 and 5.17 respectively for $p_T = 0.6$ GeV. We recall that inhomogeneity is more in MCG than OG initial conditions. Therefore, this study gives us an opportunity to learn how the local fluctuations (due to δf) evolve with the inhomogeneities in the expanding background *i.e.* how the inhomogeneous background affects the evolution of perturbation.

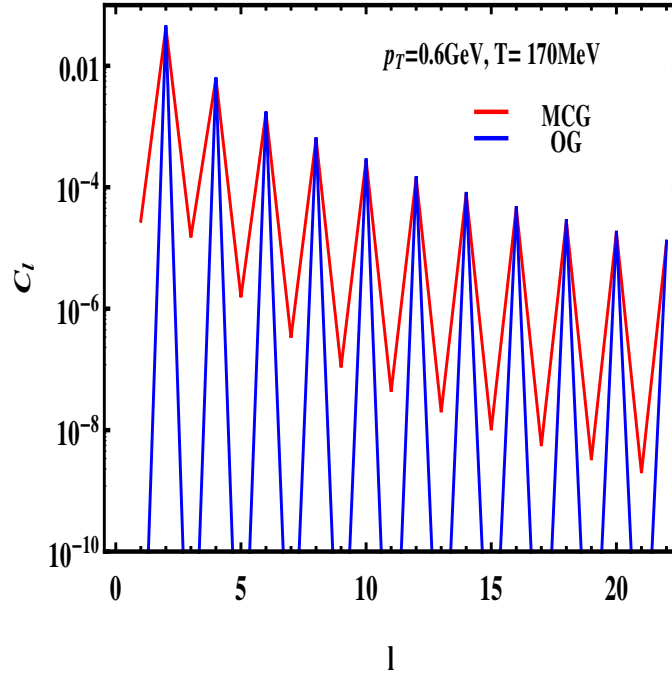


Figure 5.17: Same as Fig. 5.15 at $T = 170$ MeV.

We find that the spectrum with OG initial condition remains largely unaltered. However, the amplitude of the spectrum with MCG initial conditions changed significantly. For both the initial conditions C_l 's for odd l 's are small at large T . This is because the perturbation, δf for $n = 2$ has a symmetry under the transformation $\theta \leftrightarrow -\theta$ indicating the dominance of even l through spherical harmonics. However, for MCG initial condition C_l with odd l appear to be non-zero. The presence of non-zero inhomogeneity in the background in MCG initial condition breaks the $\theta \leftrightarrow \theta$ symmetry at lower T (later time) and consequently C_l 's with odd l 's appear. Therefore, emergence of odd l 's in this particular case indicate the presence of inhomogeneous background. It is to be noted that for small perturbations, characterized by $\delta\epsilon/\epsilon < 1$ the C_l 's with perturbation are close to C_l 's without perturbation. The power spectrum with perturbation at $p_T = 1.5$ GeV are displayed in Figs. 5.18, 5.19 and 5.20. The amplitude of the spectrum is qualitatively similar but quantitatively smaller at all temperatures compared to the case with $p_T = 0.6$ GeV. We find significant enhancement of odd l 's at $T = 170$ MeV.

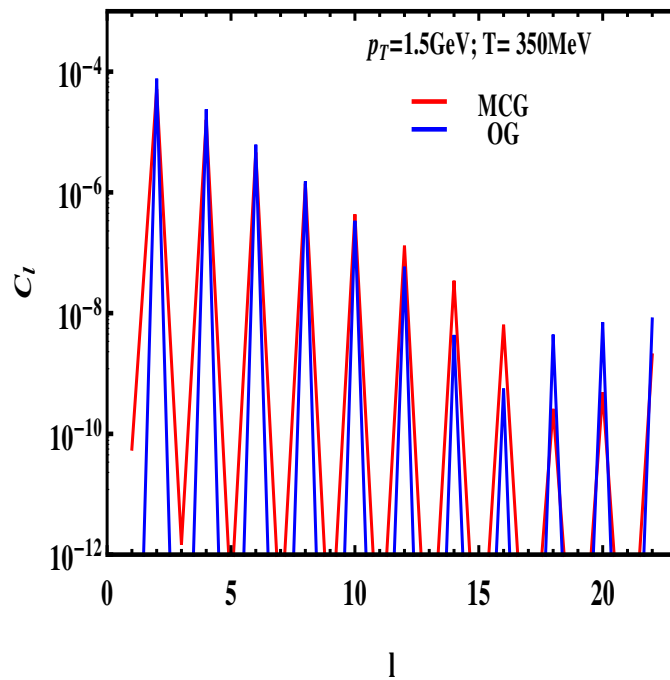


Figure 5.18: Same as Fig 5.15 for $p_T = 1.5 \text{ GeV}/c$

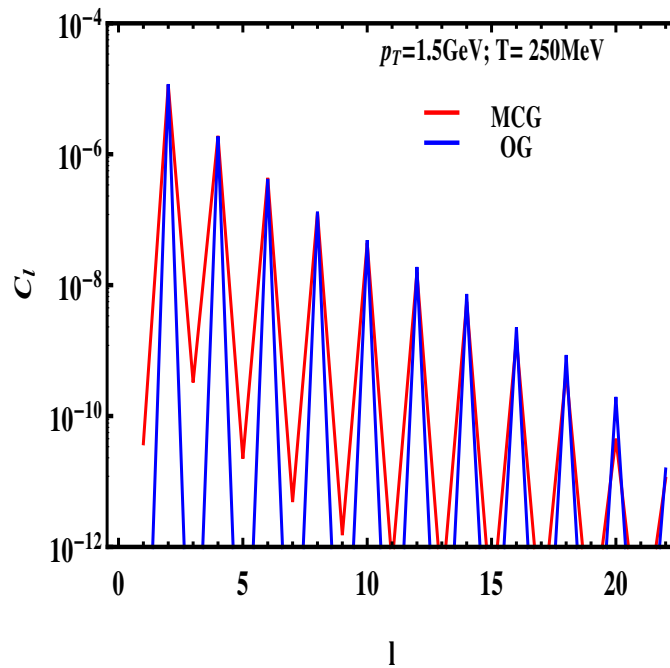


Figure 5.19: Same as Fig 5.16 at $T = 170 \text{ MeV}$

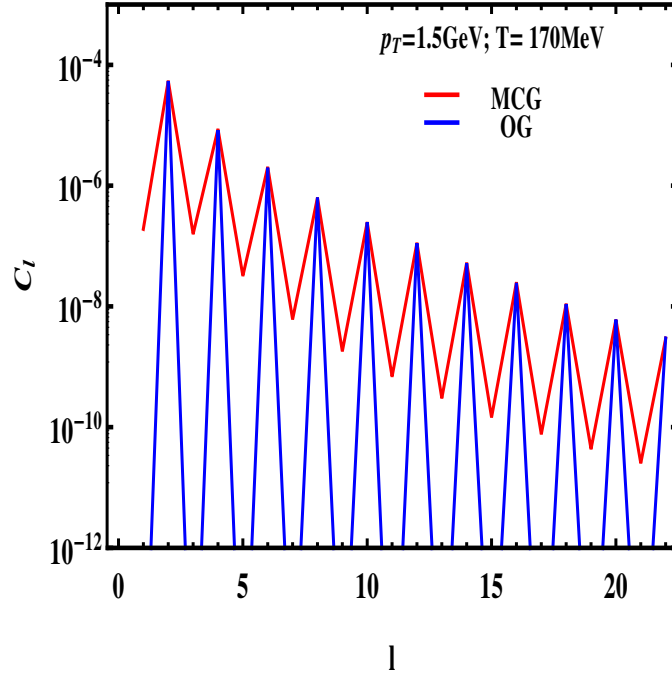


Figure 5.20: Same as Fig 5.17 for $p_T = 1.5 \text{ GeV}/c$

5.5.6 Variation of C_l with T

(i) First we discuss the variation of C_l with T without perturbation. The variation of power spectrum with T for different l has been displayed in Fig. 5.21. The C_l 's for small l decrease with T monotonically at low T and reach a plateau at higher T . The C_l 's for larger (smaller angular scale) l does not show much variation with T . Similar quantities have been depicted in Fig. 5.22 for MCG initial condition. The fall is faster in case of MCG initial conditions. In Fig. 5.23 the variation of power spectrum with T for odd l has been depicted. We clearly observe that the C_l for odd l falls faster with T as compared to even l . At small T (late time) fluctuation with smaller angular scale appear.

(ii) Now we discuss the T variation of power spectrum with inclusion of perturbation (δf) for even l (the values with odd l 's are very small). In Fig. 5.24 (Fig. 5.25) the C_l is plotted as a function of temperature for $p_T = 0.6 \text{ GeV}$ for OG (MCG) initial condition. The variation is similar to case (i). This is because at low $p_T \sim 0.6 \text{ GeV}$

particles from background dominates, *i.e.* perturbation has hardly any effect.

Fig. 5.26 shows T variation of C_l without perturbation for particles with $p_T = 3$ GeV. We find that C_l is smaller at low T than at high T because of the Boltzmann suppression of $p_T = 3$ GeV particles at low temperature in the background. However, a very different T variation of C_l is observed with the introduction of p_T dependent perturbation as given in Eq. 5.13. In the intermediate p_T we find non-zero C_l which is arising entirely due to the presence of perturbations Fig. 5.27.

To study the dependence of C_l on the strength of perturbation we change δf such that the corresponding $\delta\epsilon/\epsilon = 0.3$. With this value of δf we estimate C_l and plot its variation with T for different l in Fig. 5.28. We find that with increase in strength of perturbation the effect of background gets suppressed.

We have observed a similar behavior for OG initial conditions also. It is also observed that the variation of C_l with T for odd l with and without perturbation look similar. However, for even l the variation without (Fig. 5.26) and with (Fig. 5.27) perturbation are distinctly different and this difference originates from the perturbation with $\theta \leftrightarrow -\theta$ symmetry introduced thorough initial δf . Therefore, this distinct behavior of C_l in the presence of perturbation traces the non-equilibrium aspects of the system.

5.5.7 Relation between flow harmonics and power spectrum

The η and p_T dependence of various flow harmonics can be calculated from the power spectrum using the following relation (see appendix B.2 for derivation):

$$2\pi \frac{dN}{p_T dp_T dy} v_k = \sum_{l \geq k}^{\infty} \sqrt{\frac{2l+1}{4\pi} \frac{(l-k)!}{(l+k)!}} [a_{l,k} + (-1)^k a_{l,-k}] P_l^k(\cos \theta)$$

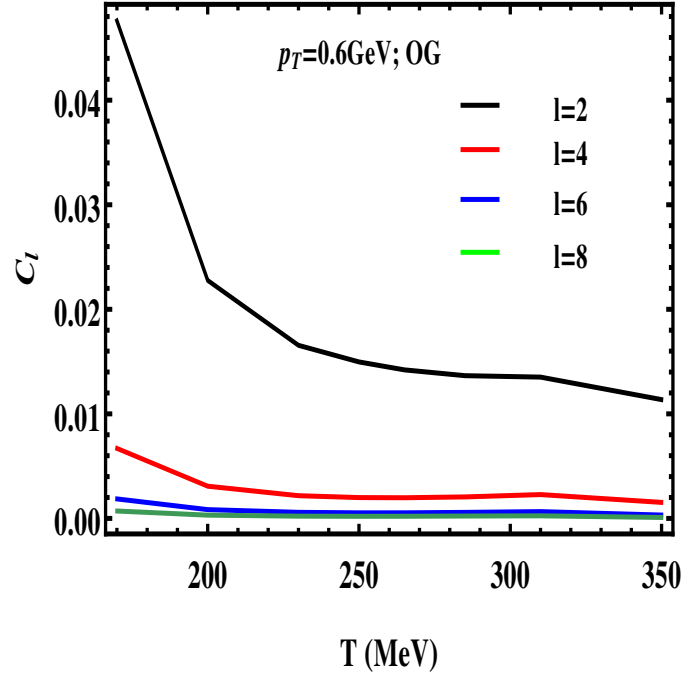


Figure 5.21: The temperature variation of power spectrum with OG initial condition for different l values.

For example, the elliptic flow can be calculated by using values of P_l^k as:

$$v_2 = \left(\frac{dN}{2\pi p_T dp_T dy} \right)^{-1} \text{sech}^2 \eta [a'_{22} + a'_{32} \tanh \eta + a'_{42} (7 \tanh^2 \eta - 1) + \dots] \quad (5.20)$$

where

$$a'_{22} = \frac{1}{3} \sqrt{\frac{5}{12\pi}} a_{22}, \quad a'_{32} = 15 \sqrt{\frac{7}{120\pi}} a_{32}, \quad a'_{42} = \frac{15}{2} \sqrt{\frac{1}{40\pi}} a_{42}, \quad (5.21)$$

where a_{lm} is a function of p_T and given by Eq. 5.18. The fluctuations in v_2 and its dependence on kinematic variables can also be estimated from the analysis of EdN/d^3p presented here. The fluctuations of other harmonics and its dependence on p_T , η can also be calculated using similar procedure. In principle this mathematical expression will be very useful in estimating the fluctuations in various harmonics due to perturbations.

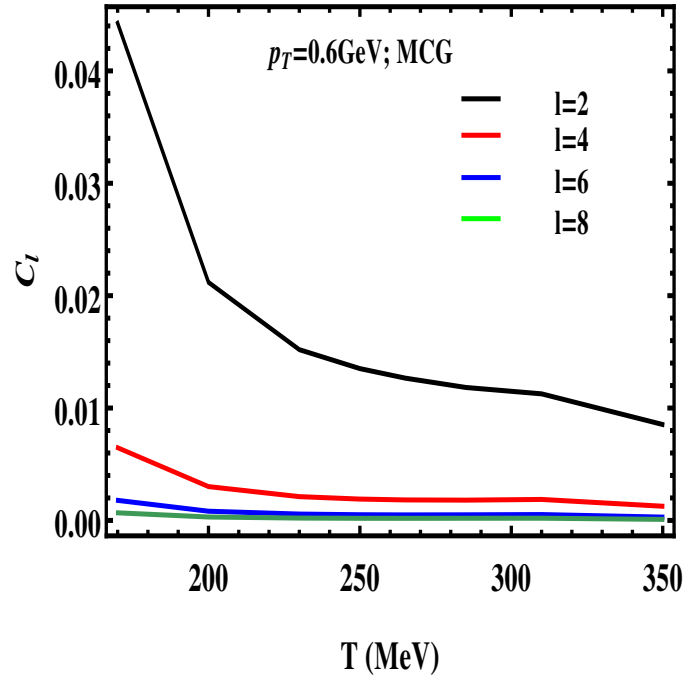


Figure 5.22: The variation of power spectrum for even l with temperature for MCG initial condition.

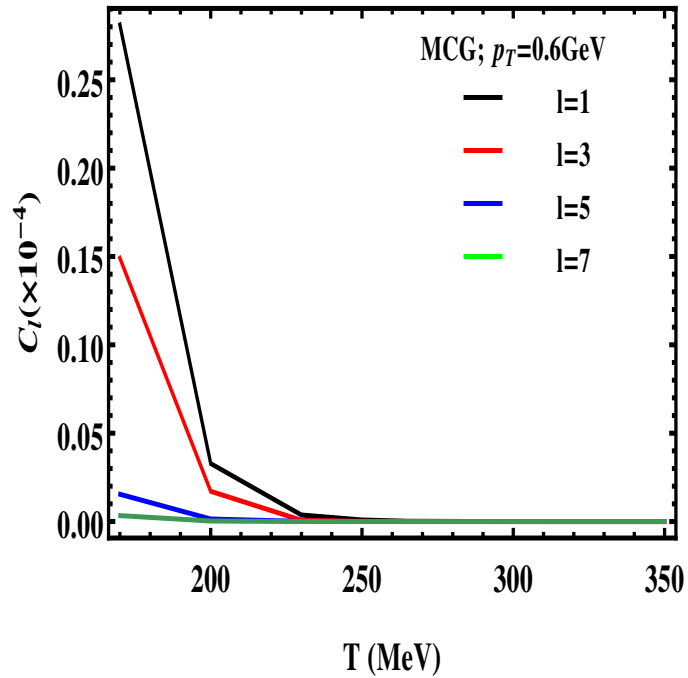


Figure 5.23: The variation of power spectrum for odd l with temperature for MCG initial condition.

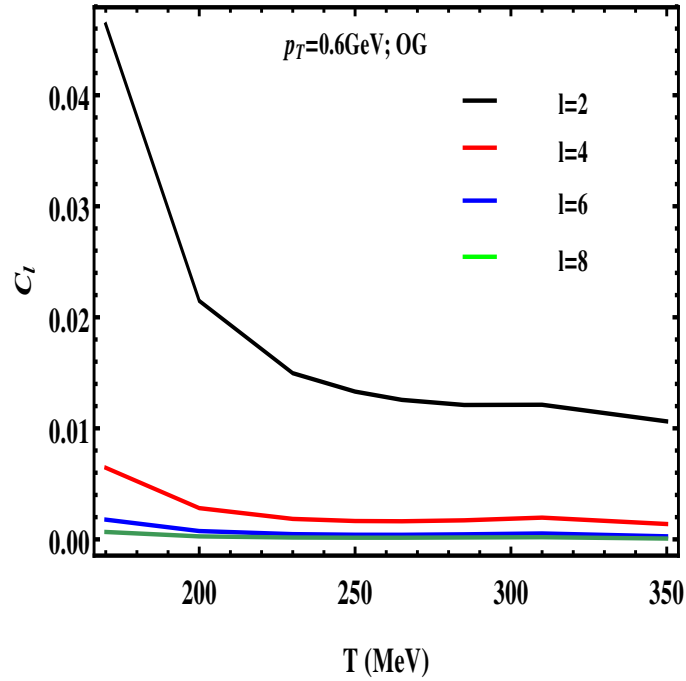


Figure 5.24: The variation of power spectrum with temperature for OG initial condition with perturbation at $p_T = 0.6$ GeV/ c (see text for details).

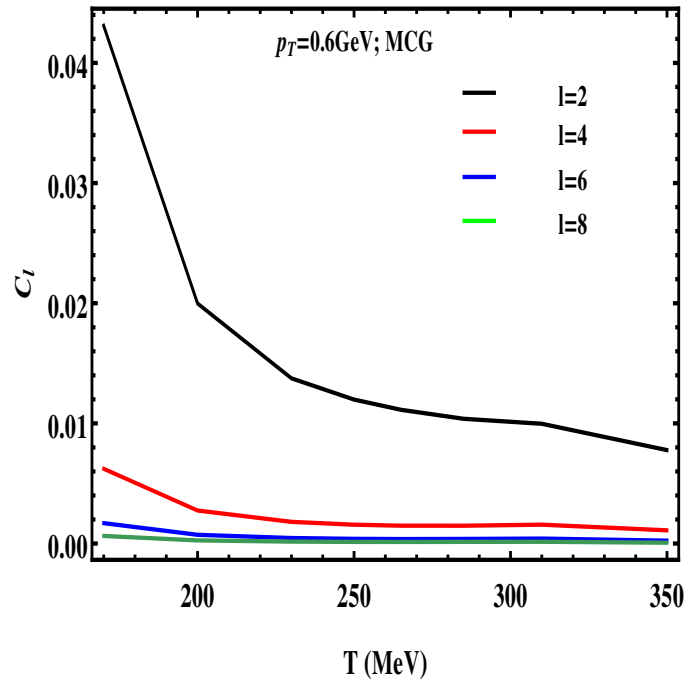


Figure 5.25: The variation of power spectrum of even l with temperature for MCG initial condition with perturbation at $p_T = 0.6$ GeV/ c (see text for details).

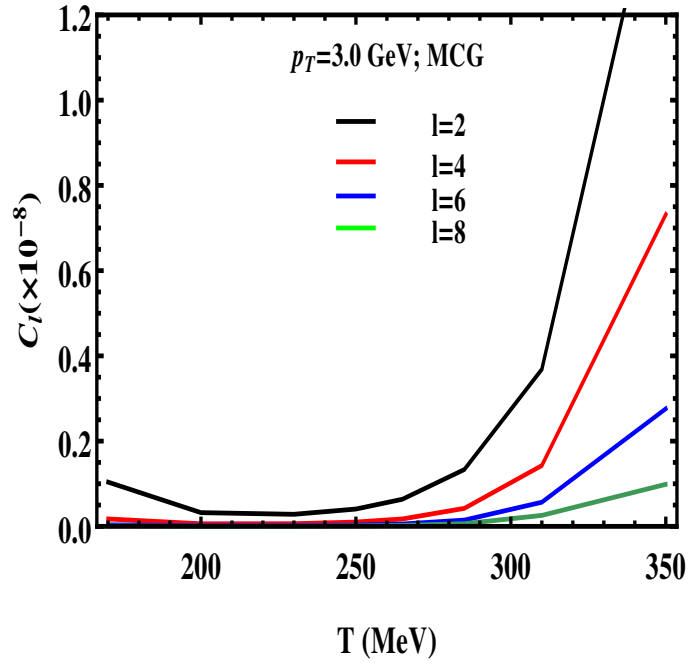


Figure 5.26: Same as Fig 5.22 for $p_T = 3$ GeV/ c (without perturbation).

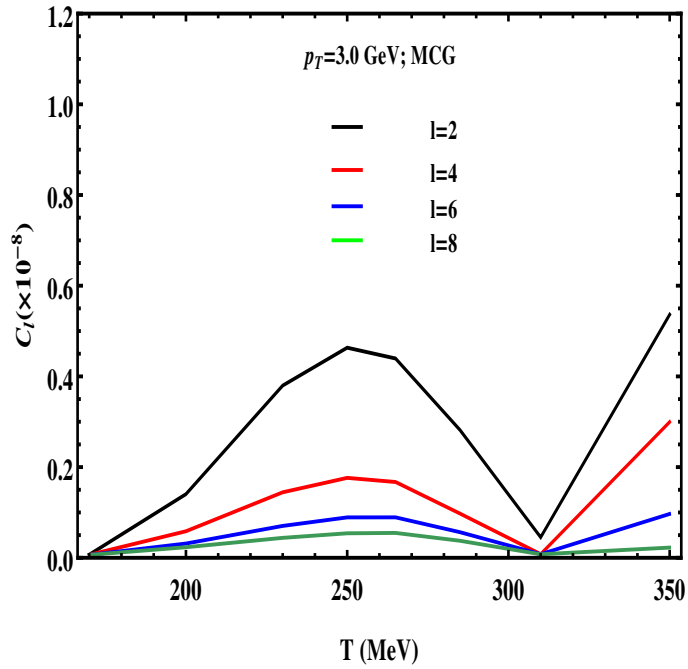


Figure 5.27: Same as Fig 5.25 for $p_T = 3$ GeV/ c (with perturbation $\delta\epsilon/\epsilon \sim 0.01$).

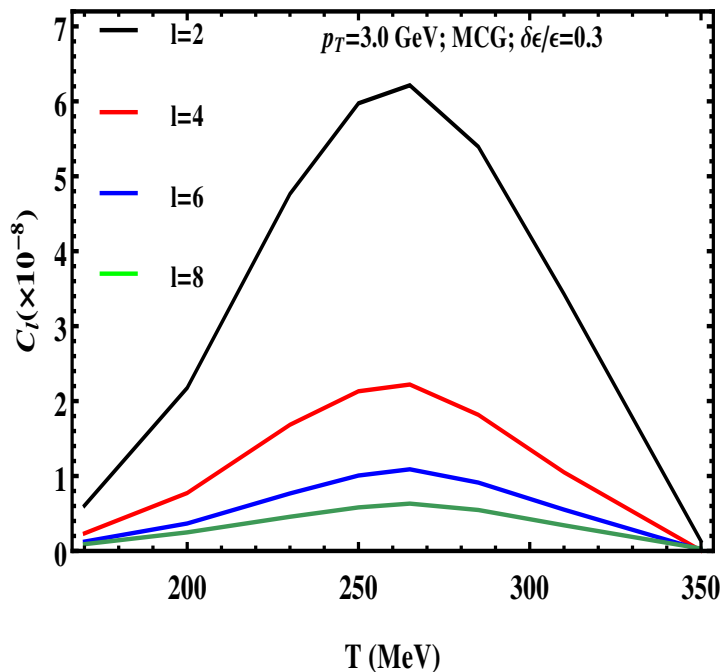


Figure 5.28: Same as Fig 5.27 for $p_T = 3$ GeV/ c , but the perturbation δf , corresponds to $\delta\epsilon/\epsilon \sim 0.3$.

5.6 Summary and discussions

The hot and dense system formed in heavy ion collisions at relativistic energies has been evolved using (3+1) dimensional relativistic hydrodynamics. The initial energy density profiles required to solve the hydrodynamics has been derived from OG and MCG models. The power spectrum of momentum distribution of particles due to fluctuations in initial conditions for both OG and MCG models have been estimated at different surfaces of constant temperatures following the analysis procedure that is used for CMBR spectrum. This enable us to study the evolution of the power spectrum with decrease in temperature and hence effectively with increase in time. We observe that the power spectrum with OG initial conditions for central collisions does not change significantly with the progression of time because the initial system is symmetric. However, the power spectrum for MCG initial condition with negligible values for odd l 's changes, showing non-zero values for odd l 's at later time.

The power spectrum for perturbation introduced through phase space distribution which derive the system away from equilibrium has also been estimated. It has been observed that the temperature variation of power spectrum with perturbation is distinctly different from the one without perturbation at higher p_T - clearly indicating the trace of non-equilibrium in the system. Such studies will help in constraining the initial states [145, 146]. A relation between the power spectrum with the flow harmonics has been derived. This relation can be used to estimate the pseudo-rapidity and p_T dependence of the flow harmonics. The power spectrum of phase space perturbation can be used to estimate the fluctuations in flow harmonics and its dependence on kinematic variables. The connection between the experiments and the present type of works has been nicely discussed in Ref. [126].

In this work a general method for estimating the power spectrum of an expanding fluid has been studied. It is also shown how the power spectrum of perturbation in the fluid that is induced through phase space distribution can be calculated. The input required for these calculations are the initial conditions and EoS for solving relativistic hydrodynamical equations, initial conditions for solving Boltzmann equations governing the evolution of perturbations. In the present works these inputs are taken for matter formed in RHIC-E.

The present work remained theoretical. However, experimental data from RHIC-E on the invariant momentum distribution of particles as a function of p_T , θ or η and ϕ will be very useful to contrast this work with experiments.

CHAPTER 6

Bulk Viscosity and Fluctuations

This chapter contains part of papers [81] and [147]. Here the evolution of correlation of pressure perturbations in QGP and the use of this correlation in the estimate of bulk viscosity of QGP is discussed. We have also estimated the bulk viscosity of hadronic system for the purpose of comparison with the bulk viscosity of QGP. Although a different method is used for estimation of bulk viscosity of hadron resonance gas as discussed below.

6.1 Introduction

It is well known that hydrodynamics is the study of the slowly varying degrees of freedom of the system involving continuity equations of the conserved charges of the underlying microscopic interactions. Viscous relativistic hydrodynamics has been a very successful framework to describe the evolution of the fireball created in heavy ion collisions at relativistic energies (RHIC-E) with a few free parameters which are extracted by fits to data [148, 149].

$T^{ij}(i, j = 1, 2, 3)$ for a non-viscous hydrodynamical system 3.5 in the local rest frame

is given by,

$$T_{ij} = P\delta_{ij} \quad (6.1)$$

where P is the isotropic thermodynamic pressure of the system. In case of Navier Stokes viscous hydrodynamics, the system's response to the gradients of the fluid flow four velocity u^μ can be taken into account by viscous coefficients. Upto first order in derivatives of u^μ two such transport coefficients, namely shear (η) and bulk (ζ) viscosities appear as,

$$T_{ij} = P\delta_{ij} + \eta \left(\frac{\partial u_i}{\partial x^j} + \frac{\partial u_j}{\partial x^i} - \frac{2}{3}\delta_{ij}\nabla \cdot u \right) + \zeta\delta_{ij}\nabla \cdot u \quad (6.2)$$

That is the leading order correction (δT_{ij}) to the energy momentum tensor due to dissipation is introduced through the shear (η) and bulk (ζ) viscous coefficients such that $T_{ij} = P\delta_{ij} + \delta T_{ij}$. The two-point correlation function (δT_{ij}) is related to the viscosities. The effects of these transport coefficients on the hydrodynamic evolution of the strongly interacting fireball and on various observable in RHIC-E, *e.g.* the elliptic flow, spectra of hadronic and electromagnetically interacting particles, etc have been studied extensively [150–155]. The general consensus reached is that the matter created in heavy ion collisions behaves almost like a perfect liquid [156–160] with η/s close to the KSS (Kovtun, Son and Starinets) bound [161]. On the other hand, the issue of bulk viscosity is far from settled. In the earlier works the contribution of ζ was neglected. Inspired by the AdS/CFT correspondence, the $\mathcal{N} = 4$ supersymmetric Yang-Mills theory has been used by several authors to estimate the shear viscosity of the QGP and other strongly correlated system [161]. The ζ/s is always zero in this approach. However, it is shown in [162] that $\zeta/s \sim 0.1$ for certain classes of black hole solutions. Moreover, the lattice QCD (LQCD) based studies [163, 164] has indicated that the bulk viscosity could be as large as shear viscosity at the vicinity of the QCD phase transition. Similar conclusions have also

been drawn from calculations done by using QCD inspired effective models [165–167]. Thus, there have been studies where ζ was included into hydrodynamic simulations. It was found that ζ affects the low momentum hadron spectra as well as the elliptic flow significantly [168].

The phenomenological relevance of ζ has fueled efforts to estimate it by using various models. In this work we provide an estimate of ζ for QGP by using the pressure correlation estimated using the formalism discussed in Ch. 3, 4. ζ for hadrons has been estimated within the ambit of HRG model which has been quite successful in describing the low temperature QCD thermodynamics. Lately, bulk viscosity of the hadronic medium has been computed in various schemes [169–176]. In this work we intend to study the role played by the phase space in deciding the bulk viscosity of the hadronic medium.

This chapter is organized as follows. In the next section discuss evolution of pressure correlation in QGP phase as discussed in Chapter 4 and estimate the temperature variation of bulk viscosity in QGP medium using evolution equation of fluctuations and time correlation of pressure. Then discuss the the estimation of bulk viscosity of HRG phase.

6.2 Correlation in pressure fluctuation and bulk viscosity in QGP phase:

The auto-correlation function for fluctuation in pressure arising from perturbations is defined as:

$$C_{\Delta P}(r, t, \Delta\phi) = \int d\phi \delta P(r, \phi, t) \delta P(r, \phi + \Delta\phi, t) \quad (6.3)$$

We evaluate $C_{\Delta P}$ at fixed r (= 3 fm here) as a function of t and $\Delta\phi$. The solution of δf has been used to estimate δP . The variation of $C_{\Delta P}$ with the angular separation

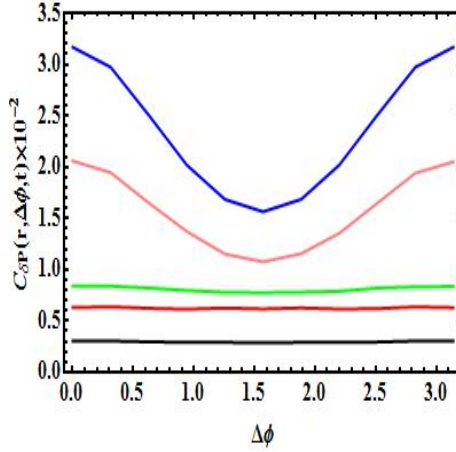


Figure 6.1: The angular auto-correlation of pressure is shown at $r = 3$ fm as a function of $\Delta\phi$. The $\Delta\phi$ variation of $C_{\delta P}$ is displayed at different times such as 0.6 fm/c (blue) 1 fm/c (orange), 2.5 fm/c (green), 3.5 fm/c (red) and 4 fm/c (black line).

$\Delta\phi$ is plotted in Fig. 6.1 for perturbation with elliptic geometry ($n = 2$) of the QGP background as discussed in section. 4.3 at different times as indicated. For $t = 0.6$ fm/c the correlation function decreases with $\Delta\phi$ attains a dip at $\Delta\phi \sim \pi/2$ and again increases to produce a symmetric behavior about the dip. At $t = 1$ fm/c the $\Delta\phi$ variation of $C_{\Delta P}$ is similar to earlier time with an overall reduction in the magnitude. At a later time, $t = 2.5$ fm/c the $C_{\Delta P}$ evolves to a plateau. This indicates that the power spectrum, $[\delta P(\tilde{k})]^2$ is a Dirac delta function. It is also interesting to note that the $C_{\Delta P}$ at a given r and $\Delta\phi$ decreases monotonically with time *i.e.* the correlation becomes weaker in real space as the perturbation reduces and the system approaches toward equilibrium with the progress of time. The evolution of correlation in the pressure fluctuation is crucial for the study of flow harmonics in RHIC-E. The angular differential pressure will give rise to various non-zero flow coefficients like, elliptic flow. The measured anisotropy can be extrapolated backward in time through theoretical model to characterize the early state of the matter formed in RHIC-E.

The bulk viscosity of matter created in RHIC-E is a field of high contemporary interest [177]. We use the current formalism to estimate the bulk viscous coefficient (ζ). The fluctuations in thermodynamic quantities can be used to estimate various

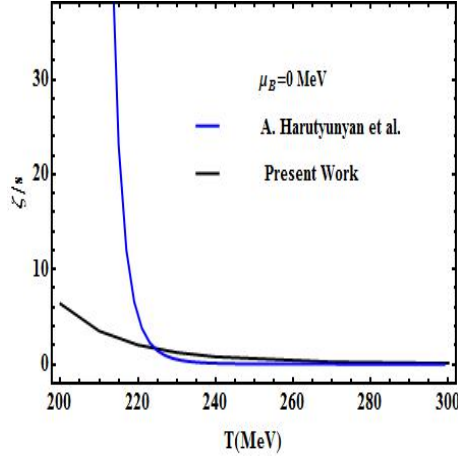


Figure 6.2: The variation of bulk viscosity to entropy ratio (ζ/s) as a function of temperature.

transport coefficients. For example, the fluctuations in pressure ($\delta P \ll \bar{P}$) determined by the δf (Eq. 3.25) can be employed to calculate the bulk viscous coefficient (several methods have been employed in the literature to estimate bulk viscosity of QGP some of these are discussed in [177]) of the quarks with thermal mass [178] by using Green-Kubo relation [179] in the domain of linear response. The bulk viscosity (ζ) is related to the correlation of time dependent pressure fluctuation as follows [180]:

$$\zeta = \frac{V}{T} \int_0^\infty dt \langle \delta P(t) \delta P(0) \rangle \quad (6.4)$$

We estimate the ζ by using this relation and compare the bulk viscosity to entropy density (s) ratio as a function of temperature to the results obtained in Ref. [181] in the strong coupling limit with two flavor NJL model (Fig 6.2). We observe that the behavior of ζ/s in the high $T (> 225 \text{ MeV})$ regime is similar to that obtained in Ref. [181]. This is reasonable because the relaxation time used in the present work has been estimated for weakly coupled QGP [105] which may be realized at the high T regime. The ζ/s calculated in [181] rises very fast with lowering of T (for $T < 225 \text{ MeV}$) due to multi-loop contributions, inclusion of such contributions is beyond the scope of the present work. However, it has been verified that the ζ/s obtained here is similar to the ζ/s reported in Ref. [181] with single loop contribution which may

be a good approximation for weakly coupled system.

6.3 Estimation of bulk viscosity in HRG phase

6.3.1 Formalism

A fluid in equilibrium can fluctuate to a non-equilibrium state in many ways. Depending on the mode of fluctuation there is an onset of the corresponding dissipative process to counter this fluctuation for maintaining the equilibrium. Within the ambit of linear response theory, the medium response allows us to compute the transport coefficients like η , ζ etc. As seen in Eq. 6.2, η is connected to the traceless part of T_{ij} given by Eq. 6.2 and ζ is related to the trace of T_{ij} for a compressible fluid warned by the presence of $\nabla \cdot u$ which is related to the rate of change of volume (V) associated with the uniform expansion or compression through the continuity equation:

$$\frac{\partial n}{\partial t} + \vec{\nabla} \cdot (n\vec{v}) = 0 \quad (6.5)$$

substituting the density $n = N/V$ in Eq. 6.5 (N is the total number and V is the volume), one obtains $\nabla \cdot u = V^{-1}dV/dt$ [169]. This also indicates that the bulk viscosity will vanish for an incompressible fluid. The deviation in the pressure due to change in the bulk not followed from the equation of state (EoS) can be connected to the bulk viscosity as follows:

$$\delta P = \zeta \nabla \cdot \vec{v} \quad (6.6)$$

In this work we will consider the situation where such flow field arises due to change in hadron yield from the equilibrium number. For a single component hadron gas

assuming adiabaticity, it has been shown in [182] that:

$$\delta P = \left(\frac{\partial P}{\partial n} \right)_{\epsilon} \frac{\partial n}{\partial s} s \nabla \cdot \vec{v} \tau_R \quad (6.7)$$

where τ_R is the relaxation time scale of the system, which is the inverse of the rate of number changing process responsible to maintain chemical equilibrium. Now within the HRG formalism, the total pressure P is given by sum over the partial pressure, P_i due to each hadron species, i ,

$$P = \sum P_i \quad (6.8)$$

Thus the fluctuation in the total pressure P can be expressed as

$$\delta P = \sum_i \delta P_i = \left[\sum_i \left(\frac{\partial P_i}{\partial n_i} \right)_{\epsilon_i} \frac{\partial n_i}{\partial s_i} s_i \tau_R^i \right] \nabla \cdot \vec{v} \quad (6.9)$$

τ_R^i is the relaxation time of the species, i . The fluid flow velocity field, u^i being a hydrodynamic variable is same for all the hadron species. On comparing Eqs. 6.6 and 6.9, we find the expression for ζ

$$\zeta = \sum_i \left(\frac{\partial P_i}{\partial n_i} \right)_{\epsilon_i} \frac{\partial n_i}{\partial s_i} s_i \tau_R^i \quad (6.10)$$

This relation can be used to derive the expression for bulk viscosity (see appendix C for details) as,

$$\zeta = \sum_i \left[\frac{\left(\frac{\partial P_i}{\partial T} \right) \left(\frac{\partial \epsilon_i}{\partial \mu_i} \right) - \left(\frac{\partial P_i}{\partial \mu_i} \right) \left(\frac{\partial \epsilon_i}{\partial T} \right)}{\left(\frac{\partial n_i}{\partial T} \right) \left(\frac{\partial \epsilon_i}{\partial \mu_i} \right) - \left(\frac{\partial n_i}{\partial \mu_i} \right) \left(\frac{\partial \epsilon_i}{\partial T} \right)} \right] \left[\left(\frac{\partial n_i}{\partial T} \right) \left(\frac{\partial T}{\partial s_i} \right) + \left(\frac{\partial n_i}{\partial \mu_i} \right) \left(\frac{\partial \mu_i}{\partial s_i} \right) \right] s_i \tau_R^i \quad (6.11)$$

In order to estimate τ_R^i we need to know the cross sections of all the possible processes through which hadron, i interacts with all the hadrons and resonances. As all these

required cross sections are not known presently and we are interested in studying the effects of phase space on ζ , a constant cross sections for all the hadronic processes is assumed in the spirit of Ref. [183] and treat the relaxation time as a constant to write down the ratio ζ/τ_R as:

$$\frac{\zeta}{\tau_R} = \sum_i \left[\frac{\left(\frac{\partial P_i}{\partial T}\right) \left(\frac{\partial \epsilon_i}{\partial \mu_i}\right) - \left(\frac{\partial P_i}{\partial \mu_i}\right) \left(\frac{\partial \epsilon_i}{\partial T}\right)}{\left(\frac{\partial n_i}{\partial T}\right) \left(\frac{\partial \epsilon_i}{\partial \mu_i}\right) - \left(\frac{\partial n_i}{\partial \mu_i}\right) \left(\frac{\partial \epsilon_i}{\partial T}\right)} \right] \left[\left(\frac{\partial n_i}{\partial T}\right) \left(\frac{\partial T}{\partial s_i}\right) + \left(\frac{\partial n_i}{\partial \mu_i}\right) \left(\frac{\partial \mu_i}{\partial s_i}\right) \right] \quad (6.12)$$

Eq. 6.12 has been used to estimate the ζ for HRG in this work. Each term in Eq. 6.12 can be computed from P_i and its derivatives, where P_i is given by,

$$\begin{aligned} P_i &= \frac{T}{V} \ln Z_i(T, V, \mu_i) \\ &= \sum_i \frac{ag_i}{2\pi^2} T^4 \int_0^\infty dx x^2 \ln \left[1 + a \exp \left[- \left(\sqrt{x^2 + \left(\frac{m_i}{T}\right)^2} - \frac{\mu_i}{T} \right) \right] \right] \end{aligned} \quad (6.13)$$

where $a = -1$ for mesons (Bosons) and $+1$ for baryons (Fermions). Consequently the corresponding entropy density (s_i), number density (n_i) and energy density (ϵ_i) are given by,

$$s_i = \frac{\partial P_i}{\partial T}, \quad n_i = \frac{\partial P_i}{\partial \mu_i}, \quad \epsilon_i = T \frac{\partial P_i}{\partial T} - P_i + \mu_i \frac{\partial P_i}{\partial \mu_i} \quad (6.14)$$

It can be easily checked from Eqs. 6.12, 6.13 and 6.14 that when the hadron, i is massless with $\epsilon_i = 3P_i$ then ζ_i vanishes as $\left(\frac{\partial P_i}{\partial T}\right) \left(\frac{\partial \epsilon_i}{\partial \mu_i}\right) - \left(\frac{\partial P_i}{\partial \mu_i}\right) \left(\frac{\partial \epsilon_i}{\partial T}\right) = 0$. Eqs. 6.13 and 6.14 can be used to reproduce the known thermodynamic expressions for pressure, entropy density, number density, energy density, etc., both for relativistic and non-relativistic limits. In turn these quantities can be used in Eq. 6.12 to estimate the bulk viscosity to relaxation time ratio.

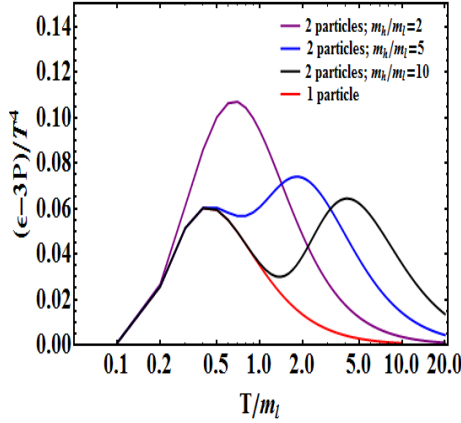


Figure 6.3: Variation of $(\epsilon - 3P)/T^4$ with T/m_l for different values of the ratio of the masses of the heavy to light particle, m_h/m_l for vanishing chemical potential.

6.4 Results

The bulk viscosity, ζ for a HRG system can be calculated by using Eq. 6.12 where all the particles as listed in the Particle Data Book [184] of mass upto 2.5 GeV are included. In order to understand the results for the full HRG, we first investigate a system with single species of hadrons of mass, m_l and then the other with two different hadronic species of masses m_l and m_h with $m_h > m_l$. We study the interplay of the two different mass scales on the temperature dependence of ζ and its correlation with the CSB (conformal symmetry breaking) measure, $\Delta = \epsilon - 3P$ [185].

We have plotted Δ/T^4 as function of T in Fig. 6.3 for systems with different composition and masses to elucidate the role of hadronic masses in Δ and subsequently in bulk viscosity (Fig.6.5). The curves in Fig.6.3 stand for different values of the ratio, m_h/m_l . The qualitative features of the plots remain same when we replace the bosons by fermions. Results displayed in Fig. 6.3 indicate that $\Delta/T^4 \rightarrow 0$ both for the non-relativistic $m/T \gg 1$ and massless limits $m/T \rightarrow 0$. To understand the variation of Δ/T^4 with T/m , first consider a system at temperature T with single species of mass m_l . In the high temperature limit the pressure-energy density

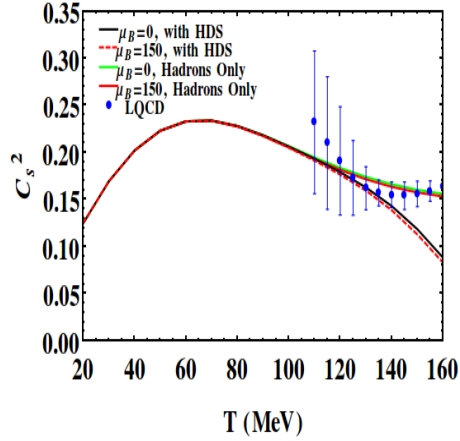


Figure 6.4: Variation of the square of the speed of sound with T for zero and non-zero net baryon density.

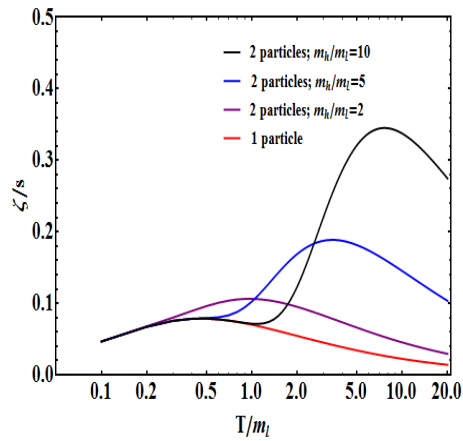


Figure 6.5: Variation of ζ/s with T/m_l for different values of the ratio of the masses of the heavy to light particle, m_h/m_l for vanishing chemical potential.

relation becomes $P = \epsilon/3$ giving rise to $\Delta = 0$. In the limit of large m/T (small T/m) the CSB measure varies as: $\Delta \sim e^{-m/T}$, becomes vanishingly small. That is for both small and large T , $\Delta \rightarrow 0$, with an intermediary peak at $T/m_l \sim 0.5$.

Now we consider a two-particle system with masses m_l and m_h ($m_h > m_l$). First consider the case with $m_h/m_l = \infty$. The heavier particle does not contribute to the thermodynamics. Hence this is essentially a single particle system. We find a single peak around $T \sim 0.5m_l$. Next, we plot for the case with $m_h/m_l = 10$. The large separation in the masses of the two particles results in distinct two peaks at $T/m_l \sim 0.5$ and $T/m_l \sim 5$ (i.e. at $T/m_h \sim 0.5$). For $m_h/m_l = 5$, similar structure is found with closer peaks and reduced dip between the two peaks. We observe that the peak associated with the lighter particle has converted to a shoulder-like structure. Finally for $m_h/m_l = 2$, the peaks have partially merged and we are left with only a single (broader) peak at $T \sim 0.5(0.5m_l + 0.5m_h) = 0.75m_l$.

The presence of the massive hadrons does not allow the system to satisfy the relation $\epsilon = 3P$ i.e. the conformal symmetry is broken for the entire range of T both for zero and non-zero μ_B . This is evident from the estimation of the speed of sound (c_s^2) which remains below $1/\sqrt{3}$ (Fig. 6.4) for the entire T range considered.

It is expected that the temperature and mass dependences of CSB discussed above will be reflected on ζ/s as these quantities are correlated [186]. For demonstrating the phase space dependence of ζ we assume $\tau_R \sim 1$ fm/c. The results are depicted in Fig. 6.5. The peaks corresponding to the single and two particles systems (with $m_h/m_l = 2$) get blurred. For $m_h/m_l = 5$ and 10 the peaks at lower T/m_l get smeared, however, for higher T/m_l the peaks become broader but distinctly visible. In summary, the ζ and Δ have similar T -variation with broader peaks in the later quantity. For a system with many particles the ζ will be a superposition of results obtained for each of the different hadrons with their respective masses. We use Eqs. 6.12, 6.13 and 6.14 to estimate the ratio ζ/τ_R for a system of single particles

with mass m in the limits of $m/T \rightarrow 0$ and $m/T \rightarrow \infty$. We find that $\zeta/\tau_R \sim (m/T)^2$ for $m/T \ll 1$ and $\zeta/\tau_R \sim e^{-(m-\mu)/T}$ for $m/T \gg 1$, *i.e.* the bulk viscosity vanishes both in the relativistic and non-relativistic limits - a well known result in the literature.

Now we turn our attention to the HRG system. The study of HRG is important because lattice QCD results indicate that at lower temperatures, the HRG is a good approximation for the effective degrees of freedom of the strongly interacting matter. Therefore, it will be very useful to study the properties of HRG if it is away from equilibrium. We estimate the bulk viscosity of the HRG when it is slightly away from equilibrium - a situation may be confronted during the evolution of matter formed in nuclear collisions at relativistic energies.

The lightest hadron is the pion with $m_\pi \sim 140$ MeV and the next hadron (kaon) is heavier by about 350 MeV. The hadronic degrees of freedom are expected to survive upto $T \sim 150 - 160$ MeV. Thus, in this temperature domain, $m/T \gg 1$ for all hadrons except pion. This implies that for the full HRG system, we should expect to see features qualitatively similar to the non-relativistic end of the plots in Fig. 6.5 *i.e.* we should see an increasing trend of ζ with T for constant τ_R .

In Figs. 6.6 and 6.7 we have displayed the temperature variation of ζ/ζ_0 and $R_\zeta = (\zeta/s)/(\zeta_0/s_0)$ [$\zeta_0 = \zeta(T = 150 \text{ MeV})$ $s_0 = s(T = 150 \text{ MeV})$] respectively for different values of baryonic chemical potential, μ . Please note that in the ratios of ζ the effects of the constant relaxation time get cancelled. We find that the bulk viscosity increases with both temperature and baryonic density as expected from the discussions above.

The results displayed so far may be improved by the following two considerations: (i) by making the τ_R a T and μ dependent quantity. We have taken constant τ_R so far, however, the relaxation time τ_R should depend on the thermodynamic state of the matter, *i.e.* it should vary with T and μ . To get the T and μ dependence of τ_R

we can use the relation,

$$\tau_R^j = \frac{1}{\sum_i \sigma_{ij} n_i \frac{\langle p_i \rangle}{\langle E_i \rangle}} \quad (6.15)$$

However, as mentioned above we will assume constant cross section *i.e.* $\sigma_{ij} = \sigma$ and a single relaxation time for the system, $\tau_R^j = \tau_R$. We find that the relaxation time, τ_R reduces with the T and μ *i.e.* the hotter and denser systems relax faster.

(ii) By including the Hagedorn density of states (HDS) [187, 188] for counting the resonances at higher temperatures in estimating the bulk viscosity [189]. For this purpose we have used the following mass spectrum in evaluating relevant thermodynamic quantities:

$$\rho(m) = \sum_i d_i \delta(m - m_i) + \frac{a_0}{(m^2 + m_0^2)^{5/2}} e^{m/T_H} \quad (6.16)$$

where the first part is the standard discrete contribution from all the PDG resonances while the second part is the additional contribution from the continuous HDS. $d_i = 2S_i + 1$ is the degeneracy due to the spin of the i th hadron with mass m_i . a_0 , m_0 and T_H are parameters extracted from fits of the HDS to the observed spectrum. Here we have used $a_0 = 0.744 \text{ GeV}^{3/2}$, $m_0 = 0.529 \text{ GeV}$ and $T_H = 180 \text{ MeV}$ as in [188]. The thermodynamic quantities like the energy density (ϵ) may be calculated by using the formula: $\epsilon = \int dm \rho(m) \int \frac{d^3 p}{(2\pi)^3} \sqrt{p^2 + m^2} f(p)$, where $f(p)$ is the appropriate thermal distribution for Bosons or Fermions.

With the inclusion of these two effects as described above the temperature dependence of R_ζ , the normalized bulk viscosity has been evaluated and the result is displayed in Fig. 6.8. The T and μ dependence of τ_R has changed the results both quantitatively and qualitatively. In sharp contrast to the results displayed in Fig. 6.7 the ratio decreases with temperature as observed also in Refs. [169, 170]. However, we recall that the results depicted in Fig. 6.8 contains temperature dependent τ_R which decreases with T as: $\tau_R^{-1} \propto T^2 e^{-m/T}$ (due to T dependent density and av-

erage velocity) for constant cross sections. This temperature variation seems to be stronger than the T dependent growth of the right hand side (rhs) of Eq.6.12. As a result the ratio, R_ζ which is a product of these two factors - rhs of Eq. 6.12 and τ_R decreases with T . The outcome of the present work has particularly been compared with the results obtained by solving Boltzmann equation - in (a) relaxation time approximation with excluded volume effects in HRG [172] and (b) Chapman-Enskog approximations for interacting pion gas [170]. At higher temperature all the results converge. At lower temperature the results from different models tend to differ. However, the outcome of the present work with the inclusion of HDS (solid line) agrees well with the results of Ref. [170].

In Fig.6.9 the variation of CSB measure with temperature is displayed for HRG system with (solid line) and without (dashed line) HDS. A significant enhancement of CSB is observed for temperature above pion mass, more so for the case where HDS are used in addition to the standard PDG hadrons. This is expected as the inclusion of additional Hagedorn resonances result in a stronger breaking of the conformal symmetry. We have compared the CSB measure obtained in the HRG model with that of LQCD data and found good agreement upto about $T \sim 1.1m_\pi$ which is the region of interest here. It is expected that the observed variation of CSB with T will also reflect in the T dependence of ζ .

In RHIC-E, for a given $\sqrt{s_{NN}}$ a hot and dense medium is created with entropy, S and net baryon number, N_B . For an isentropic expansion of the system, the S/N_B ratio remains constant throughout the evolution. Therefore, the system will evolve along a trajectory in the $T - \mu$ plane corresponding to a constant S/N_B contour. We use this evidence to evaluate ζ along the constant S/N_B contours in the $T - \mu$ plane for $S/N_B = 30, 45$ and 300 . These values of S/N_B may correspond to AGS (FAIR), SPS and RHIC collision conditions [190] (see also [191]). The variation of R_ζ with T along these contours are depicted in Fig. 6.10. The relaxation time is estimated by using Eq. 6.15 with the value of cross section, $\sigma = \pi \text{ fm}^2$ as in [183]. It is observed

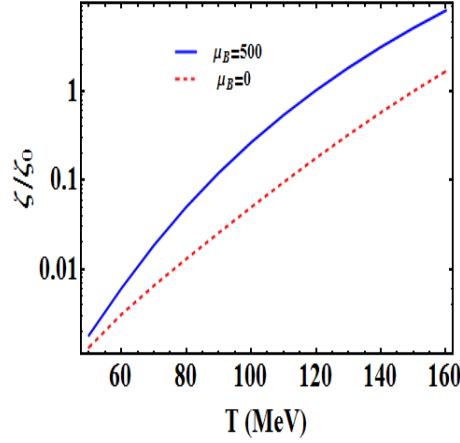


Figure 6.6: The temperature variation of $\zeta(T)/\zeta_0$ is shown here with $\zeta_0 = \zeta(T = 150)$ MeV.

that the magnitude of ζ/s at low temperature domain is higher for $S/N_B = 30$ (corresponds to higher μ) compared to $S/N_B = 300$. At higher temperatures the values of bulk viscosity seems to converge for all the values of S/N_B .

In RHIC-E the centre of mass energy ($\sqrt{s_{NN}}$) can be connected to the values of T and μ at the chemical freeze-out curve by analyzing the hadronic yields [192, 193] as follows. In Ref. [193] the chemical freeze-out curve has been parametrized as: $T(\mu) = 0.166 - 0.139\mu^2 - 0.053\mu^4$ and the $\sqrt{s_{NN}}$ dependence of μ has been fitted with $\mu = 1.308(1 + 0.273\sqrt{s_{NN}})^{-1}$. Using these parameterizations the normalized bulk viscosity has been estimated and the results have been displayed as a function of $\sqrt{s_{NN}}$ in Fig 6.11 with (dashed line) and without (solid) incorporating the HDS. At high $\sqrt{s_{NN}}$ the inclusion of Hagedorn spectra does not make any difference, however, at lower values of $\sqrt{s_{NN}}$ Hagedorn spectra enhances the bulk viscosity. The important point to be noted here is that at lower beam energy the bulk viscosity is larger (for larger μ). Therefore, ζ will play a more important role at FAIR than LHC experiments.

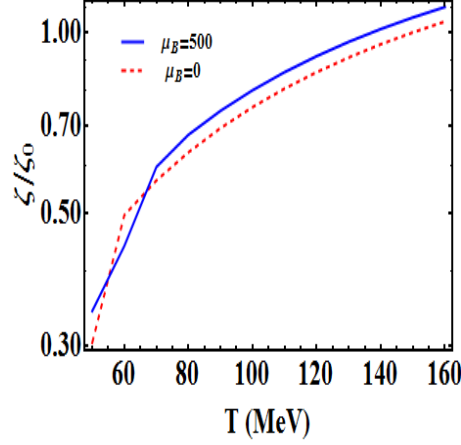


Figure 6.7: Depicts the temperature variation of the bulk viscosity to entropy density ratio normalized to the value of the ratio at $T = 150$ MeV (see text) with constant relaxation time.

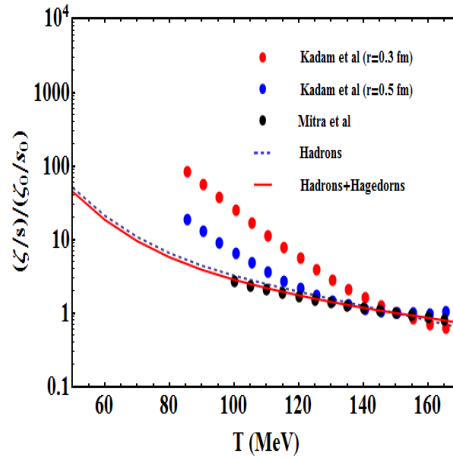


Figure 6.8: Variation of R_ζ (see text) as a function of T for hadronic resonances upto mass 2.5 GeV with (red line) and without (blue dashed line) HDS including T dependent relaxation time estimated by using Eq. 6.15. We have also displayed the same quantity as obtained in other works [170, 172].

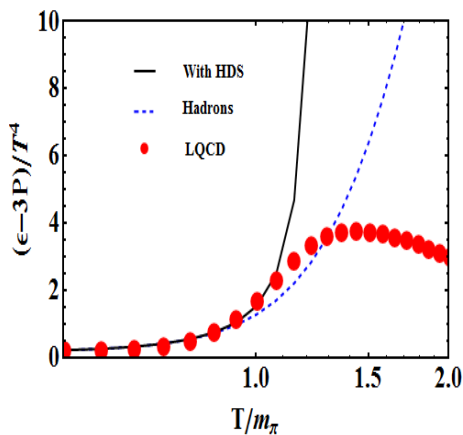


Figure 6.9: The variation $(\epsilon - 3P)/T^4$ with T/m_π with (solid line) and without (dashed line) HDS. A comparison has been made with continuum extrapolated (2+1) lattice QCD data with physical quark masses [194].

6.5 Summary and discussions

The evolution of correlations of perturbation in pressure has been studied using the solution of BTE and shown that the correlation between two points in real space reaches a plateau at later time. We have used the calculated correlation in pressure fluctuation to estimate the bulk viscous coefficient [180].

Using grand canonical ensemble the bulk viscosity of the hadronic medium has been estimated within the ambit of the HRG model approach. The grand canonical ensemble of HRG provides the mean hadron number as well as the fluctuations in the chemical composition of the hadronic medium. These fluctuations grant a non-zero divergence for the hadronic fluid flow velocity, offering an opportunity to evaluate the hadronic bulk viscosity ζ up to a relaxation time. First we have considered both single and two hadronic systems with different masses to exemplify the role of hadronic masses on the CSB and bulk viscosity. Then we proceed to evaluate the ζ for HRG model and eventually include the HDS in the calculations. We find that the inclusion of HDS enhances the bulk viscosity of the system at lower $\sqrt{s_{NN}}$. We would like to note here that recently it has been shown that a considerable improve-

ment in the HRG framework in describing LQCD data is obtained by simultaneous inclusion of the HDS as well as a hard core repulsion between the hadrons within an excluded volume approach [195]. In the low temperature domain ($T \simeq 150$ MeV) it is found that the pressure and energy density estimated without excluded volume effect remain within error bars of the lattice QCD results [195]. However, the agreement with the energy density turns to be better at higher T with excluded volume effect. We leave this interesting exercise about the simultaneous role of the finite size of the hadrons as well as the HDS on the bulk viscosity of the hadronic medium for the future. We also estimate ζ along the constant S/N_B contours and find that ζ/s is enhanced for lower S/N_B . ζ/s has also been evaluated along the chemical freeze-out curve obtained from the parameterization of hadronic yields [193] and found that the ζ/s is larger at FAIR than LHC energy region. This indicates that the bulk viscosity will play more crucial role in nuclear collision at FAIR than LHC energies.

A few words on the T and μ dependence of the bulk viscosity arising from the phase space factors are in order here. In the present work we have assumed a constant σ for all the hadronic processes, however, in reality the situation could be more complex with T and μ dependent cross sections to be considered for all types of possible reactions undergoing in the medium. As mentioned earlier the cross sections for the hadronic reactions involving all the resonances and Hagedorn states are not known presently. Therefore, we have assumed a constant cross section [183] and demonstrated the T and μ dependence of the bulk viscosity originating from the phase space factors only. The lack of these cross sections does not allow us to estimate the relaxation time from microscopic interactions. Therefore, we assume that the relaxation time of a hadron h is $\tau_h = \tau_R \pm \delta_h$, where τ_R is the average relaxation time scale of the full system and δ_h is the deviation of τ_h from it. In this work, it is assumed that $\tau_R \gg \delta_h$ for all h . The deviation of a system from equilibrium can be regarded as its response to some external perturbation.

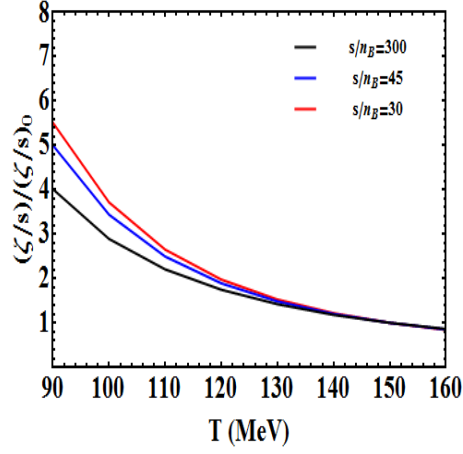


Figure 6.10: The variation of bulk viscosity to entropy density ratio (normalized at $T = 150$ MeV) with temperature along constant S/N_B contours for $S/N_B = 30, 45$ and 300.

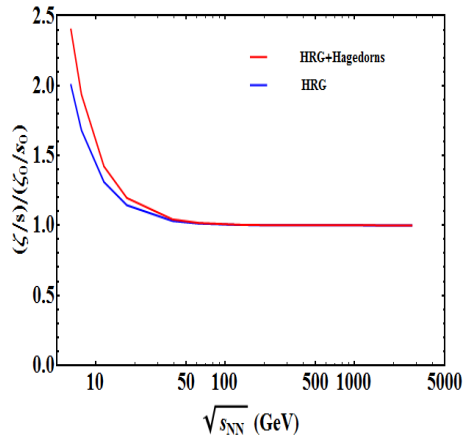


Figure 6.11: The variation of R_ζ as a function of $\sqrt{s_{NN}}$ with (red line) and without (blue line) HDS.

CHAPTER 7

Summary and Outlook

The evolution of perturbation in relativistic fluid introduced through the phase space distribution function has been studied using Boltzmann transport equation in relaxation time approximation. The perturbation evolves in an expanding QGP background governed by $(3 + 1)$ dimensional relativistic hydrodynamics. The relaxation time appearing in the solution of the Boltzmann equation is a temperature dependent quantity. The space time dependence of temperature is governed by relativistic hydrodynamics. Thus the perturbation is coupled to the background through relaxation time.

We have derived a relation between the fluctuations in energy density with the transport coefficients, e.g. shear viscosity and thermal conductivity. We have also analyzed and demonstrated how the various Fourier modes of the perturbations get mixed in an expanding background. It is shown that if a perturbation is created near the boundary of the system then it has a better chance of getting detected.

The evolution of the power spectrum of the invariant momentum distribution of particles has been estimated for Optical Glauber as well as Monte-Carlo Glauber initial conditions. The power spectrum of the momentum distribution of the particles due to perturbations imparted through the phase space distribution have been

evaluated at different surfaces of fixed temperatures(T). We observe that the non-equilibrium effects introduced as perturbations in the phase space distributions can be traced from the temperature variation of the power spectrum of particles of higher transverse momentum which is distinctly different from the case of vanishing perturbation. A relation has been derived between the power spectrum and the flow harmonics.

The evolution of correlation function for the perturbation in pressure has been studied and shown that the initial correlation between two neighboring points in real space evolves to a constant value at later time which gives rise to Dirac delta function for the correlation function in Fourier space.

The solution of the Boltzmann equation obtained here can be used to estimate various other physical quantities. For example, we have used this solution to estimate the fluctuation in pressure and subsequently the bulk viscosity of the QGP with the help of Kubo relation. We find that the bulk viscosity is quite high at low temperature (~ 200 MeV).

The bulk viscosity of hadronic system has been calculated by using HRG model and the Hagedorn density of states. The fluctuation in thermodynamic pressure has been used to determine the ζ of QGP. The bulk viscosity to entropy ratio (ζ/s) has been estimated by using HRG model and Hagedorn density of states. We have studied the role played by the phase space in deciding the bulk viscosity of the hadronic medium.. The bulk viscosity of hadronic system is found to decrease with temperature. The result obtained here has been compared with other similar results available in the literature.

Given the possibility to trace of the non-equilibrium effect in the power spectrum analysis of momentum anisotropy of produced particles, it would be very interesting to extend the analysis further and investigate such effects in actual data. In this regard the focus of this work would be to investigate it further, and estimate and

analyze the fate of different scales of fluctuations in QGP. This will help selecting suitable events where non-equilibrium processes are less present, and hence extracting hydrodynamic quantities like shear viscosity in a more unambiguous way. It can also help to point out the nature of the origin of finite azimuthal anisotropy in most central collisions.

The procedure presented in the present dissertation may be used to estimate temperature fluctuation in little bangs. The fluctuation in temperature, ΔT in different azimuthal bins ($\Delta\phi$) can be calculated as follows. Since the average transverse momentum ($\langle p_T \rangle$) is directly proportional to the temperature of the QGP the fluctuation in temperature in a bin $\Delta\phi$ is given by the relation,

$$\frac{\Delta T}{\Delta y} \sim \int_{\phi_1}^{\phi_2} d\phi \int_0^\infty p_T dp_T \int d^3x \delta f \quad (7.1)$$

Therefore, the $\Delta\phi$ variation of temperature fluctuation in little bang *i.e.* for the system formed in RHIC-E can be estimated analogous to the temperature fluctuation in the universe in the recombination era. This analysis will help us justify the name "little bang" that created in the laboratory in the collision of two nuclei at relativistic energy.

APPENDIX A

Correlations of Fluctuations

In this appendix, we evaluate the correlation, $\langle \Delta(\hat{n}_1)\Delta(\hat{n}_2) \rangle$. The fluctuations, $\Delta(\vec{x}, \hat{n}, t)$ can be written as:

$$\Delta(\vec{x}, \hat{n}, t) = \sum_{l,m} a_{lm}(\vec{x}, t) Y_{lm}(\hat{n}), \quad (\text{A.1})$$

with $a_{lm} = (-i)^l 4\pi \int d^3\hat{n} Y_{lm}^*(\hat{n}) \Delta(\vec{x}, \hat{n}, t)$ and $\langle a_{lm} a_{l'm'}^* \rangle = C_l(\vec{x}, t) \delta_{ll'} \delta_{mm'}$. Using Eq. A.1 we can find the correlations in the following way,

$$\begin{aligned} \langle \Delta(\vec{x}, \hat{n}_1, t) \Delta(\vec{x}, \hat{n}_2, t) \rangle &= \sum_{l,m,l',m'} \langle a_{lm} a_{l'm'}^* \rangle Y_{lm}(\hat{n}_1) Y_{l'm'}^*(\hat{n}_2), \\ &= \sum_{l,m,l',m'} C_l(\vec{x}, t) \delta_{ll'} \delta_{mm'} Y_{lm}(\hat{n}_1) Y_{l'm'}^*(\hat{n}_2), \\ &= \sum_{l,m} C_l(\vec{x}, t) Y_{lm}(\hat{n}_1) Y_{lm}^*(\hat{n}_2), \end{aligned} \quad (\text{A.2})$$

which leads to

$$\langle \Delta(\vec{x}, \hat{n}_1, t) \Delta(\vec{x}, \hat{n}_2, t) \rangle = \frac{1}{4\pi} \sum_l (2l+1) C_l(\vec{x}, t) P_l(\hat{n}_1 \cdot \hat{n}_2),$$

since, $P_l(\hat{n}_1 \cdot \hat{n}_2) = \frac{4\pi}{2l+1} \sum_{m=-l}^l Y_{lm}(\hat{n}_1) Y_{lm}^*(\hat{n}_2)$. Eq. A.2 defines the correlations of

fluctuations observed from two different directions in terms of co-efficient C_l s. C_l 's are the angular power spectrum which contains the information of the anisotropies. Work is under progress to estimate these coefficients by solving the hydrodynamical equations with the initial conditions taken from Glauber Monte-Carlo method. Similarly, one can define these co-efficients corresponding to k -space presentation of fluctuations. Time evolution of these co-efficients can be obtained from evolution of energy density fluctuation, $\Delta(\vec{k}, \hat{n}, t)$ given by Eq. 3.34. Therefore, we have

$$\langle \Delta(\vec{x}, \hat{n}_1, t) \Delta(\vec{x}, \hat{n}_2, t) \rangle = \int \frac{d^3k}{(2\pi)^3} \frac{d^3k'}{(2\pi)^3} e^{i(\vec{k}-\vec{k}')\cdot\vec{x}} \langle \Delta(\vec{k}, \hat{n}_1, t) \Delta(\vec{k}', \hat{n}_2, t) \rangle \quad (\text{A.3})$$

Now,

$$\begin{aligned} \langle \Delta(\vec{k}, \hat{n}_1, t) \Delta(\vec{k}', \hat{n}_2, t) \rangle &= \langle \Delta(\vec{x}, \hat{n}_1, t_0) \Delta(\vec{x}, \hat{n}_2, t_0) \rangle L(\vec{k}, t_0; \vec{k}', t_0) \\ &+ \langle \Theta(\vec{x}, \hat{n}_1, t_0) \Theta(\vec{x}, \hat{n}_2, t_0) \rangle M(\vec{k}, t_0; \vec{k}', t_0) \\ &+ \langle \Delta(\vec{x}, \hat{n}_1, t_0) \Theta(\vec{x}, \hat{n}_2, t_0) \rangle N(\vec{k}, t_0; \vec{k}', t_0), \end{aligned} \quad (\text{A.4})$$

where,

$$\begin{aligned} L(\vec{k}, t, \vec{k}', t_0) &= e^{-\frac{2(t-t_0)}{\tau}} \left\{ \frac{\sin k(t-t_0)}{k(t-t_0)} \right\} \left\{ \frac{\sin k'(t-t_0)}{k'(t-t_0)} \right\}, \\ M(\vec{k}, t, \vec{k}', t_0) &= e^{-\frac{2(t-t_0)}{\tau}} \left(\frac{40}{3} \frac{\eta}{s\bar{T}} \right)^2 \left\{ \frac{\sin k(t-t_0)}{k(t-t_0)} + \frac{3 \cos k(t-t_0)}{(k(t-t_0))^2} - \frac{3 \sin k(t-t_0)}{(k(t-t_0))^3} \right\} \\ &\times \left\{ \frac{\sin k'(t-t_0)}{k'(t-t_0)} + \frac{3 \cos k'(t-t_0)}{(k'(t-t_0))^2} - \frac{3 \sin k'(t-t_0)}{(k'(t-t_0))^3} \right\} \\ N(\vec{k}, t, \vec{k}', t_0) &= e^{-\frac{2(t-t_0)}{\tau}} \frac{40}{3} \left(\frac{\eta}{s\bar{T}} \right) \left\{ \frac{\sin k(t-t_0)}{k(t-t_0)} \right\} \\ &\times \left\{ \frac{\sin k'(t-t_0)}{k'(t-t_0)} + \frac{3 \cos k'(t-t_0)}{(k'(t-t_0))^2} - \frac{3 \sin k'(t-t_0)}{(k'(t-t_0))^3} \right\} \end{aligned} \quad (\text{A.5})$$

For two functions Δ and Θ , defining the correlation as: $\langle \Delta(\vec{k}, \hat{n}_1, t) \Theta(\vec{k}', \hat{n}_2, t) \rangle = (2\pi)^3 \delta(\vec{k}-\vec{k}') \delta_{\Delta\Theta} \langle \Delta(k, \hat{n}_1, t) \Theta(k, \hat{n}_2, t) \rangle$ and $\Delta(\vec{k}, \hat{n}, t) = \sum_{l,m} a_{lm}^\Delta(\vec{k}, t) Y_{lm}(\hat{n})$, $\langle a_{lm}^\Delta \cdot a_{l'm'}^{\Theta*} \rangle = C_l^{\Delta\Theta}(\vec{k}, t) \delta_{ll'} \delta_{mm'}$, we get

$$\begin{aligned}
 \langle \Delta(\vec{k}, \hat{n}_1, t) \Delta(\vec{k}', \hat{n}_2, t) \rangle &= (2\pi)^3 \delta(\vec{k} - \vec{k}') \sum_l \frac{2l+1}{4\pi} P_l(\hat{n}_1 \cdot \hat{n}_2) \\
 &\quad \times \{C_l^{\Delta\Delta}(k, t_0) L(k, t, k, t_0) + C_l^{\Theta\Theta}(k, t_0) M(k, t, k, t_0)\}.
 \end{aligned} \tag{A.6}$$

Using $\langle \Delta(\vec{k}, \hat{n}_1, t) \Delta(\vec{k}', \hat{n}_2, t) \rangle = (2\pi)^3 \delta(\vec{k} - \vec{k}') \sum_l \frac{2l+1}{4\pi} C_l^{\Delta\Delta}(k, t) P_l(\hat{n}_1 \cdot \hat{n}_2)$, in Eq. A.6 we get,

$$C_l^{\Delta\Delta}(\vec{k}, t) = C_l^{\Delta\Delta}(k, t_0) L(k, t, k, t_0) + C_l^{\Theta\Theta}(k, t_0) M(k, t, k, t_0). \tag{A.7}$$

Using Eq. A.2, A.7 in Eq A.3, we get

$$C_l^{\Delta\Delta}(\vec{x}, t) = \int d^3k \{C_l^{\Delta\Delta}(k, t_0) L(k, t, k, t_0) + C_l^{\Theta\Theta}(k, t_0) M(k, t, k, t_0)\} \tag{A.8}$$

This provides the correlations at different angular scales at time t for a given correlations at initial time, t_0 ($t > t_0$).

APPENDIX B

Equations State Parameters and Flow Coefficients

B.1 Parameters for EoS:

In this appendix we provide the expressions for f_n 's appearing in Eq. 5.8.

$$f_0 = 1 + \frac{3N_f}{32}(7 + 120\hat{\mu}_q^2 + 240\hat{\mu}_q^4) \quad (\text{B.1})$$

$$f_2 = -\frac{15}{4} \left[1 + \frac{N_f}{12}(5 + 72\hat{\mu}_q^2 + 144\hat{\mu}_q^4) \right] \quad (\text{B.2})$$

$$f_3 = 30 \left[1 + \frac{N_f}{6}(1 + 12\hat{\mu}_q^2) \right]^{3/2} \quad (\text{B.3})$$

$$\begin{aligned} f_4 = & 237.223 + (15.963 + 124.773\hat{\mu}_q^2 - 319.849\hat{\mu}_q^4)N_f - (0.415 + 15.926\hat{\mu}_q^2 + 106.719\hat{\mu}_q^4)N_f^2 \\ & + \frac{135}{2} \left[1 + \frac{N_f}{6}(1 + 12\hat{\mu}_q^2) \right] \ln \left[\left(\frac{\alpha_s}{\pi} \right) \left(1 + \frac{N_f}{6}(1 + 12\hat{\mu}_q^2) \right) \right] \\ & - \frac{165}{2} \left[1 + \frac{N_f}{12}(5 + 72\hat{\mu}_q^2 + 144\hat{\mu}_q^4) \right] \left(1 - \frac{2N_f}{33} \right) \ln \hat{M} \end{aligned} \quad (\text{B.4})$$

$$\begin{aligned}
 f_5 = & -\sqrt{1 + \frac{N_f}{6}(1 + 12\hat{\mu}_q^2)[799.149 + (21.963 - 137.33\hat{\mu}_q^2 + 482.171\hat{\mu}_q^4)N_f]} \\
 & + (1.926 + 2.0749\hat{\mu}_q^2 - 172.07\hat{\mu}_q^4)N_f^2 + \frac{495}{12}[6 + N_f(1 + 12\hat{\mu}_q^2)] \left(1 - \frac{2N_f}{33}\right) \ln \hat{M}
 \end{aligned} \tag{B.5}$$

$$\begin{aligned}
 f_6 = & - [659.175 + (65.888 - 341.489\hat{\mu}_q^2 + 1446.514\hat{\mu}_q^4)N_f + (7.653 + 16.225\hat{\mu}_q^2 - 516.210\hat{\mu}_q^4)N_f^2 \\
 & - \frac{1485}{2} \left(1 + \frac{N_f}{6}(1 + 12\hat{\mu}_q^2)\right) \left(1 - \frac{2N_f}{33}\right) \ln \hat{M}] \ln \left[\left(\frac{\alpha_s}{\pi}\right) \left(1 + \frac{N_f}{6}(1 + 12\hat{\mu}_q^2)\right) 4\pi^2 \right] \\
 & - 475.587 \ln \left[\left(\frac{\alpha_s}{\pi}\right) 4\pi^2 C_A \right]
 \end{aligned} \tag{B.6}$$

B.2 C_l and v_n :

In this appendix we derive a relation between anisotropic flow coefficients, v_n and the coefficients, a_{lm} . The p_T distribution can be written as:

$$\frac{dN}{d^2p_T dy}(p_T, \theta, \phi) = \frac{1}{2\pi} \frac{dN}{p_T dp_T dy} \left(1 + \sum_{n=1}^{\infty} v_n \cos(n\phi)\right) \tag{B.7}$$

which can also be written as:

$$\frac{dN}{d^2p_T dy}(p_T, \theta, \phi) = \bar{N} + \sum_{l=1}^{\infty} \sum_{m=-l}^l a_{lm} Y_{lm}(\theta, \phi) \tag{B.8}$$

which leads to

$$\frac{1}{2\pi} \frac{dN}{p_T dp_T dy} \left(1 + \sum_{n=1}^{\infty} v_n \cos(n\phi)\right) = \bar{N} + \sum_{l=1}^{\infty} \sum_{m=-l}^l a_{lm} Y_{lm}(\theta, \phi)$$

Multiplying both sides of the above Eq. by $\cos(k\phi)$ and integrating over ϕ we get,

$$\int_0^{2\pi} d\phi \cos(k\phi) \frac{1}{2\pi} \frac{dN}{p_T dp_T dy} \left(1 + \sum_{n=1}^{\infty} v_n \cos(n\phi) \right) = \int_0^{2\pi} d\phi \cos(k\phi) \left(N_0 + \sum_{l=1}^{\infty} \sum_{m=-l}^l a_{lm} Y_{lm}(\theta, \phi) \right)$$

This gives

$$\frac{1}{2\pi} \frac{dN}{p_T dp_T dy} \int_0^{2\pi} d\phi \cos(k\phi) \sum_{n=1}^{\infty} v_n \cos(n\phi) = \int_0^{2\pi} d\phi \cos(k\phi) \sum_{l=1}^{\infty} \sum_{m=-l}^l a_{lm} Y_{lm}(\theta, \phi)$$

Now v_k can be expressed as:

$$\frac{1}{2\pi} \frac{dN}{p_T dp_T dy} v_k = \int_0^{2\pi} d\phi \cos(k\phi) \sum_{l=1}^{\infty} \sum_{m=-l}^l a_{lm} Y_{lm}(\theta, \phi)$$

Writing Y_{lm} in terms of associated Legendre polynomials and $e^{im\phi}$ we obtain,

$$\frac{1}{2\pi} \frac{dN}{p_T dp_T dy} v_k = \int_0^{2\pi} d\phi \cos(k\phi) \sum_{l=1}^{\infty} \sum_{m=-l}^l a_{lm} \sqrt{\frac{2l+1}{4\pi} \frac{(l-m)!}{(l+m)!}} P_l^m(\cos \theta) [\cos(m\phi) + i \sin(m\phi)]$$

Performing the ϕ integration we get,

$$\frac{1}{2\pi} \frac{dN}{p_T dp_T dy} v_k = \sum_{l \geq k}^{\infty} \sqrt{\frac{2l+1}{4\pi}} \left[a_{l,k} \sqrt{\frac{(l-k)!}{(l+k)!}} P_l^k(\cos \theta) + a_{l,-k} \sqrt{\frac{(l+k)!}{(l-k)!}} P_l^{-k}(\cos \theta) \right]$$

On simplification we obtain the relation between the flow harmonics and $a_{l,k}$ as:

$$\frac{1}{2\pi} \frac{dN}{p_T dp_T dy} v_k = \sum_{l \geq k}^{\infty} \sqrt{\frac{2l+1}{4\pi} \frac{(l-k)!}{(l+k)!}} [a_{l,k} + (-1)^k a_{l,-k}] P_l^k(\cos \theta)$$

APPENDIX C

Phase Space Derivatives

In this appendix we will show in details the computation of the bulk viscosity. For simplicity we assume that the state of the hadronic matter under consideration can be described by two independent thermodynamic variables: *i.e.* temperature (T) and baryonic chemical potential (μ). When we take partial derivative w.r.t. T it is understood that μ is constant and vice-versa and hence we do not mention this explicitly. The differential of $P(T, \mu)$ can be written as

$$\begin{aligned}dP &= \left(\frac{\partial P}{\partial T}\right) dT + \left(\frac{\partial P}{\partial \mu}\right) d\mu \\ \frac{\partial P}{\partial n} &= \left(\frac{\partial P}{\partial T}\right) \frac{\partial T}{\partial n} + \left(\frac{\partial P}{\partial \mu}\right) \frac{\partial \mu}{\partial n} \\ \left(\frac{\partial P}{\partial n}\right)_\epsilon &= \left(\frac{\partial P}{\partial T}\right) \left(\frac{\partial T}{\partial n}\right)_\epsilon + \left(\frac{\partial P}{\partial \mu}\right) \left(\frac{\partial \mu}{\partial n}\right)_\epsilon\end{aligned}$$

where $\left(\frac{\partial n}{\partial T}\right)_\epsilon = \left(\frac{\partial n}{\partial T}\right) + \left(\frac{\partial n}{\partial \mu}\right) \left(\frac{\partial \mu}{\partial T}\right)_\epsilon$, $\left(\frac{\partial n}{\partial \mu}\right)_\epsilon = \left(\frac{\partial n}{\partial \mu}\right) + \left(\frac{\partial n}{\partial T}\right) \left(\frac{\partial T}{\partial \mu}\right)_\epsilon$. We have $\left(\frac{\partial T}{\partial \mu}\right)_\epsilon = -\frac{\left(\frac{\partial \epsilon}{\partial \mu}\right)}{\left(\frac{\partial \epsilon}{\partial T}\right)}$ along the constant ϵ trajectory and finally $\frac{\partial n}{\partial s}$ can be written as $\left(\frac{\partial n}{\partial s}\right) = \left(\frac{\partial n}{\partial T}\right) \left(\frac{\partial T}{\partial s}\right) + \left(\frac{\partial n}{\partial \mu}\right) \left(\frac{\partial \mu}{\partial s}\right)$. Thus, bulk viscosity to entropy density ratio in units of the

relaxation time scale can be expressed as:

$$\begin{aligned}
 \frac{\zeta}{s\tau_R} &= - \left(\frac{\partial P}{\partial n} \right)_\epsilon \left(\frac{\partial n}{\partial s} \right) \\
 &= - \left(\frac{\left(\frac{\partial P}{\partial T} \right)}{\left(\frac{\partial n}{\partial T} \right) - \left(\frac{\partial n}{\partial \mu} \right) \left(\frac{\partial \epsilon}{\partial T} \right)} + \frac{\left(\frac{\partial P}{\partial \mu} \right)}{\left(\frac{\partial n}{\partial \mu} \right) - \left(\frac{\partial n}{\partial T} \right) \left(\frac{\partial \epsilon}{\partial \mu} \right)} \right) \left(\left(\frac{\partial n}{\partial T} \right) \left(\frac{\partial T}{\partial s} \right) + \left(\frac{\partial n}{\partial \mu} \right) \left(\frac{\partial \mu}{\partial s} \right) \right)
 \end{aligned} \tag{C.1}$$

Now all the derivatives in Eq. C.1 can be evaluated starting from the expression of $\ln Z$ within the HRG model. To begin with, the partition function $Z(T, V, \mu)$ is given by

$$\ln Z^{GC}(T, V, \{\mu_i\}) = \sum_i \frac{g_i}{2\pi^2} VT^3 \sum_{n=1}^{\infty} \frac{(\mp 1)^{(n+1)}}{n^4} x_i^2 K_2(x_i) e^{y_i}$$

The pressure P is obtained by operating $T \frac{\partial}{\partial V}$ on $\ln Z^{GC}$

$$P^{GC}(T, V, \{\mu_i\}) = \sum_i \frac{g_i}{2\pi^2} T^4 \sum_{n=1}^{\infty} \frac{(\mp 1)^{(n+1)}}{n^4} x_i^2 K_2(x_i) e^{y_i}$$

where $x_i = nm_i/T$ and $y_i = n\mu_i/T$ introduced for brevity in notation. Further the derivatives of P are obtained as

$$\begin{aligned}
 \left(\frac{\partial P^{GC}}{\partial T} \right) &= \frac{1}{V} \left\{ \ln Z^{GC} + \frac{1}{T} \left(E^{GC} - \sum_i \mu_i N_i^{GC} \right) \right\} \\
 \left(\frac{\partial P^{GC}}{\partial \mu_i} \right) &= \frac{1}{V} \sum_i N_i^{GC}
 \end{aligned}$$

The particle number and its derivatives are given by

$$\begin{aligned}
 N_i^{GC}(T, V, \mu_i) &= T \frac{\partial \ln Z^{GC}}{\mu_i} \\
 N_i^{GC}(T, V, \mu_i) &= \frac{g_i}{2\pi^2} V T^3 \sum_{n=1}^{\infty} \frac{(\mp 1)^{(n+1)}}{n^3} x_i^2 K_2(x_i) e^{y_i} \\
 \left(\frac{\partial N_i^{GC}}{\partial T} \right) &= \frac{g_i V m_i^2}{2\pi^2} \sum_{n=1}^{\infty} \frac{(\mp 1)^{n+1}}{n} e^{y_i} \left[\frac{x_i}{2} K_1(x_i) + (1 - y_i) K_2(x_i) + \frac{x_i}{2} K_3(x_i) \right] \\
 \left(\frac{\partial N_i^{GC}}{\partial \mu} \right)_T &= \frac{B_i g_i}{2\pi^2} V T^2 \sum_{n=1}^{\infty} \frac{(\mp 1)^{(n+1)}}{n^2} x_i^2 K_2(x_i) e^{y_i}
 \end{aligned}$$

The energy and its derivatives are given by

$$E^{GC}(T, V, \{\mu_i\}) = T^2 \frac{\partial \ln Z^{GC}}{\partial T} + \sum_i \mu_i N_i^{GC}$$

$$\begin{aligned}
 E^{GC}(T, V, \{\mu_i\}) &= \sum_i C_i T \sum_{n=1}^{\infty} \frac{(\mp 1)^{(n+1)}}{n^2} e^{y_i} \left[\frac{x_i}{2} K_1(x_i) \right. \\
 &\quad \left. + (1 - y_i) K_2(x_i) + \frac{x_i}{2} K_3(x_i) \right] + \sum_i \mu_i N_i^{GC}
 \end{aligned} \tag{C.2}$$

$$\begin{aligned}
 \left(\frac{\partial E^{GC}}{\partial T} \right)_\mu &= \sum_i C_i \sum_{n=1}^{\infty} \frac{(\mp 1)^{n+1}}{n^2} e^{y_i} \left[\frac{x_i^2}{4} K_0(x_i) + (-x_i y_i + x_i) K_1(x_i) \right. \\
 &\quad \left. + (y_i^2 + \frac{x_i^2}{2}) + 2(1 - y_i) K_2(x_i) + (-x_i y_i + x_i) K_3(x_i) + \frac{x_i^2}{4} K_4(x_i) \right] + \sum_i \mu_i \frac{\partial N_i}{\partial T}
 \end{aligned} \tag{C.3}$$

$$\begin{aligned}
 \left(\frac{\partial E^{GC}}{\partial \mu} \right)_T &= \sum_i C_i \sum_{n=1}^{\infty} \frac{(\mp 1)^{(n+1)}}{n} e^{y_i} \left[\frac{x_i}{2} K_1(x_i) - y_i K_2(x_i) + \frac{x_i}{2} K_3(x_i) \right] \\
 &\quad + \sum_i \left(N_i + \mu_i \frac{\partial N_i}{\partial \mu} \right)
 \end{aligned} \tag{C.4}$$

where

$$\mathcal{C}_i = g_i \frac{VT}{2\pi^2} m_i^2 \quad (\text{C.5})$$

Finally the entropy and its derivatives are given by

$$\begin{aligned} S^{GC}(T, V, \{\mu_i\}) &= \frac{1}{T} \left\{ E^{GC}(T, V, \{\mu_i\}) + P^{GC}(T, V, \{\mu_i\})V - \sum_i \mu_i N_i^{GC}(T, V, \mu_i) \right\} \\ \left(\frac{\partial S^{GC}}{\partial T} \right) &= -\frac{S}{T} + \frac{1}{T} \left\{ \left(\frac{\partial E^{GC}}{\partial T} \right) + V \frac{\partial P}{\partial T} - \sum_i \mu_i \left(\frac{\partial N_i^{GC}}{\partial T} \right) \right\} \\ \left(\frac{\partial S^{GC}}{\partial \mu} \right) &= \frac{1}{T} \left\{ \left(\frac{\partial E^{GC}}{\partial \mu} \right) + V \frac{\partial P}{\partial \mu} - \sum_i N_i - \sum_i \mu_i \left(\frac{\partial N_i^{GC}}{\partial \mu} \right) \right\} \end{aligned}$$

where we have used

$$\frac{\partial}{\partial \mu} = \sum_i \frac{\partial \mu_i}{\partial \mu} \frac{\partial}{\partial \mu_i}$$

The speed of sound, c_s can be used as a regulator for CSB. A system with $c_s^2 \rightarrow 1/3$ will indicate the restoration of CSB. Therefore, we the expression to estimate, c_s within the ambit of present model is recalled below.

$$\begin{aligned} c_s^2 &= \left(\frac{\partial P}{\partial \epsilon} \right)_{s/n_B} \\ &= \left(\frac{\partial P}{\partial T} \right) \left(\frac{\partial T}{\partial \epsilon} \right)_{s/n_B} + \left(\frac{\partial P}{\partial \mu} \right) \left(\frac{\partial \mu}{\partial \epsilon} \right)_{s/n_B} \end{aligned}$$

Now for constant s/n_B , $d(s/n_B) = \frac{\partial(s/n_B)}{\partial T} dT + \frac{\partial(s/n_B)}{\partial \mu} d\mu = 0$. This implies that

$$\left(\frac{\partial T}{\partial \mu} \right)_{s/n_B} = -\frac{\frac{\partial(s/n_B)}{\partial \mu}}{\frac{\partial(s/n_B)}{\partial T}}. \text{ Thus}$$

$$\begin{aligned} \left(\frac{\partial \epsilon}{\partial T} \right)_{s/n_B} &= \frac{\partial \epsilon}{\partial T} - \frac{\partial \epsilon}{\partial \mu} \left(\frac{\frac{\partial(s/n_B)}{\partial T}}{\frac{\partial(s/n_B)}{\partial \mu}} \right) \\ \left(\frac{\partial \epsilon}{\partial \mu} \right)_{s/n_B} &= \frac{\partial \epsilon}{\partial \mu} - \frac{\partial \epsilon}{\partial T} \left(\frac{\frac{\partial(s/n_B)}{\partial \mu}}{\frac{\partial(s/n_B)}{\partial T}} \right) \end{aligned}$$

Thus finally the expression for c_s turns out to be

$$c_s^2 = \left(\frac{\left(\frac{\partial P}{\partial T}\right)_\mu}{\left(\frac{\partial \epsilon}{\partial T}\right)_\mu - \left(\frac{\partial \epsilon}{\partial \mu}\right)_T \frac{\left(\frac{\partial(s/n_B)}{\partial T}\right)}{\left(\frac{\partial(s/n_B)}{\partial \mu}\right)}} + \frac{\left(\frac{\partial P}{\partial \mu}\right)_T}{\left(\frac{\partial \epsilon}{\partial \mu}\right)_T - \left(\frac{\partial \epsilon}{\partial T}\right)_\mu \frac{\left(\frac{\partial(s/n_B)}{\partial \mu}\right)}{\left(\frac{\partial(s/n_B)}{\partial T}\right)}} \right).$$

Bibliography

- [1] D. Griffiths, "Introduction to Elementary Particles" Wiley-VCH, Weinheim, 2008.
- [2] F. Halzen and A.D. Martin, "QUARKS AND LEPTONS: An Introductory Course Modern Particle Physics" Wiley-India, New Delhi, 1984.
- [3] L. H. Ryder, Chapter 1: "Quantum Field theory" Cambridge University Press, Cambridge 1985, 1996
- [4] M. E. Peskin and D. V. Schroeder, "An Introduction to Quantum Field Theory" Levant Books, Kolkata, 1995.
- [5] T. Muta, "Foundations of Quantum Chromodynamics: An Introduction to Perturbative Methods in Gauge Theories" World Scientific Lecture Notes in Physics - Vol. **57**, 1994.
- [6] C. Quigg, "Gauge Theories of the Strong, Weak and Electromagnetic", Addison-Wesley Publishing Company, 1994.
- [7] D. J. Gross and F. Wilczek, Phys. Rev. Lett. **30**, 1343 (1973).
- [8] D. J. Gross and Frank Wilczek, Phys. Rev. D, **8** 3633 (1973).
- [9] H. D. Politzer, Phys. Rev. Lett. **30**, 1346 (1973).
- [10] S. Bethke, J. Phys G **26**, R27 (2000).

- [11] J. C. Collins and M. J. Perry, Phys. Rev. Lett. **34**, 1353 (1975).
- [12] F. Karsch, Lect. Notes Phys.**583** 209 (2002) [arXiv:hep-lat/0106019]; Nucl. Phys. A **698**, 199 (2002)
- [13] F. Karsch, E. Laermann and A. Peikert, Phys. Lett. B 478, 447 (2000).
- [14] E. Shuryak, Rev. Mod. Phys. **61**, 71 (1980).
- [15] M. Riordan and W. A. Zajc, Sci. Am. **294**,N5, 24 (2006) [Spektrum Wiss. 2006N11, 36 (2006)].
- [16] A. Akmal, V. R. Pandharipande and D. G. Ravenhall, Phys. Rev. C **58**, 1804 (1998) [nucl-th/9804027].
- [17] J. M. Torres-Rincon, Introduction to Relativistic Heavy Ion Collisions. In: Hadronic Transport Coefficients from Effective Field Theories, Springer Theses (Recognizing Outstanding Ph.D. Research). Springer, Cham (2014)[arXiv:1205.0782].
- [18] Kliemant, M. et al. "Global Properties of Nucleus–Nucleus Collisions". Lect. Notes Phys. **785**,23–103 (2010).
- [19] G.-Y. Qin, Int.J.Mod.Phys. E **24**, 1530001 (2015).
- [20] E. Eichten, K. Gottfried, T. Kinoshita, K. D. Lane and T. M. Yan, Phys. Rev. D **17**, 3090 (1978).
- [21] E. Eichten, K. Gottfried, T. Kinoshita, K. D. Lane and T. M. Yan, Phys. Rev. D **21**, 203 (1980).
- [22] T. Matsui and H. Satz, Phys. Lett. B **178** , 416 (1986).
- [23] T. Hashimoto, O. Miyamura, K. Hirose, and T. Kanki Phys. Rev. Lett. **57** 2123 (1986).

- [24] J. Alam, *Pramana* **84** 861(2015).
- [25] L. McLerran and T. Toimela, *Phys. Rev. D* **31**, 545 (1985).
- [26] C. Gale and J.I. Kapusta, *Nucl. Phys. B* **357**, 65 (1991).
- [27] R. Chatterjee, L. Bhattacharya and D. K. Srivastava, arXiv:0901.3610v1 [nucl-th].
- [28] K.J. Eskola, hep-ph/9911350.
- [29] M. Gyulassy, I. Vitev, X. N. Wang, and B.W. Zhang, in *QuarkGluon Plasma 3*, edited by R. C. Hwa and X. N.Wang (World Scientific, Singapore, 2004) [arXiv:nucl-th/ 0302077].
- [30] J.D. Bjorken, FERMILAB-PUB-82-59-THY (1982).
- [31] J. Adams et al. (STAR Collaboration) *Nucl. Phys. A* **757**, 102 (2005).
- [32] K. Adcox et al. (PHENIX Collaboration), *Nucl. Phys. A* **757**, 184 (2005).
- [33] J. Y. Ollitrault, *Phys. Rev. D* **46**, 229 (1992).
- [34] S. Voloshin and Y. Zhang, *Z.Phys.C* **70**, 665 (1996).
- [35] P. Huovinen, P.V. Ruuskanen, *Ann. Rev. Nucl. Part. Sci.* **56**, 163 (2006)
- [36] P. Huovinen and P. V. Ruuskanen, *Ann. Rev. Nucl. Part. Sci.* **56**, 163 (2006).
- [37] D. A. Teaney, arXiv:0905.2433 [nucl-th].
- [38] S. S. Adler et al. (PHENIX Collaboration), *Phys. Rev. Lett.* **91**, 182301 (2003).
- [39] K. H. Ackemann et al. (STAR Collaboration), *Phys. Rev. Lett.* **86**, 402 (2003).
- [40] U. Heinz and P. F. Kolb, *Nucl. Phys. A* **702**, 269 (2002).90
- [41] P. F. Kolb and U.W. Heinz, in *QuarkGluon Plasma 3*, edited by R. C. Hwa and X. N.Wang (World Scientific, Singapore, 2004) [arXiv:nucl-th/0305084].

BIBLIOGRAPHY

- [42] J. Adams et al. (STAR Collaboration), Phys. Rev. Lett. **92**, 052302 (2004).
- [43] J. Adams et al. (STAR Collaboration), Phys. Rev. C **72**, 014904 (2005).
- [44] J. Adams et al. (STAR Collaboration), Phys. Rev. Lett. **95**, 122301 (2005).
- [45] A. Adare et al. (PHENIX Collaboration), Phys. Rev. Lett. **98**, 162301 (2007).
- [46] A. Adare et al. (PHENIX Collaboration), Phys. Rev. Lett. **99**, 052301 (2007).
- [47] J. Adams et al. (STAR Collaboration), Phys. Rev. C **77**, 054901 (2008).
- [48] R.A.Lacey and A.Taranenko, PoS(CFRNC2006)021.
- [49] C.-J. Zhang and J. Xu Phys. Rev. C **93**, 024906(2016).
- [50] J. Rafelski and B. Muller, Phys. Rev. Lett. **48**, 1066 (1982); (E) **56** 2334 (1986).
- [51] P. Koch, B. Muller and J. Rafelski, Phys. Rep. **142**, 167 (1986).
- [52] J. Rafelskia, Eur. Phys. J ST **155**, 139, (2008)89.
- [53] M. Gazdzicki, J. Phys. G **30**, S701 (2004).
- [54] J. Cleymans, H. Oeschler, K. Redlich and S. Wheaton, Eur.Phys.J.A **29**, 119 (2006).
- [55] S. Jeon, V. Koch, Quark–Gluon Plasma 3(2004), World Scientific [arXiv:hep-ph/0304012].
- [56] B.Friman, Nucl.Phys. A **928** (2014) 198.
- [57] S. K. Das, J. Alam, PoS WPCF2011 (2011) 059; S.K. Das, Heavy Flavor Production and Propagation in Heavy Ion Collision (Thesis) (<http://www.hbni.ac.in/students/phdlist.html>).
- [58] A. K. Chaudhuri, A Short Course on Relativistic Heavy Ion Collisions, Institute of Physics Publishing, 2014.

BIBLIOGRAPHY

- [59] H. Wang, Study of particle ratio fluctuations and charge balance functions at RHIC [Ph.D. thesis], Michigan State University, 2013, <http://arxiv.org/abs/1304.2073>.
- [60] E. Shuryak *Rev. Mod. Phys.* **89**, 035001(2017).
- [61] P. Braun-Munzinger and J. Stachel, *Nature*, **448**, 302 (2007).
- [62] J. I. Kapusta, B. Muller and M. Stephanov, *Phys. Rev. C* **85**, 054906 (2012).
- [63] S. Gavin and G. Moschelli, *Phys. Rev. C* **85**, 014905 (2012); S. Gavin and G. Moschelli, *Phys. Rev. C* **86**, 034902 (2012); S. Gavin and M. Abdel-Aziz, *Phys. Rev. Lett.* **97**, 162302 (2006); S. Gavin, *Phys. Rev. Lett.* **92**, 162301 (2004).
- [64] S. Jeon and U. Heinz, *Int. J. Mod. Phys. E* **24**, 1530010 (2015),
- [65] Amaresh Jaiswal and Victor Roy, "Relativistic Hydrodynamics in Heavy-Ion Collisions: General Aspects and Recent Developments," *Advances in High Energy Physics*, vol. 2016, Article ID 9623034, 39 pages, 2016.
- [66] L D Landau, E.M. Lifshitz, *Fluid Mechanics* (Elsevier, New Delhi, 2011)
- [67] S. Weinberg, *Gravitation and Cosmology* (John Wiley & Sons, New York, 1972)
- [68] P. I. Kovtun, *J. Phys. A: Math. Theor.* **45** 473001(2012).
- [69] A. Kumar, J. R. Bhatt, A. P. Mishra, *Nucl. Phys. A* **925**, 199 (2014)
- [70] P. Kovtun, Guy D. Moore, and Paul Romatschke, *Phys. Rev. D* **84**, 025006 (2011)
- [71] Y. Akamatsu, A. Mazeliauskas, and D. Teaney, *Phys. Rev. C* **95**, 014909 (2017)
- [72] S. R. de Groot, W. A. van Leeuwen and C. G. van Weert, *Relativistic kinetic theory : principles and applications*, North-Holland Publishing Co., Amsterdam, 1980.

- [73] C. Cercignani and G. M. Kremer, *The relativistic Boltzmann equation: theory and applications*, Springer Basel AG, 2002.
- [74] J. Steinheimer, M. Bleicher, H. Petersen, S. Schramm, H. Stöcker, and D. Zschesche, *Phys. Rev. C*, **77**, no. 3, Article ID 034901, 2008.
- [75] L. Pang, Q. Wang, and X. Wang, *Phys. Rev. C*, **86**, no. 2, Article ID 024911, 2012.
- [76] R. S. Bhalerao, A. Jaiswal, and S. Pal, *Phys. Rev. C*, **92**, no. 1, Article ID 014903, 2015.
- [77] B. Zhang, C. M. Ko, B. A. Li, and Z. W. Lin, *Phys. Rev. C*, **61**, Article ID 067901, 2000.
- [78] Z. W. Lin, C. M. Ko, B. A. Li, B. Zhang, and S. Pal, *Phys. Rev. C*, **72**, Article ID 064901, 2005.
- [79] X.-N. Wang and M. Gyulassy, *Phys. Rev. D*, **44**, no. 11, Article ID 3501, 1991.
- [80] M. Gyulassy and X.-N. Wang, *Computer Physics Communications*, **83**, no. 2-3, pp. 307–331, 1994.
- [81] G. Sarwar and J. Alam, *Int. J. Mod. Phys. A* **33**, 1850040 (2018).
- [82] R. Durrer, *The Cosmic Microwave Background*, Cambridge University Press, 2008.
- [83] P. Staig and E. Shuryak, *Phys. Rev. C* **84**, 034908; *Phys. Rev. C* **84**, 044912 (2011).
- [84] S. Floerchinger and U. A. Wiedemann, *Phys. Rev. C* **88**, 044906 (2013), S. Floerchinger and U. A. Wiedemann, *Phys. Lett. B* **728**, 407 (2014).
- [85] S. Shi, J. Liao and P. Zhuang, *Phys. Rev. C* **90**, 064912 (2014).

BIBLIOGRAPHY

- [86] A. P. Mishra, R. K. Mohapatra, P. S. Saumia and A. M. Srivastava, *Phys. Rev. C* **81**, 034903 (2010).
- [87] G.-Y. Qin and B. Mueller, *Phys. Rev. C* **85**, 061901(R) (2012).
- [88] M. A. Stephanov, K. Rajagopal and E. V. Shuryak, *Phys. Rev. Lett.* **81**, 4816 (1998).
- [89] M. A. Stephanov, K. Rajagopal and E. V. Shuryak, *Phys. Rev. D* **60**, 114028 (1999).
- [90] M. Asakawa, U. Heinz and B. Muller, *Phys. Rev. Lett.* **85**, 2072 (2000).
- [91] S. Jeon and V. Koch, *Phys. Rev. Lett.* **83**, 5435 (1999).
- [92] S. Jeon and V. Koch, *Phys. Rev. Lett.* **85**, 2076 (2000).
- [93] M. A. Stephanov, *Phys. Rev. D* **81**, 054012 (2010).
- [94] S. Mrowczynski, *Phys. Rev. C* **57**, 1518 (1998).
- [95] A. Rafiei and K. Javidan, *Phys. Rev. C* **94**, 034904 (2016).
- [96] Y. Xu, P. Moreau, T. Song, M. Nahrgang, S. A. Bass, and E. Bratkovskaya, *Phys. Rev. C* **96**, 024902 (2017).
- [97] E. Iancu and Bin Wu, *Nuclear Physics A* **956** (2016) 581–584, [http://dx.doi.org/10.1007/JHEP10\(2015\)155](http://dx.doi.org/10.1007/JHEP10(2015)155).
- [98] E. M. Lifshitz and L. P. Pitaevskii, *Physical Kinetics* (Elsevier, New York, 1987).
- [99] H. K.-Suonio, "Cosmology I" (lecture notes), <http://www.helsinki.fi/hkurkisu/cosmology/Cosm10.pdf>.
- [100] E. Flowers and N. Itoh, *Astrophys. J.* **230**, 847 (1979).

BIBLIOGRAPHY

- [101] C. -P. Ma and E. Bertschinger, *Astro. Phys. J.* **455**, 7 (1995).
- [102] W. Florkowski, R. Ryblewski, M. Strickland, *Phys. Rev. C* **88**, 024903 (2013).
- [103] W. Florkowski, R. Ryblewski, M. Strickland, *Phys. Rev. D* **86**, 085023 (2012).
- [104] Y. Hatta, M. Martinez and B. -W. Xiao, *Phys. Rev. D* **91**. 085024 (2015).
- [105] M. H. Thoma, *Phys. Rev. D* **49**, 451 (1994).
- [106] G.S. Denicol et al, *Phys. Rev. Lett.* **113**, 202301 (2014)
- [107] D. Bazow et al, *Phys. Rev. Lett.* **116**, 022301 (2016)
- [108] J. Tindall, J. M. Torres-Rincon, J. B. Rose and H. Petersen, *Phys. Lett. B* **770**, 532 (2017).
- [109] H. Levine, *Partial Differential Equations*, American Mathematical Society (1997).
- [110] J. D. Bjorken, *Phys. Rev. D* **27**, 140 (1983).
- [111] S. K. Singh *et al.* under preparation.
- [112] M. Luzum and H. Petersen, *J. Phys. G: Nucl. Part. Phys.* **41** 063102 (2014)
- [113] G. Sarwar, S. K. Singh and J. Alam. *Int. J.M.Phys. A* **33**, (2018)1850121.
- [114] W. Hu and S. Dodelson, *Ann. Rev. Astron. Astrophys.* **40**, 171 (2002)
- [115] S. Jeon, V. Koch, arXiv:hep-ph/0304012
- [116] B. Schenke, S. Jeon, and C. Gale, *Phys. Rev. Lett.* **106**, 042301 (2011).
- [117] D. Teaney and L. Yan, *Phys. Rev. C* **83**, 064904 (2011).
- [118] R. A. Lacey, et al., *Phys. Rev. C* **83**, 044902 (2011).
- [119] L. X. Han, et al., *Phys. Rev. C* **84**, 064907 (2011).

- [120] R. S. Bhalerao, M. Luzum, and J.-Y. Ollitrault, Phys. Rev. C **84** , 034910 (2011);
- [121] E. Retinskaya, M. Luzum, J.-Y. Ollitrault, Phys. Rev. C **89**, 014902 (2014);
J.-Y. Ollitrault, A. M. Poskanzer, and S. A. Voloshin, Phys. Rev. C **80**, 014904 (2009)
- [122] G. Giacalone, J. Noronha-Hostler, and J.-Y. Ollitrault, Phys. Rev. C **95**, 054910 (2017)
- [123] B. Alver et al., Phys. Rev. C **77**, 014906(2008)
- [124] A. Mocsy and P. Sorensen, Nucl. Phys. A **855**, 241 (2011).
- [125] P. Naselsky *et al.*, Phys. Rev. C **86**, 024916 (2012).
- [126] F. J. Llanes-Estrada and J. L. M. Martinez, Nucl.Phys. A **970**, 107 (2018);
arXiv:1612.05036 [hep-ph].
- [127] X.- N. Wang and M. Gyulassy, Phys. Rev. D **44**, 3501 (1991).
- [128] M. L. Miller, K. Reygers, S. J. Sanders and P. Steinberg, Ann. Rev. Nucl. Part. Sci. **57**, 205 (2007). DOI:10.1146/annurev.nucl.57.090506.123020
- [129] M. Bleicher *et al.*, J. Phys G. **25**, 1859 (1999).
- [130] J. Adams et al, Phys. Rev. Lett., 97(16), [162301]
- [131] Iu. Karpenko, P. Huovinen, M. Bleicher, Comp. Phys. Comm. **185**, 3016 (2014).
- [132] M. Albright, J. Kapusta and C. Young, Phys. Rev. C **56**, 024915 (2014)
- [133] G. D. Yen, M. I. Gorenstein, W. Greiner and S.N. Yang, Phys. Rev. C **56** (1997) 2210
- [134] A. Vuorinen, Phys. Rev. D **67**, 074032 (2003); **68**, 054017 (2003)

- [135] N. Haque, M. G. Mustafa and M. Strickland, Phys. Rev. D **87**, 105007 (2013)
- [136] Particle data Group, J. Beringer *et al.*, Phys. Rev. D. **86**, 010001 (2012).
- [137] S. Borsányi *et al.*, Phys. Lett. B **370** (2014) 99-104
- [138] F. Cooper, G. Frye, Phys. Rev. D **10** (1974) 186.
- [139] J. Admas *et al.* (for ALICE collaboration) Phys. Rev. Lett. **117**, 182301 (2016).
- [140] N. Borghini, J.Y. Ollitrault, Phys. Lett. B **642**, 227 (2006).
- [141] U. Heinz and R. Snellings, Ann. Rev. Nucl. Part. Sci. **63**, 63 (2013).
- [142] P. B. Arnold, C. Dogan, and G. D. Moore, Phys. Rev. D **74**, 085021 (2006).
- [143] F. G. Gardin, F. Grassi, M. Luzum and J. Noronha-Hostler, Phys. Rev. C **95**, 034901 (2017).
- [144] J. Adams *et al.* (for ALICE collaboration), Phys. Rev. Lett. **117** 182310 (2016).
- [145] E. Retinsaya, M. Luzum and J. Y. Ollitrault, Phys. Rev. C **89**, 014902 (2014).
- [146] H. Petersen, C. Coleman-Smith, S. A. Bass and R. Wolpert, J. Phys. G **58**, 045102 (2011).
Phys. Lett. B **730**, 99 (2014).
- [147] G. Sarwar, S. Chatterjee and J. Alam, J. Phys. G: Nucl. Part. Phys. **44** 055101 (2017).
- [148] U. Heinz and S. Raimond, Ann. Rev. Nucl. Part. Sci., **63**, 123 (2013).
- [149] C. Gale, S. Jeon and B. Schenke, Int. J. Mod. Phys. A **28**, 1340011 (2013).
- [150] P. Romatschke and U. Romatschke, Phys. Rev. Lett., **99**, 172301 (2007).

BIBLIOGRAPHY

- [151] H. Song, Nucl. Phys. A **904**, 114c (2013).
- [152] B. Alver and G. Roland, Phys. Rev. C **81**, 054905 (2010).
- [153] F. G. Gardim, F. Grassi, M. Luzum, J.-Y. Ollitrault, Phys. Rev. C **85**, 024908 (2012).
- [154] H. Niemi, G. S. Denicol, H. Holopainen and P. Huovinen, Phys. Rev. C **87**, 054901 (2013).
- [155] K. Dusling and T. Schäfer, Phys. Rev. C **85**, 044909 (2012).
- [156] M. Gyulassy and L. McLerran, Nucl. Phys. A **750**, 30 (2005).
- [157] I. Arsene *et al.* (for BRAHMS collaboration), Nucl. Phys. A **757**, 1 (2005).
- [158] K. Adcox *et al.* (for PHENIX collaboration), Nucl. Phys. A **757**, 184 (2005).
- [159] B. B. Back *et al.* (for PHOBOS collaboration), Nucl. Phys. A **757**, 28 (2005).
- [160] J. Adams *et al.* (for STAR collaboration) Nucl. Phys. A **757**, 102 (2005).
- [161] P. Kovtun, D. T. Son and A. O. Starinets, Phys. Rev. Lett. **94**, 111601 (2005).
- [162] S. S. Gubser, A. Nellore, S. S. Pufu, F. D. Rocha Phys. Rev. Lett. **101**, 131601 (2008).
- [163] H. B. Meyer, Phys. Rev. Lett. **100**, 162001 (2008).
- [164] F. Karsch, D. Kharzeev and K. Tuchin, Phys. Lett. B **663**, 217 (2008).
- [165] A. Dobado and J. M. Torres-Rincon, Phys. Rev. D **86**, 074021 (2012).
- [166] S. Ghosh *et al.*, Phys Rev C **93**, 045205 (2016).
- [167] A. Tawfik, A. M. Diab and T. M. Hussein, Int. J. Adv. Research Phys. Science **3**, 4 (2016)

BIBLIOGRAPHY

- [168] S. Ryu, J.-F. Paquet, C. Shen, G. S. Denicol, B. Schenke and C. Gale, Phys. Rev. Lett. **115**, 132301 (2015).
- [169] E. Lu and G. D. Moore, Phys. Rev. C **83**, 044901 (2011).
- [170] S. Mitra and S. Sarkar, Phys. Rev. D **87**, 094026 (2013).
- [171] A. Dobado, F. J. Llanes-Estrada and J. M. Torres-Rincon, Phys. Lett. B **702**, 43 (2011).
- [172] G. P. Kadam and H. Mishra, Phys. Rev. C **92**, 035203 (2015).
- [173] P. Chakraborty and J. I. Kapusta, Phys. Rev. C **83**, 014906 (2011).
- [174] J. -W. Chen and J. wang, Phys. Rev. C **79**, 044913 (2009).
- [175] C. Sasaki and K. Redlich, Phys. Rev. C **79**, 055207 (2009).
- [176] J. Noronha-Hostler, J. Noronha and F. Grassi, Phys. Rev. C **90**, 034907 (2014).
- [177] J. S. Moreland, S. A. Bass, J. Liu, and U. Heinz, Phys. Rev. C **94**, 024907 (2016); P. Božek Phys. Rev. C **95**, 054909 (2017); G.S. Denicol, Nucl. Phys. A **956**, 67 (2016); G. S. Denicol, T. Kodama, T. Koide, and Ph. Mota Phys. Rev. C **80**, 064901 (2009); K. Dusling and T. Schäfer Phys. Rev. C **85**, 044909(2012); A.S. Khvorostukhin et al. Nuc. Phys. A **845**, 106 (2010); C. Sasaki and K. Redlich, Phys. Rev. C **79** , 055207 (2009); V. Chandra, Phys.Rev. D **86**, 114008 (2012); A.S. Khvorostukhin, V.D. Toneev, and D.N. Voskresensky Nucl. Phys. A **845** 106 (2010); M. Bluhm, B. Kämpfer, and K. Redlich, Phys. Lett. B **709**, 77 (2012).
- [178] M. le Bellac, Thermal Field Theory, Cambridge University Press (1996)
- [179] R. Zubarev and O. Morozov, Statistical Mechanics of Non-Equilibrium Processes Vol. 2: Relaxation and Hydrodynamics Processes (Akademie Verlag,

- Berlin, 1996); R. Kubo M. Toda N. Hashitsume, Statistical Physics II (Nonequilibrium Statistical Mechanics), Springer-Verlag Berlin Heidelberg (1985)
- [180] H. Okumuraa, F. Yonezawab, Physica A **321** (2003) 207 – 219; J. H. Hansen, I.R. McDonald, Theory of Simple Liquids, Academic Press, London, 1986, p. 253 (Chapter 8).
- [181] A. Harutyunyan, and A. Sedrakian, Phys. Rev. D **96**, 034006 (2017)
- [182] K. Paech and S. Pratt, Phys. Rev. C **74**, 014901 (2006).
- [183] G. S. Denicol, C. Gale, S. Jeon and J. Noronha, Phys. Rev. C **88**, 064901 (2013).
- [184] K. A. Olive *et al.* (Particle Data Group), Chin. Phys. C **38** 090001 (2014).
- [185] D. Fernandez-Fraile and A. Gomez Nicola, Phys. Rev. Lett. **102**, 121601 (2009).
- [186] M. Cheng *et al.*, Phys. Rev. D **77**, 014901 (2008).
- [187] S. Chatterjee, R. M. Godbole and S. Gupta, Phys. Rev. C **81**, 044907 (2010).
- [188] P. M. Lo, M. Marczenko, K. Redlich and C. Sasaki, Phys. Rev. C **92**, 055206 (2015).
- [189] A. Tawfik and M. Wahba, Annalen Phys. **522**, 849-856 (2010).
- [190] S. Ejiri, F. Karsch, E. Laermann and C. Schmidt, Phys. Rev. D **73**, 054506 (2006).
- [191] A. Tawfik, E. Gamal, H. Magdy, arXiv:1301.1828 [nucl-th].
- [192] J. Cleymans and K. Redlich, Phys. Rev. Lett. **81**, 5284 (1998).
- [193] J. Cleymans, H. Oeschler, K. Redlich, and S. Wheaton, Phys. Rev. C **73**, 034905 (2006).

[194] S. Borsányi *et. al.*, Physics Letters **B 730**, 99 (2014).

[195] V. Vovchenko, D.V. Anchishkin and M.I. Gorenstein, Phys. Rev. **C 91**, 024905 (2015).